

**Universität Stuttgart**

Keio University



**Institute for Microintegration**

**Institute Director**

Univ.-Prof. Dr.-Ing. André Zimmermann

**Yan Laboratory**

**Institute Director**

Prof. Jiwang Yan, Ph.D.

Student Research Project

# **Fabrication and Characterization of Press-Molded Polymer Microlens Arrays**

by:

Holger Rühl

Matriculation no. 3323043

presented to:

Institute for Micro Integration

Prof. Dr.-Ing. André Zimmermann

Advisor:

Prof. Jiwang Yan, Ph.D.

Yan Laboratory for Precision Machining and Nano Processing

Faculty of Science and Technology

Keio University, Yokohama 223-8522, Japan

Date of issue:

April 22, 2019

Date of submission:

October 22, 2019



# Table of Contents

List of Figures.....	iii
List of Tables.....	vi
List of Formula.....	viii
List of Abbreviations .....	ix
List of Symbols.....	xi
List of Appendices .....	xiii
1 Introduction.....	1
2 Microlens and Microlens Arrays.....	4
2.1 Definition of Terms .....	4
2.2 Requirements for Microlenses and Microlens Arrays .....	6
2.3 Applications of Microlens Arrays .....	8
3 Optical Plastics.....	11
3.1 Optical Properties of Plastic Materials .....	12
3.1.1 Refraction and Dispersion.....	12
3.1.2 Birefringence.....	13
3.1.3 Transmittance and Transmission .....	13
3.2 Selected Polymers in Optical Applications.....	15
4 Fabrication of Microlens Arrays .....	17
4.1 Direct Fabrication Methods .....	17
4.1.1 Thermal Reflow .....	17
4.1.2 Inkjet Printing .....	18
4.1.3 Ultraprecision Machining.....	19
4.2 Indirect Fabrication Methods.....	21
4.2.1 Injection Molding .....	21
4.2.2 Compression Molding and Hot Embossing .....	22
4.2.3 Injection-Compression Molding.....	24
5 Compression Molding .....	26
5.1 Compression Molding Process.....	26
5.2 Compression Presses.....	29
5.3 Optical Mold Fabrication .....	30
5.4 Advantages and Disadvantages of Compression Molding.....	31

6	Design of Experiments.....	33
6.1	Design and Fabrication of a Compression Molding Tool .....	33
6.1.1	Mold and Microlens Array Design.....	33
6.1.2	Mold Fabrication.....	36
6.2	Press Molding Machine at Yan Laboratory .....	38
6.3	Selection of Optical Polymers .....	42
6.3.1	High-Density Polyethylene.....	42
6.3.2	Polycarbonate .....	45
6.3.3	PMMA.....	47
6.4	Measuring Equipment.....	50
6.4.1	Balance SHIMADZU TW323N .....	50
6.4.2	Scanning Probe Microscope OLYMPUS OLS4100 .....	50
6.4.3	Digital Microscope KEYENCE VH-Z100UR .....	52
6.4.4	Laser Probe 3D Measuring Instrument MITAKA Series.....	52
6.4.5	Scanning Electron Microscope .....	54
6.5	Experimental Documentation .....	54
7	Experimental Results and Discussion.....	55
7.1	Mold Dimensions Before Compression Molding.....	55
7.2	Compression Molding of Test Series 1 – HDPE.....	62
7.3	Compression Molding of Test Series 3 – HDPE.....	64
7.4	Compression Molding of Test Series 2 - Polycarbonate.....	72
7.5	Compression Molding of Test Series 4 – PMMA.....	84
7.6	Mold Microstructure After Compression Molding.....	91
8	Summary.....	94
	List of Cited Literature.....	97
	Appendix.....	105
	Mold – Technical Drawings and Datasheets .....	105
	Extracts from Polymer Data Sheets.....	116
	Press-Molding Parameters to be set at the Toshiba GMP211 .....	123
	Experiment Documentation .....	124

## List of Figures

Figure 2-1: Microlens dimensions.....	5
Figure 2-2: Microlens array arrangement; left: rectangular packaging; right: hexagonal packaging.....	5
Figure 2-3: Relation between wavefront and ray aberrations; a) Rayleigh criterion; b) Maréchal criterion [14].....	7
Figure 2-4: Optical utilization of MLA for 1) collimation or 2) focusing of light, 3) illumination and 4) imaging [7].....	8
Figure 2-5: MLA used in collimating and focusing light; left: optical fiber coupling [18]; right: focusing incident light into the active areas of a sensor array [3] .....	9
Figure 2-6: MLA used in illumination; liquid crystal application [3].....	9
Figure 2-7: MLA used in illumination; left: MLA arrangement in an optical projector [21]; right: Welcome light carpet in the BMW 7 Series [22].....	10
Figure 2-8: MLA used in imaging; microlens objective arranged in an array in photo-lithography [7] .....	10
Figure 3-1: Comparison of refractive index $nd$ and Abbe number $vd$ of different glasses and optical polymers [30].....	12
Figure 3-2: Transmission of optical plastics for a sample thickness of $t = 3.2$ mm [30].....	14
Figure 4-1: Thermal reflow process .....	18
Figure 4-2: Inkjet printing of polymer microlenses on transparent substrates; 1: ejecting and forming of hemispherical microlenses; 2: UV curing of the polymer .....	18
Figure 4-3: Ultraprecision machining; left: processing of a microlens [17]; right: cross-sectional topography of a diamond turned surface [50] .....	20
Figure 4-4: Mold insert with heating system [57] .....	21
Figure 4-5: left: hot embossing; right: compression molding .....	23
Figure 4-6: Injection-compression molding process sequence [65].....	24
Figure 5-1: Schematic of compression molding process.....	27
Figure 5-2: Microlens defects; left: material burst caused by overpressure during the molding and cooling step; right: shrinkage defect in lens center [10].....	28

Figure 5-3: Comparison of different manufacturing techniques for optical molds [54] .....	31
Figure 6-1: Compression molding tool used in this study (CAD exploded drawing).....	34
Figure 6-2: Numeration of microlenses on a substrate in this study .....	36
Figure 6-3: Mold parts (upper mold part already with diamond cut microlens array) .....	36
Figure 6-4: Ultra-precision diamond cutting of the microlens array.....	37
Figure 6-5: Compression molding press GMP211 (Toshiba Machine Corp., Japan).....	39
Figure 6-6: Machine setup for compression molding process .....	40
Figure 6-7: Manual adjustment of the amount of thermal energy supplied by the IR lamps; left: display for lower mold; right: display for upper mold .....	41
Figure 6-8: Toshiba GMP211 compression molding process.....	41
Figure 6-9: Naming convention in this study to describe the test series, a sample within a test series or a ML within an array .....	42
Figure 6-10: Preparation of cylindrical polycarbonate sheets; left: milling of samples; right: Diameter measurement using a micrometer .....	46
Figure 6-11: Preparation of cylindrical PMMA sheets; left: laser cutting; right: image of marks and void formation caused by heat input of the laser machine on the substrate (100x-magnification).....	48
Figure 6-12: Olympus OLS4100 .....	51
Figure 6-13: Laser probe 3D measuring instrument [83]; left: MITAKA NH-3SP; right: MITAKA MLP-3 .....	52
Figure 6-14: MITAKA NH-3SP Lens measuring settings .....	53
Figure 7-1: Ultra-precision machined microlens array .....	55
Figure 7-2: Mold microlenses at 10x magnification; upper left: ML01; upper right: ML08; lower left: ML12; lower right: ML13.....	56
Figure 7-3: Frequency distributed microlens diameters in the mold .....	57
Figure 7-4: Comparison of microlens hole profiles with the theoretical lens profile.....	58
Figure 7-5: Surface roughness measurement perpendicular to cutting tool marks; left: ML hole 01; right: ML03 .....	60
Figure 7-6: Polished lower mold part 3 .....	60

Figure 7-7: Polymer flash caused by excess material.....	62
Figure 7-8: Compression molded HDPE microlens array .....	64
Figure 7-9: Surface roughness Ra of the press-molded samples in test series 3 .....	69
Figure 7-10: Surface roughness Rq of the press-molded samples in test series 3 .....	69
Figure 7-11: Brass particle found in TS3no405 .....	70
Figure 7-12: Air trapping in a press-molded PC sample .....	73
Figure 7-13: SEM picture of a compression molded polycarbonate MLA .....	73
Figure 7-14: Flow lines with entrapped gas (900x-magnification).....	74
Figure 7-15: PC sample sticking to the mold after demolding .....	74
Figure 7-16: Form error of test series 2 left: TS2no202; TS2no212 .....	79
Figure 7-17: Surface roughness Ra of the press-molded samples in test series 2 .....	79
Figure 7-18: Surface roughness Rq of the press-molded samples in test series 2 .....	80
Figure 7-19: Surface roughness Ra of the press-molded samples in test series 4 .....	88
Figure 7-20: Surface roughness Rq of the press-molded samples in test series 4 .....	88
Figure 7-21: Mold microstructures after the press-molding experiments at 10x magnification; upper left: ML01; upper right: ML08; lower left: ML12; lower right: ML13 .....	91
Figure 7-22: Microlens in the mold after pressing in 50x-magnification. ....	93
Figure 7-23: Thermal oxidation of the lower mold part 2 after the compression molding experiments .....	93

## List of Tables

Table 2-1: Important characteristics and their parameters of optical components [8].....	6
Table 3-1: Properties of PMMA, PC and HDPE [15], [25], [30], [39], [40].....	15
Table 6-1: Process parameters and tool geometry for the ML diamond cutting of mold2.....	38
Table 6-2: Material properties of LINKLON HM600A [37].....	43
Table 6-3: Press molding parameters for test series 1 - HDPE.....	44
Table 6-4: Press molding parameters for test series 3 - HDPE.....	44
Table 6-5: Material properties of polycarbonate by C.I. TAKIRON Corporation [76].....	45
Table 6-6: Press molding parameters for test series 2 – Polycarbonate.....	47
Table 6-7: Material properties of COMOGLAS™ [77–79].....	47
Table 6-8: Press molding parameters for test series 4 – PMMA.....	49
Table 6-9: Measuring machines used to measure the mold and microlens arrays.....	50
Table 7-1: RMS and PV form error of ML hole 2 and 12.....	59
Table 7-2: Ra and Rq surface roughness values of the mold microlenses.....	59
Table 7-3: Used charge mass of every sample in test series 1 - HDPE.....	62
Table 7-4: Microlens diameters of test series 3.....	65
Table 7-5: Microlens sag height of TS3no1xx.....	66
Table 7-6: Microlens sag height of TS3no2xx.....	66
Table 7-7: Microlens sag height of TS3no3xx.....	67
Table 7-8: Microlens sag height of TS3no4xx.....	67
Table 7-9: Microlens sag height of TS3no5xx.....	68
Table 7-10: Microlens sag height of TS3no6xx.....	68
Table 7-11: PV form error results of test series 3.....	69
Table 7-12: Microlens diameters of test series 2.....	75
Table 7-13: Microlens sag height of TS2no1xx.....	76
Table 7-14: Microlens sag height of TS2no2xx.....	76
Table 7-15: Microlens sag height of TS2no3xx.....	77
Table 7-16: Microlens sag height of TS2no4xx.....	77
Table 7-17: Microlens sag height of TS2no5xx.....	78

Table 7-18: Microlens sag height of TS2no6xx .....	78
Table 7-19: PV form error results of TS2noxx .....	79
Table 7-20: Microlens diameters of test series 4 .....	84
Table 7-21: Microlens sag height of TS4no1xx .....	85
Table 7-22: Microlens sag height of TS4no2xx .....	85
Table 7-23: Microlens sag height of TS4no3xx .....	86
Table 7-24: Microlens sag height of TS4no4xx .....	86
Table 7-25: Microlens sag height of TS4no5xx .....	87
Table 7-26: Microlens sag height of TS4no6xx .....	87
Table 7-27: PV form error results of test series 4 .....	88
Table 7-28: Ra and Rq surface roughness values of the mold microlenses after the compression molding experiments.....	92



## List of Formula

Equation 2-1: Microlens packaging density.....	5
Equation 2-2: Total integrated scattering .....	7
Equation 3-1: Refractive index .....	12
Equation 3-2: Abbe number .....	13
Equation 3-3: Optical transmission .....	14
Equation 6-1: Aspherical lens shape equation .....	35
Equation 6-2: Calculation of microlens sag height of mold 1.....	35
Equation 6-3: Calculation of needed HDPE mass .....	43
Equation 6-4: $V_{\text{Cavity}}$ .....	45
Equation 6-5: $V_{\text{PC, sheet}}$ .....	45
Equation 6-6: Calculation of the needed PC sheet diameter $d_{\text{PC, sheet}}$ .....	45
Equation 0-1: Tolerance stack analysis - Nominal dimension .....	113
Equation 0-2: Tolerance stack analysis – Center tolerance deviation.....	113
Equation 0-3: Tolerance stack analysis – Component tolerance.....	113
Equation 0-4: Tolerance stack analysis - Required dimension.....	113
Equation 0-5: Calculation of $N_0$ .....	114
Equation 0-6: Calculation of $E_{C0}$ .....	114
Equation 0-7: Calculation of $T_0$ .....	114
Equation 0-8: Calculation of $M_0$ .....	114
Equation 0-9: Calculation of $N_0$ .....	115
Equation 0-10: Calculation of $E_{C0}$ .....	115
Equation 0-11: Calculation of $T_0$ .....	115
Equation 0-12: Calculation of $M_0$ .....	115

## List of Abbreviations

AC	alternating current
CNC	computerized numerical control
DOD	drop-on-demand
DOE	diffractive optical element
DS	datasheet
FTS	fast tool servo
HEM	hot embossing
HDPE	high-density polyethylene
JIS	Japanese Industrial Standard
IFM	Institute for Microintegration
IM	injection molding
ISO	International Organization for Standardization
IR	infrared
Imp	lower mold part
LCD	liquid crystal display
ML	microlens
MLA	microlens array
MOEMS	Micro-Opto-Electro-Mechanical Systems
NA	numerical aperture
OT	optical transmission
PE	polyethylene
PC	polycarbonate
PMMA	polymethylmethacrylate

PV	peak-to-valley
SPDT	single-point diamond turning
STS	slow tool servo
TS	test series
TIS	total integrated scattering
TD	technical drawing
UP	ultraprecision
UPM	ultraprecision machining
UV	ultraviolet
WD	working distance

## List of Symbols

Symbol	Description	Unit
$2a$	microlens diameter	mm
$a$	microlens radius	mm
$c$	phase velocity of light in material	m/s
$c_0$	speed of light in vacuum	m/s
$f$	feed rate	$\mu\text{m}/\text{min}^{-1}$
$f$	focal length	mm
$l_r$	sampling length (line roughness measurement)	mm
$n$	refractive index	-
$n_d$	refractive index for the helium-d-line	-
$n_C$	refractive index for the hydrogen-C-line	-
$n_F$	refractive index for the hydrogen-F-line	-
$t$	material thickness	mm
$v$	Abbe number	-
$D_n$	lens packaging density	$\text{mm}^{-2}$
$I$	light intensity	
$I_0$	light intensity of incident light	
$E_{Ci}$	center tolerance deviation	mm
$K$	conic constant	-
$N_i$	general dimension	mm
$N_i$	nominal dimension	mm
$P$	compression force	kN
$P_{x,y}$	microlens pitch in x- and y-direction	mm

$R(x)$	real wavefront profile	-
$R_c$	radius of curvature	mm
$R_a$	arithmetical mean deviation line surface roughness	nm
$R_q$	root-mean-square line surface roughness	nm
$T$	temperature	°C
$T_i$	component tolerance	mm
$T_g$	glass transition temperature	°C
$OT$	optical transmission	%
$W(x)$	ideal wavefront profile	-
$TIS$	total integrated scattering	-
$\lambda$	wavelength of light	nm
$\lambda_c$	cut-off wavelength (line surface roughness measurement)	nm
$\rho$	material density	g/cm <sup>3</sup>
$\tau$	transmittance	-
$\Psi_{RMS}$	root-mean-square wavefront aberration	-
$\Psi_{PV}$	peak-to-valley wavefront aberration	-

## **List of Appendices**

### **Mold - Technical Drawings and Datasheets**

- (1) TD Upper Mold – Yan Lab Design
- (2) TD Lower Mold 1 – Yan Lab Design
- (3) TD Lower Mold 2 – Yan Lab Design
- (4) TD Lower Mold 3 – Yan Lab Design
- (5) TD Upper Mold
- (6) TD Lower Mold 1
- (7) TD Lower Mold 2
- (8) TD Lower Mold 3
- (9) DS compression springs DC519 by Accurate Inc., Japan
- (10) Tolerance stack analysis – Axial guidance length between Imp 1 and Imp 2
- (11) Tolerance stack analysis – Plunger length at upper mold part

### **Extracts from Polymer Material Data Sheets**

- (12) C.I. Takiron Polycarbonate Material Data Sheet
- (13) Kuraray Co. Ltd. PMMA Material Data Sheet
- (14) Kuraray Co. Ltd. PMMA Safety Data Sheet

### **Press-Molding Parameters to be set at the Toshiba GMP211**

- (15) Explanation of the compression molding parameters

### **Experiment Documentation**

- (16) TS3no1xx
- (17) TS3no2xx
- (18) TS3no3xx
- (19) TS3no4xx
- (20) TS3no5xx
- (21) TS3no6xx

- (22) TS2no1xx
- (23) TS2no2xx
- (24) TS2no3xx
- (25) TS2no4xx
- (26) TS2no5xx
- (27) TS2no6xx
- (28) TS4no1xx
- (29) TS4no2xx
- (30) TS4no3xx
- (31) TS4no4xx
- (32) TS4no5xx
- (33) TS4no6xx

# 1 Introduction

This research work deals with a theoretical and experimental elaboration on the *fabrication and characterization of press-molded polymer microlens arrays*. The theoretical part of this research elaborates the terms *microlens arrays*, *polymers in optical applications* and the *fabrication of microlenses* in general. Based on the description of microlens fabrication technologies, microlens compression molding is discussed more detailed in order to lead to the experimental part of this study. In the following, an experimental part is conducted in which microlens arrays are compression molded out of different polymer materials. Prior to starting the experiments, the following steps must be prepared. Firstly, an array of microlenses with a microlens diameter  $\varnothing = 1 \text{ mm}$  has to be designed. Specific requirements needed to fulfill a certain application do not have to be considered. The microlens array is then micro structured into a mold by diamond turning. A first dimensional mold design is provided by the Yan Laboratory, but the detailed design and tolerancing is carried out within the framework of this study. After cutting, the microlens mold geometry has to be measured for comparison with the press-molded samples within the evaluation. Three different polymers are to be used in the compression molding experiments. The use of polycarbonate as one of the three materials is determined by the topic. The other two materials can be freely selected. The optical polymer polymethyl-methacrylate is chosen as a second optical material. High-density polyethylene, which is not a classic optical polymer, completes the material selection. After finishing the beforementioned preparations, the three chosen materials are compression molded under different pressing conditions. Crucial process parameters are temperature, compression force and processing times. Reference values for the molding can be extracted from the material data sheets and recent scientific publications. In a last step of the press-molding experiments, the molded samples are characterized by conducting different contactless measurements. Finally, the molded microstructure is optically observed to assess the wear which occurred during the molding experiments.

The objective of the theoretical part of this research is to give an introduction about the topic. An extensive overview about microlenses in arrays as well as the optical characteristics of polymers is given. These fundamentals are needed to fully understand the behavior of optical polymers during the characterization and in the later



applications. It is later seen that the optical characterization of transparent materials is challenging. An impression about the state of research in the fabrication of microlens arrays is given by presenting recent achievements using different technologies. The objective of the experimental part of this study is to press-mold three different optical plastics with one specific microlens geometry and to characterize the molded samples in comparison to each other. Recent scientific publications mostly describe the molding of microlens arrays for one material. An intermediate goal of this study is the precision cutting of the optical mold as the mold geometry represents the geometry to be replicated in the compression molding process. Thus, the mold quality is crucial for the experimental results. The organization of this research is of theoretical, engineering and experimental nature. All machining processes were executed independently unless other persons or departments like the manufacturing center are named.

This research work is presented and submitted to the *Institute for Microintegration (IFM)* of the *University of Stuttgart*. The IFM is connected with the Hahn-Schickard Institute Stuttgart by personal union [1]. Head of both institutes is Prof. Dr. André Zimmermann. Beside other areas, one research focus lies on microstructuring processes, micromolding techniques and the development of optical microsystems. The execution and elaboration of this research is conducted during a study abroad in Japan at the Yan Laboratory for Precision Machining and Nano Processing of Keio University. The Yan Laboratory is headed by Prof. Jiwang Yan, Ph.D. and researches on ultraprecision manufacturing technologies based on machining and material processing [2]. One research area is the ultra-precision micro forming which includes compression molding. Due to the similar fields of research, the execution of this research work in Japan was enabled by both research institutions. Limiting aspects of this research were the temporary stay of 5 months at the Yan Laboratory and the operating language of some machines in Japanese in the lab.

After this introduction to the topic, **chapter 2** gives a general overview of microlenses and microlens arrays. The terms microlens and microlens arrays are defined. The requirements on these optical parts and certain applications based on the main functions of microlenses are presented in the following. **Chapter 3** is devoted to the main optical properties of plastic materials which have to be understood by engineers

and researches who work in the field of optical (micro)systems. Moreover, the optical properties of the three selected polymers used in the experiments conducted in this study are elaborated. In **chapter 4**, the most common microlens array fabrication technologies including recent research results are explained. Chapter 4.2.2 should be mentioned here in particular, as in this chapter common features and differences between the two processes *compression molding* and *hot embossing* are discussed. During the literature review it has been noted that both terms are often mixed in scientific publications. In this regard, the term *compression molding* is defined in **chapter 5** followed by an in-depth look on the process. The design of compression presses and the fabrication technologies for optical molds are explained in this chapter, finalized in a discussion of the advantages and disadvantages of compression molding in chapter 5.4. **Chapter 6** deals with the design of experiments of this research. The design and fabrication of the compression molding tool, the selection of optical polymers, the equipment used for the microlens characterization as well the result documentation is described. The experimental results for the mold fabrication and the press-molded microlens arrays are presented and discussed in **chapter 7**. A summary about this study is drawn in **chapter 8**.

## 2 Microlens and Microlens Arrays

Hereafter the terminology microlenses in arrays, the requirements for them and their applications are described.

### 2.1 Definition of Terms

Even though the term *microlens* implies the description of lenses in the micron size, a clear definition is not drawn in most of the papers and articles. This also applies for the term *microlens array*. Because no standard definition exists in academia, the definition provided in the ISO standard 14880-1 should be stated here. In it, a microlens (ML) is defined as a

*“lens in an array with an aperture of less than a few millimeters including lenses which work by refraction at the surface, refraction in the bulk of the substrate, diffraction or a combination of these”* [3].

With current fabrication methods achievable dimensions range from around 1 mm down to few nanometers [4], [5]. The standard aperture of microlenses is circular in shape, but other shapes are not unheard-of. The lens shape depends on the required optical function of the lens [6]. In refractive optical elements, for example in convex or concave lenses and all types of variants with one plane side, a ray of light is shaped by refraction. In diffractive optical elements (DOE) the light is focused by diffraction [3]. Crucial dimensions of microlenses are the *diameter*  $2a$  (footprint diameter of the lens), the *radius of curvature*  $R_C$  and the *focal lengths*  $f$ .  $R_C$  describes the radius at the vertex of the microlens. These dimensions are shown in Figure 2-1 for a plano-convex ML.

Besides the geometrical and optical properties of the single lenslets, the properties of the entirety of lenses forming the microlens array (MLA) must be described. With reference to the standard ISO 14880-1, a microlens array is defined as a

*“regular arrangement of microlenses on/in a single substrate”*. [3]

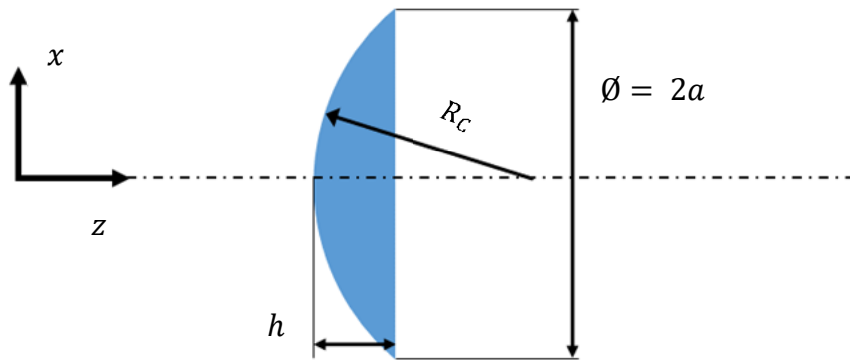


**Figure 2-1: Microlens dimensions**

The substrate can be homogenous or laminated. The most common geometrical arrangements are the rectangular and hexagonal array as depicted in Figure 2-2. The distance between the centers of adjacent lenses in the x- and y-direction is described by the *lens pitch*  $P_x$  and  $P_y$  [7]. Depending on the lens pitch and ML diameter, the number of lenses on the substrate surface is defined by the *packing density*  $D_n$  given in equation (2-1).

$$D_n = \frac{a^2 \pi}{P_x \cdot P_y} \quad (2-1)$$

The possible maximum fill factor of rectangular MLA arrangements is 78.5 % ( $\pi/4$ ), hexagonal arrays can be packed up to 99.7 % ( $\pi/\sqrt{3}$ ).

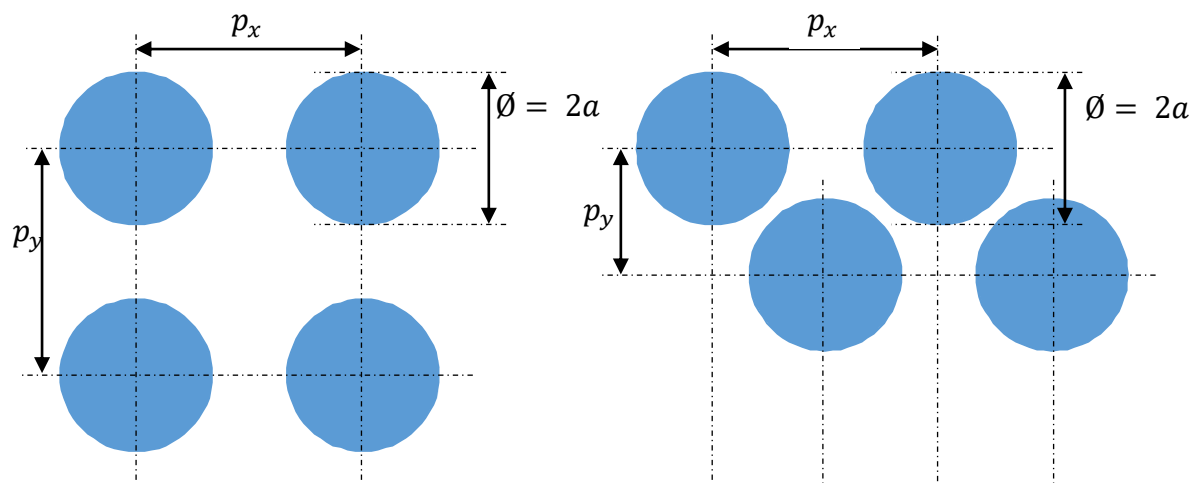


**Figure 2-2: Microlens array arrangement; left: rectangular packaging; right: hexagonal packaging**

## 2.2 Requirements for Microlenses and Microlens Arrays

The quality of an optical system is mostly affected by the characteristics of its optical components. These characteristics influence directly the light intensity, propagation direction and the polarization state of rays [8], [9]. The consistency of the focal length, low wavefront aberrations and the durability over the specified lifetime of the lenslets is therefore essential [10]. For MLA, uniformity among the ML is required. A compilation of the most important parameter of optical components is given in Table 2-1. These parameters must be controlled during and after the production process to ensure the quality of a lens.

Characteristics	Parameter	Influence on optical components performance
Geometric	Lens shape	Spherical lens shapes cause monochromatic aberrations
Geometric	Shape accuracy	Inaccuracies in shape effect cause monochromatic aberrations
Physical	Surface roughness	Unevenness cause scattering and blurred imaging
Material	Strength	Effects the material deformation and the fracture susceptibility
Material	Material density	Inhomogeneities cause unwanted changes to absorption and refractive index. Occurrence of changes in phase and intensity of the ray
Optical	Sub surface damages	Cause light loss; limit durability and increase absorption

**Table 2-1: Important characteristics and their parameters of optical components [8]**

The surface roughness of a lens must be specified since scattering of light is mainly caused by the statistical surface characteristics of an optical part [11]. With reference to the standard ISO10110-8 [12], the roughness can be specified by five statistical possibilities. A proper specification is the RMS surface roughness  $R_q$  as this value is in combination with the wavelength of incident light  $\lambda$  directly related to the occurrence of total integrated scattering (TIS) [7], [11], [12]. This relation is described by equation (2-2).

$$TIS \approx \left( \frac{4\pi R_q}{\lambda} \right)^2 \quad (2-2)$$

However, it can be noted that in most of the academic publications the profile roughness was indicated by the arithmetical mean height  $R_a$ . In general, the  $R_a$  of optical mold inserts should be  $\leq 10$  nm, the  $R_a$  of microlenses between 20 and 50 nm depending on the application. High profile peaks or deep profile valleys often remain undetected by the sole indication of  $R_a$ . The determination of at least one more surface roughness value which is representative for the application, is necessary. This can be the roughness  $R_q$  for optical parts because of the aforementioned reason. Meanwhile the surface roughness can be also calculated areally [13].

Beside geometrical measurements, the optical lens quality can be determined by different approaches based on diffraction and aberrations [14]. Aberrations are caused by deviations of the lens shape from a calculated ideal lens shape. Figure 2-3 depicts the relation of aberrations between an ideal wavefront  $W(x)$  and a distorted wavefront  $R(x)$ . Based on this relation, two commonly used quality approaches are the Rayleigh criterion and the Maréchal criterion.

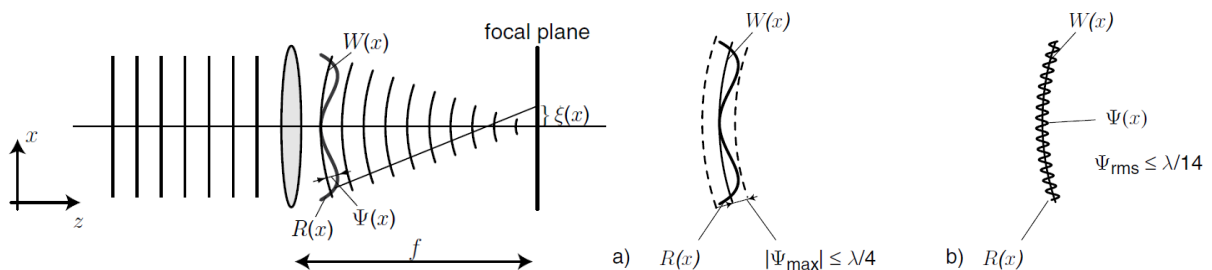


**Figure 2-3: Relation between wavefront and ray aberrations; a) Rayleigh criterion; b) Maréchal criterion [14]**

The Rayleigh criterion states that an optical system is diffraction-limited if the maximum peak-to-valley deviation  $|\psi_{PV}(x)|$  between the ideal wavefront profile  $W(x)$  and the real wavefront profile  $R(x)$  is smaller than a quarter of the wavelength of the incident light (Figure 2-3 a)). The Maréchal criterion is based on the RMS wavefront aberration  $\psi_{RMS}$ , wherein  $\psi_{RMS}$  must be less than a fourteenth of the wavelength (Figure 2-3 b)). The suitability of these criteria to evaluate the optical performance was demonstrated by Ottevaere et al., who fundamentally reviewed the optical performance of glass and polymer refractive ML produced with different fabrication methods [15]. The Rayleigh

and Maréchal criteria are of interest since not only the optical performance but also the maximum permissible form error of a microlens can be inferred from them. Examples employing these criteria to determine and evaluate the form error can be found in [16] and [17].

### 2.3 Applications of Microlens Arrays

Microlens arrays are not only limited to certain applications but are nowadays found in various technical systems in different application fields. A classification can be made on the basis of the optical utilization [7]. MLA are either used to collimate or focus light, in illumination or in imaging as shown in Figure 2-4. Exemplary applications of MLA for these functions are mentioned in the following.

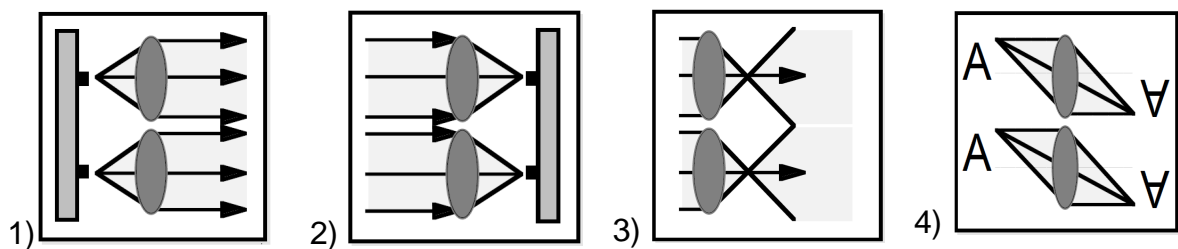


**Figure 2-4: Optical utilization of MLA for 1) collimation or 2) focusing of light, 3) illumination and 4) imaging [7]**

When big amounts of data are generated, the informations are transferred by usage of fiber-optic communication. Optical signals between two optical fibers are transferred by means of fiber couplings which contain two MLA (Figure 2-5, left) [3], [18]. The incident, individual rays of a signal are emitted at the end of the optical fiber and narrowed by a first MLA to parallel rays. To transfer the beams into the following fiber, the parallel beams are focused again on the optical fiber input by a second MLA. By using a corresponding lens design, it is even possible to switch channels. Another usage of MLA is to focus incident light on photodiodes of imaging sensors (Figure 2-5, right), which can be found in various devices like in consumer electronic products, for example smartphones [19].

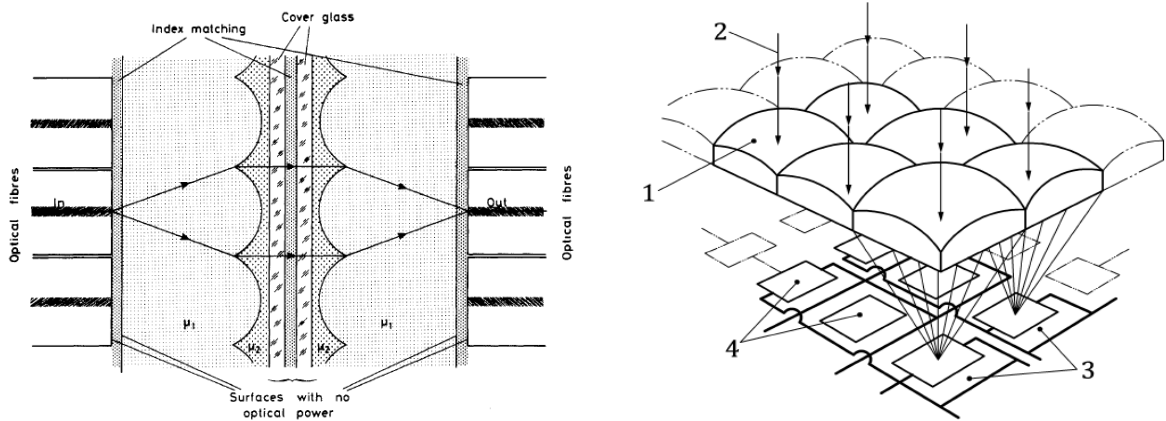


**Figure 2-5: MLA used in collimating and focusing light; left: optical fiber coupling [18]; right: focusing incident light into the active areas of a sensor array [3]**

A typical usage of MLA for illumination can be found in projection panel solutions like liquid crystal displays (LCD) [20] or organic light emitting diode (OLED) displays [4] used in consumer electronics. In LCD displays, exemplarily shown in Figure 2-6, the light is transmitted through two polarizers rotated to each other by 90 degrees. Between the polarizers, a liquid crystal layer is covered with two transparent electrode layers [20]. A microlens structure covers the backlight layer to concentrate the emitted light in order to pass it unobstructed through the different display layers and thus, increases the illumination efficiency. In the automotive sector, MLA can be found in car lighting products. A unique development is the micro-optical array projector technology presented in [21]. One condenser MLA and one projection MLA were UV-micro molded and then rearranged forming a projector. The technology was brought to the market in 2015 in the BMW 7 Series to project a light carpet on the ground [22]. The technical principle of this technology and its application are shown in Figure 2-7.

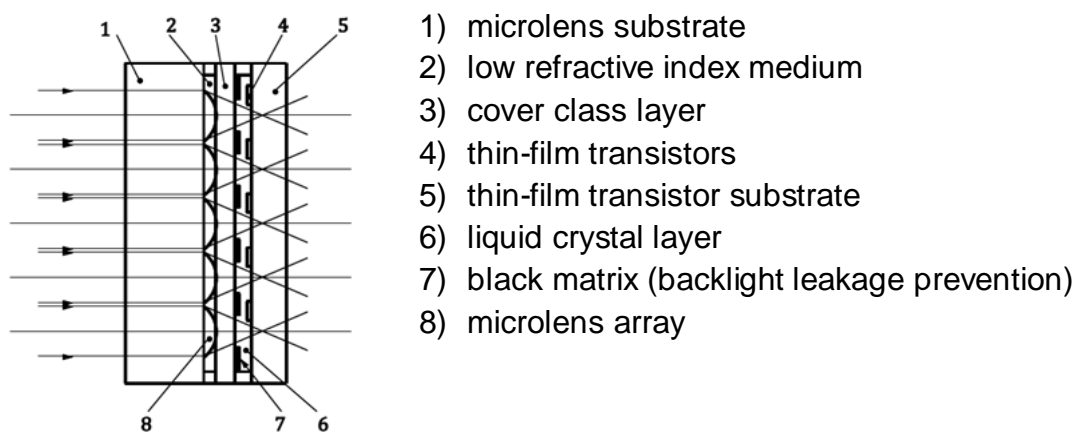


**Figure 2-6: MLA used in illumination; liquid crystal application [3]**



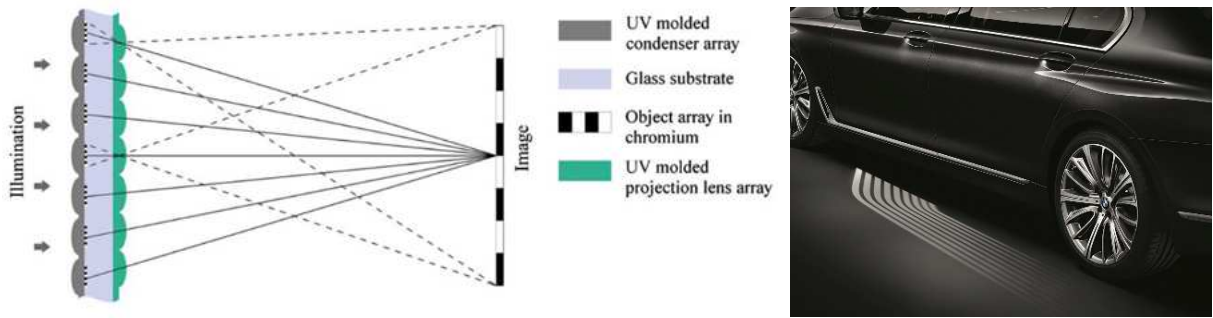


**Figure 2-7: MLA used in illumination; left: MLA arrangement in an optical projector [21]; right: Welcome light carpet in the BMW 7 Series [22]**

In imaging devices, microlens arrays are an integral part of components like photocopiers [4] or light field cameras [23]. Two MLA aligned between the main lens and the image sensor can shorten the path of light. Thus, a miniaturization of the packaging space is achieved. In photolithography systems as exemplarily shown in Figure 2-8, MLA are used as objective to replicate mask patterns on a substrate [7]. It is reported, that the depth of focus can be increased enabling micro structure patterning over large areas as needed in display fabrications or to expose thick photo resists. The usage of MLA in micro structuring devices is an example for how recent advancements in micro fabrication technologies drive the continuous development of creating smaller and smaller microstructures.

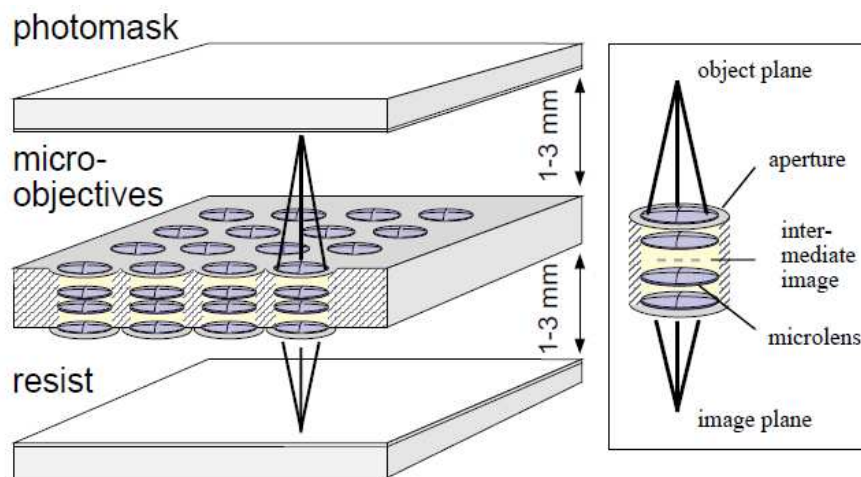


**Figure 2-8: MLA used in imaging; microlens objective arranged in an array in photolithography [7]**

### 3 Optical Plastics

As presented in chapter 2.3, micro optical systems are widely used in various applications. Microlenses are often made of optical polymers instead of optical glasses, as these offer not only better mechanical, but also superior optical material properties. Plastic materials used in optical applications are amongst others polymethylmethacrylate (PMMA), polycarbonate (PC), polystyrene (PS), cyclic olefins or O-PET [24].

One advantage of using polymers is that the lower density materials results in a lower component weight of optical elements. A reduction of weight of single parts always pushes the development of more ergonomic and efficient end products [25]. During product development not only the material properties and the functional design, but also the manufacturing costs of the end product must be considered. The high availability of plastic materials including the possibility of processing plastic parts in high quantities via molding techniques (chapter 4.2) minimize the costs per part tremendously [26–28]. Furthermore, smaller batches of parts with complex geometries, like MLA with an aspherical lens geometry, can be produced cost effectively employing appropriate molding techniques [25]. Because of these aforementioned reasons plastic optics often cost less than their glass part equivalents [4]. This is of special interest in the consumer and automotive industry where the final product costs are especially relevant.

On the other hand, glass is more appropriate for high temperature applications or areas with unstable thermal conditions due to the high thermal expansion coefficient and the poor thermal stability of plastics at high temperatures [29]. Additionally, plastic materials are soft and therefore more susceptible to scratches or other surface damages [26]. At last it can be mentioned that in comparison to the high numbers of different available optical glasses, only a small number of optical plastics is offered on the market. Nevertheless, the last-mentioned points are compensated by the freedom of shape design.

### 3.1 Optical Properties of Plastic Materials

When using plastics in optical applications, different optical properties of the materials have to be carefully taken into consideration in order to receive an optical performance which fulfills the specifications required by the application. Some properties can be influenced by the optical part manufacturing process.

#### 3.1.1 Refraction and Dispersion

The optical properties of optical materials are typically compared using one material's refractive index  $n$  and its Abbe number  $v$ . The relation of the refractive index  $n$  and the Abbe number  $v$  is shown in Figure 3-1 for different optical plastics and glasses.

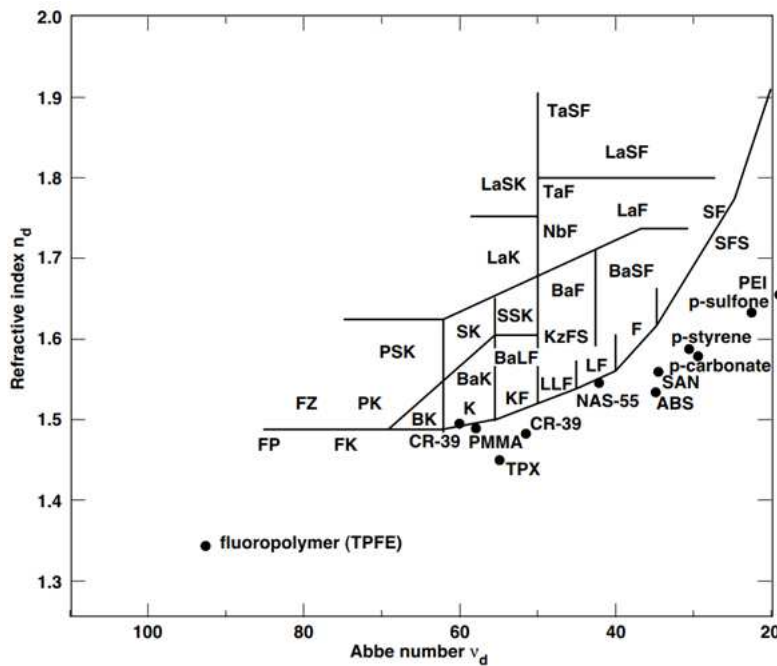


Figure 3-1: Comparison of refractive index  $n_d$  and Abbe number  $v_d$  of different glasses and optical polymers [30]

The refractive index  $n$  describes the propagation of light inside a material. It is defined according to equation (3-1) as the ratio of the speed of light  $c$  in vacuum and the phase velocity  $c$  of light in the entered material [31].

$$n = \frac{c_0}{c} \tag{3-1}$$

The refractive index is not constant for different wavelengths. For this reason, the refractive index of a material must be always referenced to the wavelength which was used for the measurement. Commonly, refractive indices are measured for the helium-d-line with a wavelength  $\lambda$  of 587.6 nm [24] or for the sodium-D-line with a wavelength  $\lambda$  of 589.3 nm. The convention of the helium-d-line for the refractive index will be followed throughout this work. In vacuum, the refractive index is defined to 1. For optical plastics the refractive index  $n_d$  is between 1.3 and 1.65 [30]. For materials with high refractive indices a ray beam is bent with a smaller refraction angle than the angle of the incident light. Spherical aberrations can be reduced with higher refractive index materials [32].

The physical phenomenon of the dependency of the refractive index on certain wavelengths is called dispersion. The dispersion of an optical material is reflected by the Abbe number  $v_d$  [33], which is defined in equation (3-2). A higher dispersion is related to a lower Abbe number. The refractive indices  $n_d$ ,  $n_F$  and  $n_C$  represent the refractive indices respectively measured for the helium-d-line, hydrogen-F-line and hydrogen-C-line. By choosing materials with high Abbe numbers chromatic aberrations can be reduced [33].

$$v_d = \frac{n_d - 1}{n_F - n_C} \quad (3-2)$$

### 3.1.2 Birefringence

Birefringence is an optical phenomenon describing the variation of the refractive index with the polarization state of light [24]. A ray of light is decomposed into two rays when passing through anisotropic material [34]. The effect occurs mostly for injection-molded parts around the sprues. Birefringence is generally caused by induced residual stress from the alignment of the polymer chains and can therefore occur for press-molded lens products, too [24], [35]. However, molding techniques which include a compression step mostly provide a better behavior in terms of birefringence.

### 3.1.3 Transmittance and Transmission

Light, which is not reflected at the material surface or absorbed within the bulk, is transmitted through optical material. The transmittance  $\tau$  is specified by the ratio

between the transmitted light intensity  $I$  and the incident light intensity  $I_0$ . For optical materials, the transmission  $OT$  is often given, which states the transmittance in percent and describes the light permeability of a material. The internal transmittance/transmission takes reflections losses into account [24]. Since the transmittance decreases with the thickness of the material, the thickness  $t$  of the material must be specified.

$$OT = 100 \% * \tau = 100\% * \frac{I}{I_0} \quad (3-3)$$

Transmittance and transmission strongly depend on the wavelengths of light. As shown in Figure 3-2, the transmission of optical plastics is high within in the visible (380 nm – 740 nm) and near infrared range between  $\lambda = 350$  nm to 2.2  $\mu\text{m}$  with slight variations depending on the plastic type [24].

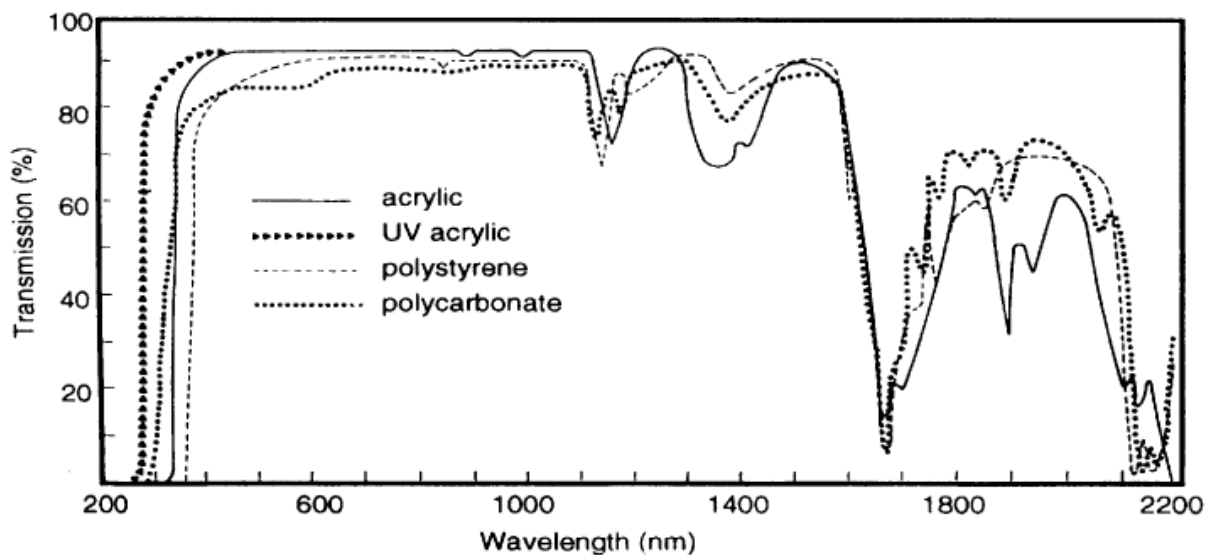


**Figure 3-2: Transmission of optical plastics for a sample thickness of  $t = 3.2$  mm [30]**

Optical plastics show high absorption rates for infrared regions  $\lambda > 2.2 \mu\text{m}$  caused by their chemical structure. In contrast, HDPE shows a transmission around 60 % for a material thickness of 500  $\mu\text{m}$  in the thermal IR wavelength range of  $\lambda = 8$  to 14  $\mu\text{m}$ . The suitability of HDPE as lens material for thermal imaging in this spectrum has been proven in [36] and [37].

### 3.2 Selected Polymers in Optical Applications

As previously mentioned, only a low number of polymers shows suitable properties to be used in optical applications. The most commonly used optical plastics are PC and PMMA. Recently, due to its good clarity in the thermal IR field, its low material costs compared to more expensive alternatives like Si or Ge and the given easy moldability, HDPE has been established for optical IR applications [37]. Optical polymers are of amorphous structure, while polyethylene is semi-crystalline. The properties of PMMA, PC and HDPE are compared in Table 3-1 to outline similarities and differences for optical applications.

Properties	PC	PMMA	HDPE
Refractive index $n_d$	1.585	1.492	1.529 <sup>*1)</sup>
Abbe number $v_d$	29.9	57.4	–
Birefringence (from 0 to 10)	7	4	–
Optical transmission $OT$ (%)	85 – 91 <sup>*2)</sup>	92 <sup>*2)</sup>	84 <sup>*3)</sup>
Density $\rho$ [g/cm <sup>3</sup> ]	1.20 – 1.24	1.15 – 1.19	0.94 – 0.96
Hardness	Rockwell M70	Rockwell M97	–
$T_g$ [°C]	145 – 150	105 – 120	< 100

\*1)  $\lambda = 9.25 \mu\text{m}$  [38]; \*2)  $t = 3.2 \text{ mm}$  [26]; \*3)  $t = 3 \mu\text{m}$ ,  $\lambda = 0.792 \mu\text{m}$  [38]

**Table 3-1: Properties of PMMA, PC and HDPE [15], [25], [30], [39], [40]**

Polycarbonate has a low percentage of polymer crystallization resulting in a sufficient transparency for the most application, but still lower transparency compared to PMMA. Its refractive index  $n_d = 1.585$  is in the medium average range of optical polymers. However due to its smaller Abbe number, PC is more susceptible to dispersion. PC has a very high impact strength [30]. The glass transition temperature  $T_g$  around 150 °C is the reason for the comparatively good mechanical properties of PC at higher temperatures [26]. On the other hand studies indicate that PC is more difficult to mold [41].

Polymethylmethacrylate (PMMA) is the most commonly used optical plastic [26], [41]. It is highly transparent and shows a very good transmission of 92 % [42]. The refractive index of  $n_d = 1.492$  is one of the lowest within the optical plastics [30], but the Abbe number is with a value of  $v_d = 57.4$  one of the highest. PMMA is hard, rigid and has good mechanical properties and a high resistance against surface damages [26]. Generally, PMMA shows a good machinability including polishability and is comparatively easy to mold [41]. Because of its good mechanical and optical properties but also its chemical resistance, acryl is used in a wide range of applications.

Polyethylene is a standard material in plastic engineering and used in wide range of application fields [39]. Since PE is of semi-crystalline structure and does not show optical properties for visible wavelengths, PE is classically not classified as an optical plastic. This might be the reason why the information about optical properties of PE are limited in scientific literature. As previously mentioned in chapter 3.1.3, HDPE shows a good transmission in the thermal infrared range for small material thicknesses. A refractive index of 1.529 comparable to the one of PC and PMMA can be measured for IR wavelength. For a material thickness of 3  $\mu\text{m}$ , which is around 1000 times smaller than the thickness used to measure the OT of PC and PMMA in [26], the transmission was measured to be 84 %.

## **4 Fabrication of Microlens Arrays**

Beginning in the last century, a wide range of methods for the fabrication of micro lens arrays has been developed, having continuously improved both the process precision and the reliability and quality of microlens products [15]. These methods can either be classified by the operating principle (mechanical, electrical, chemical, etc.) [4] or by categorization into direct and indirect methods based on the necessity of a replication tool [23], [43]. Common MLA fabrication techniques suitable for plastic materials are in the following divided according to the latter classification method and introduced briefly.

### **4.1 Direct Fabrication Methods**

The term direct fabrication describes in general the possibility to machine parts without using a replication master like a metallic mold [4]. Thus, each part is fabricated separately.

#### **4.1.1 Thermal Reflow**

The thermal reflow or resist melting method is the oldest MLA fabrication method, firstly introduced in 1988 by Popovic [18] and is commonly used to obtain spherical MLA. The great advantage of this technique is the use of standard lithography equipment and processes [7]. As shown in Figure 4-1, a photoresistive polymer layer is first coated on a substrate and cured. In the second step, the photoresist is partially exposed and dissolved in a subsequent developmental process. Isolated photoresistive cylinders are formed on the substrate. In the final reflow step (Figure 4-1 (3)), the material compound is heated above to the photoresists glass-transition temperature. Due to surface tension effects, the cylinders are shaped into spherical profiles [18], [44]. The focal length is adjusted by the thickness of the photoresistive layer before melting the cylinders. As the thermal reflow method is known for around three decades, it is well-established today. Presently, MLA with a wide variation of lens dimensions are available. However, the minimum lens diameter is limited by the photolithography process boundaries [7]. In [45], the process was used to melt square polymer cylinders into an rectangular array of square ML footprints with high density formation. The sag



heights varied from 7.3 up to 8.6  $\mu\text{m}$ . The average surface roughness  $R_a$  was 4.6 nm, measured over an area of 4 x 4  $\mu\text{m}$  at the lens vertex.

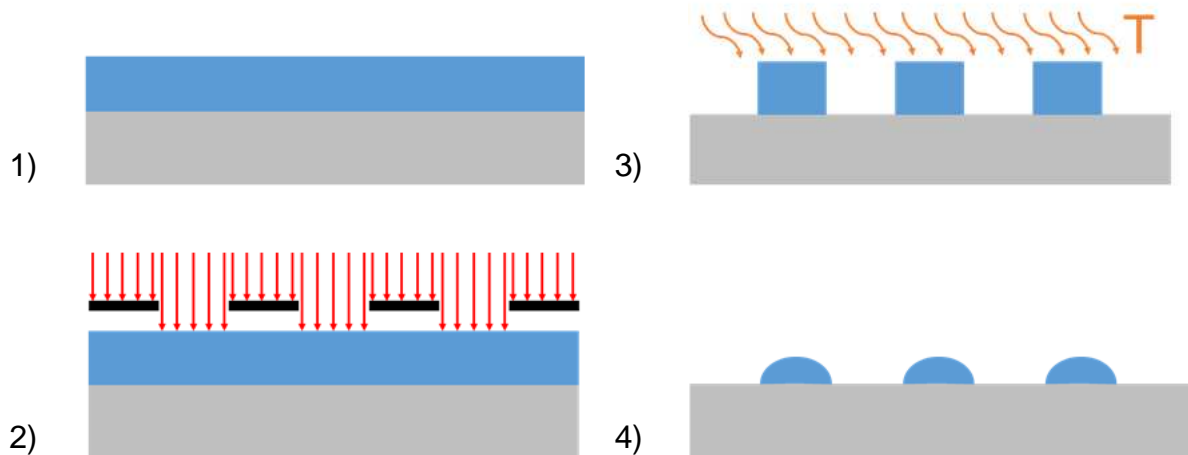


**Figure 4-1: Thermal reflow process**

#### 4.1.2 Inkjet Printing

Inkjet printing of microlenses is a technique in which small droplets of a UV-curable polymer ink are ejected in DoD-configuration from a nozzle onto a transparent substrate material [15], [23] (Figure 4-2 (1)). On the substrate the droplets merge to plano-convex hemispheres due to the surface tension effect. The liquid volume of each microlens is directly related to amount of ink and thus to the number of droplets applied for each lens. Subsequently, the formed lenses are solidified in a UV curing step forming the MLA (Figure 4-2 (2)).

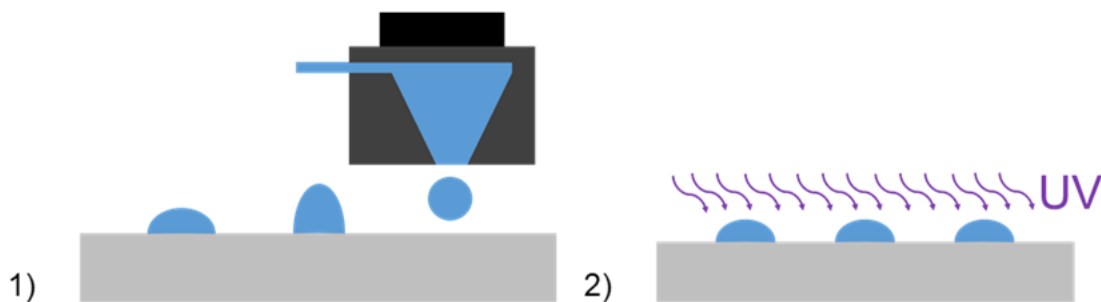


**Figure 4-2: Inkjet printing of polymer microlenses on transparent substrates;  
1: ejecting and forming of hemispherical microlenses; 2: UV curing of the polymer**

The advantage of this technique is the fabrication of microlenses of high shape accuracy over large-area substrates with an individual adjustment of the lens size and

the optical performance by varying the number of droplets [46], [47]. The amount of dropped ink is easily implantable in industrial operations by digital processes. Even a monolithic integration of inkjet printing with printing directly on optical components is possible [48]. Surface texturing of the substrate [47] or pre-patterned substrates [49] enable further process improvements and an adjustability of the lenslet's optical characteristics. Recently, as presented in [46] by Beckert et al., lenses with a ML diameter  $2a = 1$  mm were printed onto a pre-patterned substrate. By varying the number of droplets from 800 to 3500, minimal dimensions of the radius of curvature  $R_C = 1.160$  mm and a sag height  $h = 113.25 \pm 0,28$   $\mu\text{m}$  were achieved. The maximum dimensions were  $R_C = 379.79 \pm 1,4$   $\mu\text{m}$  and a sag height of  $h = 0.520$  mm. The lens height deviation was smaller than 0.4 %. The surface roughness was not measured in [46].

#### 4.1.3 Ultraprecision Machining

Ultraprecision machining (UPM) techniques are well-established in all fields of engineering. Micro optical components or their replication tools as discussed in chapter 5.3 can be ultraprecision machined in a diamond turning process. The following focuses on diamond turning, which is often termed as *single-point diamond turning* (SPDT). A diamond tool is a polished, mono-crystal diamond of gemquality [50]. Single-point diamond turning is conducted on ultraprecision lathes [16] equipped with a *slow tool servo* (STS) system as standard. The cutting tool is mounted on the tool post of the STS and driven by it in Z-direction. For certain cutting processes the lathe is equipped with an additional piezoelectrically driven *fast tool servo* (FTS) enabling smaller servo strokes and higher reciprocating frequencies. The feed rate and spindle rotation are synchronized for both servos types.

The diamond cutting process of a ML is shown in Figure 4-3 on the left. As shown in Table 2-1, the optical performance of optical components is highly influenced by the lens topography. In cutting processes, the created surface is marked by the diamond tip radius. The spacing of two grooves is in accordance to the synchronization ratio of the feed rate and the spindle speed [50]. The interdependencies are shown in Figure 4-3.

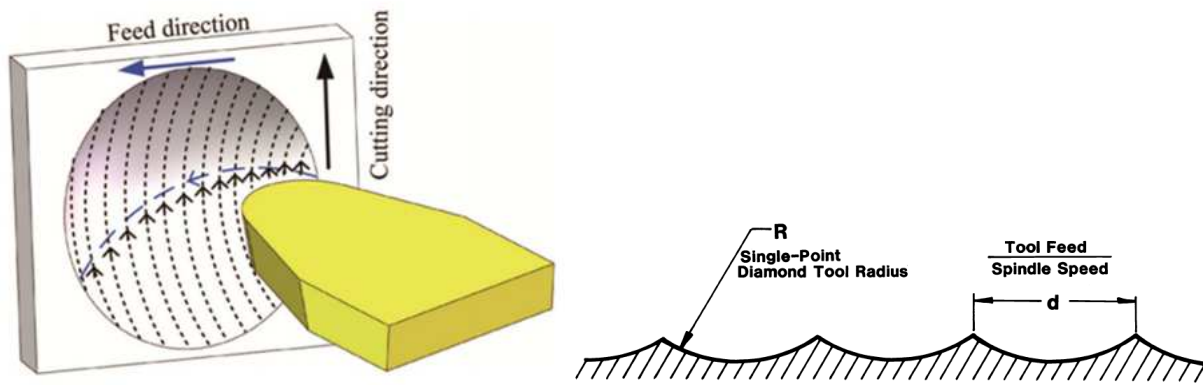


**Figure 4-3: Ultraprecision machining; left: processing of a microlens [17]; right: cross-sectional topography of a diamond turned surface [50]**

In a study conducted at the Yan Laboratory lenses of the diameter  $2a = 320 \mu\text{m}$  and a sag height of  $h = 5 \mu\text{m}$  were diamond cut on single-crystal silicon [16]. The feed rate  $f$  was varied between  $1 - 6 \mu\text{m}/\text{min}^{-1}$ . For machining in the  $\langle 100 \rangle$  direction, the minimal achieved peak-to-valley form error was  $314 \text{ nm}$  with an area surface roughness  $S_a = 6 \text{ nm}$ . The Rayleigh criterion was fulfilled for IR wavelengths. Very recently, a MLA was diamond cut in STS configuration into PMMA [17]. The lens diameter and the sag height, equivalent to the depth of cut, were  $2a = 250 \mu\text{m}$  and  $h = 7.28 \mu\text{m}$ . The feed rate was varied from  $1 \mu\text{m}/\text{min}^{-1}$  to  $10 \mu\text{m}/\text{min}^{-1}$  for a spindle speed of  $24 \text{ rpm}$ . In result, a form error of  $60 \text{ nm}$  and a surface roughness of  $8 \text{ nm}$  were achieved for a feed rate of  $2 \mu\text{m}/\text{min}^{-1}$ .

Beside the ability to machine a broad range of materials with dimensional precision while adhering to the narrowest tolerances, the processes flexibility is the most crucial reason to use SPDT for MLA fabrication. Aspherical lenses, DoE as well as freeform profiles can be obtained [51–53]. Although the possibilities of lens SPDT were proven above, diamond turning is still a time-consuming process as each lens is manufactured separately. In terms of moldable materials, ultraprecision machining is therefore more applied for the replication molds than for the ML(A) fabrication itself. This can be exemplarily seen in the publications [51], [52], [54], [55]. The achievable finish roughness using UPM for the optical mold fabrication is  $< 10 \text{ nm}$  [54].

## 4.2 Indirect Fabrication Methods

Compared to the presented direct MLA fabrication, the moldability of materials enables high-quantity production. As a consequence, materials like plastics can be fabricated in consequence with higher productivity utilizing replication processes.

### 4.2.1 Injection Molding

Injection molding (IM) is a process in which the polymer material is plasticized using heat by the injection molding machine and injected under pressure through a nozzle into the cavity of a previously closed mold. The material solidifies inside the mold into the desired shape by cooling [56]. Depending on the material shrinkage, the dimensions of the created part are almost equal to the ones of the mold. For macroscopic components, injection molding is well-known and established in science and industry for several decades. Nevertheless, the isothermal process common in conventional injection molding, results in certain problems in the microscopic world due to a reduced mold flow behavior and higher cooling rates. In microinjection molding the process can be operated variothermal.

In this configuration a micro structured tool is equipped with a heating system which should keep the mold thermally stable to the temperature level of the material to be molded [43], [57]. An mold insert with heating system is exemplified in Figure 4-4. Before demolding, the whole tool is cooled down below the materials  $T_g$ . Generally, it can be said that with this molding technique the quality of the molded parts is improved but also the process time is prolonged.



**Figure 4-4: Mold insert with heating system [57]**

A double-sided, hexagonal arranged PMMA MLA for illumination purposes was injection molded in [58]. The lens diameter was  $1450\ \mu\text{m}$ , the sag height was  $550\ \mu\text{m}$  and the radius of curvature was  $0.850\ \mu\text{m}$ . The lens design was machined into two molds by conventional CNC milling. To improve the mold surface roughness, a  $14\ \mu\text{m}$  thick layer of positive photoresist was subsequently spraycoated on one mold. One MLA was respectively injection-molded with the uncoated and the coated tool. The dimensions of the MLA molded with the uncoated mold were  $2a = 1457\ \mu\text{m}$ ,  $h = 503\ \mu\text{m}$  and  $R_C = 863\ \mu\text{m}$ . The dimensions of the MLA molded with the coated mold were  $2a = 1460\ \mu\text{m}$ ,  $h = 492\ \mu\text{m}$  and  $R_C = 869\ \mu\text{m}$ . The surface roughness of the latter MLA was  $R_a = 38\ \text{nm}$  and  $R_q = 42\ \text{nm}$  and thus two times and two and a half times better than the one of the MLA, molded with the uncoated mold. Hence, the MLA surface roughness was improved by coating the mold.

#### **4.2.2 Compression Molding and Hot Embossing**

Both compression molding (dt. Formpressen) and hot embossing (HEM) (dt. Heißprägen) are introduced in this chapter collectively since both have a high process resemblance to each other and are often mentioned together in scientific publications. Compression molding was originally introduced to mold glass components but is also used to mold thermoset and thermoplastics.

Compression molding and HEM are based on the same process steps. A polymer material is firstly inserted into the molding machine. The whole mold is then heated above the polymer glass transition temperature. By closing the mold, pressure is applied to form the substrate material into the mold insert structure. In a last step the mold and material are cooled down and the pressed part is demolded. The main difference between compression molding and hot embossing is the stage of closing the mold as it can be seen in Figure 4-5. In compression molding both mold halves are completely closed, whereas in HEM a small gap remains between the lower and upper mold part. A residual layer around the substrate remains and must be diced afterwards [29], but makes HEM less critical in terms of the charge volume. However, the open mold shows its drawback when 3D-structures should be fabricated. The advantage of both processes is that high-aspect ratios can be achieved compared to other molding processes [43], [59].



**Figure 4-5: left: hot embossing; right: compression molding**

Compression molding and HEM represent both an individual process and can be therefore mentioned individually as done in [25] and [60]. During the literature research the impression arose that the term hot embossing is mentioned more often. However, due to the process's similarities both terms are often mixed in scientific publications. Because of the not fully closed mold, hot embossing is sometimes also explained as an open-die compression molding technique [61]. The other way around, compression molding can be described in [9] as a closed-die process to produce lenses. Two years earlier, the same researchers used compression molding to mold perpendicular surfaces of a micro structured plate for display applications, but called the process closed-die hot embossing [59].

To overcome this definition problems, the terms definition of the ISO should be given as it was previously done for the terms *microlens* and *microlens array* in chapter 2.1. According to the standard ISO 472, compression molding is denoted as a “process of moulding a material in a confined cavity by applying pressure and usually heat”, whereas embossing is defined as a “process of producing a relief pattern on a surface” [62]. For a clearer distinction, an own definition of compression molding is drawn in chapter 5.1.

Recent advancements both in hot embossing and compression molding are presented in the following. An array of ML with a diameter of  $64.4\ \mu\text{m}$  and a sag height of  $3.4\ \mu\text{m}$  was hot embossed in [63] on a polycarbonate sheet after several attempts with different mold materials. The replicated MLA showed a very small deviation from the mold and a  $R_a$  surface roughness of  $11\ \text{nm}$ . The sag height of the embossed ML was enlarged due to profile deterioration caused by adhesion and friction between the polymer and the mold. In [60], microlens arrays with varying the ML diameter,  $R_c$  and the sag height between  $36 - 96\ \mu\text{m}$ ,  $20 - 60\ \mu\text{m}$  and  $17.45 - 25.08\ \mu\text{m}$  were compression molded out

of PMMA powder. It is reported that the radius of curvature and the sag height deviated from the replication master less than 0.8  $\mu\text{m}$  and 0.2  $\mu\text{m}$ . The measured  $R_q$  was 3.98 nm.

### 4.2.3 Injection-Compression Molding

Injection-compression molding (ICM) refers to the combination of microinjection molding and compression molding. ICM is a variant of IM and exploits the advantages of press-molding [43]. The full ICM process is shown in Figure 4-6. In ICM, the plasticized material is firstly injected into the cavity as it is common in conventional IM. In difference to IM, the mold is not fully closed [29]. A small gap between the two mold halves, the so called “compression gap”, is held open providing the necessary stroke length for an additional compression sequence [64], [65]. When the mold is fully closed, the compressing step is performed, and the material is pressed into the microstructures of the mold. This step is an additional holding phase. As a result of the compression step not only shrinkage effects are prevented [43], but also residual stresses inside the material are distributed more uniform resulting in a more homogenous material density [64–66]. Optical characteristics like the transmission and birefringence are improved compared to molding techniques only based on the principle of material injection.

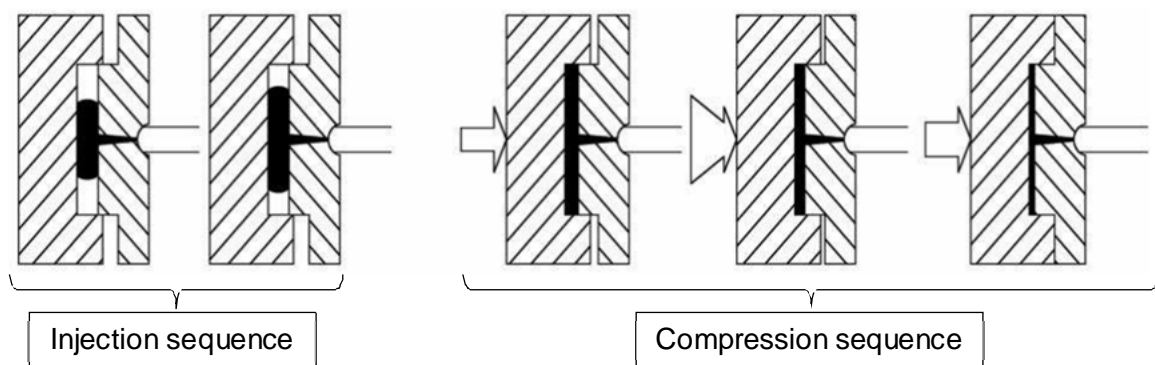


**Figure 4-6: Injection-compression molding process sequence [65]**

Whenever parts with low aspect ratios and with press-molded part quality are needed in high quantities, injection-compression molding is the suitable technique. Disadvantageous is the more complex tool design and process due to additional process parameters like gap stroke, compression speed, starting time or the applied force. The correlations between these parameters were examined in various publications and summarized comparatively in [64]. Finally, mechanical post-processing to remove the sprue must be carried out. Injection-compression process

was obtained very recently by Hahn-Schickard. A MLA containing convex-spherical 12000 ML on an area of 13 x 15 mm was injection-compression molded very recently [66]. Each lenslet was of a  $R_C$  of 1 mm and of a sag height  $h$  of 4  $\mu\text{m}$ . The ICM tool was ultraprecision milled and showed a surface roughness  $R_a = 4$  nm of a single lens and a PV form error of 39.5 nm from the specified  $R_C = 1$  mm. In result, a polymer ML with a  $R_a = 6$  nm and a PV form error of 80 nm were replicated from the mold structure.



## 5 Compression Molding

Compression molding and hot embossing were introduced briefly in the previous chapter. As the focus of this study is on press-molding experiments, the compression molding process and the needed equipment is further elaborated in the following starting with an own definition.

### 5.1 Compression Molding Process

Despite the differences between compression molding and hot embossing, the comparison of both terms in chapter 4.2.2 showed that there is no clear definition of the compression molding process in academia. An initial description was given based on the standard ISO 472, but even this definition does not provide a sufficient description of the individual process steps and their parameters. For this reason, compression molding is defined in this study separately as follows.

*Compression molding is a molding technique in which a substrate material is placed in the lower part of a mold, melted by heating the entire mold above the substrate material glass transition temperature, pressed into a form by closing the mold completely and then cooled before demolding.*

Before a molding process can be started, some pre-setting activities of the machine must be carried out. Firstly, the compression press is to be equipped with the mold tool, the gas supply needs to be provided and the parameters for each process step are to be set. Then, press-molding can be conducted following the schematic compression molding sequence shown in Figure 5-1. Characteristic processing parameters are molding temperature, molding pressure, molding time, cooling rate and demolding temperature. These parameters influence viscosity characteristics, the occurrence of plastic deformations and the replication quality.

The substrate material for the mold charge is inserted in a presetting step. Initial forms like powder [10], [60], granules [37], plates [59], [63] were used in different scientific investigations. Moreover, preformed blanks [67] and even liquid films can be inserted [28]. Powders and granules have a higher heat absorption capacity due to their enhanced surface. The operating time can be reduced as these forms show a

faster rise in temperature. In automated industry processes the material is often preheated to reduce the process time and to boost productivity. To obtain a repeatable uniformity and thus a high process reliability, the amount of fed material has to be weighed precisely [28].

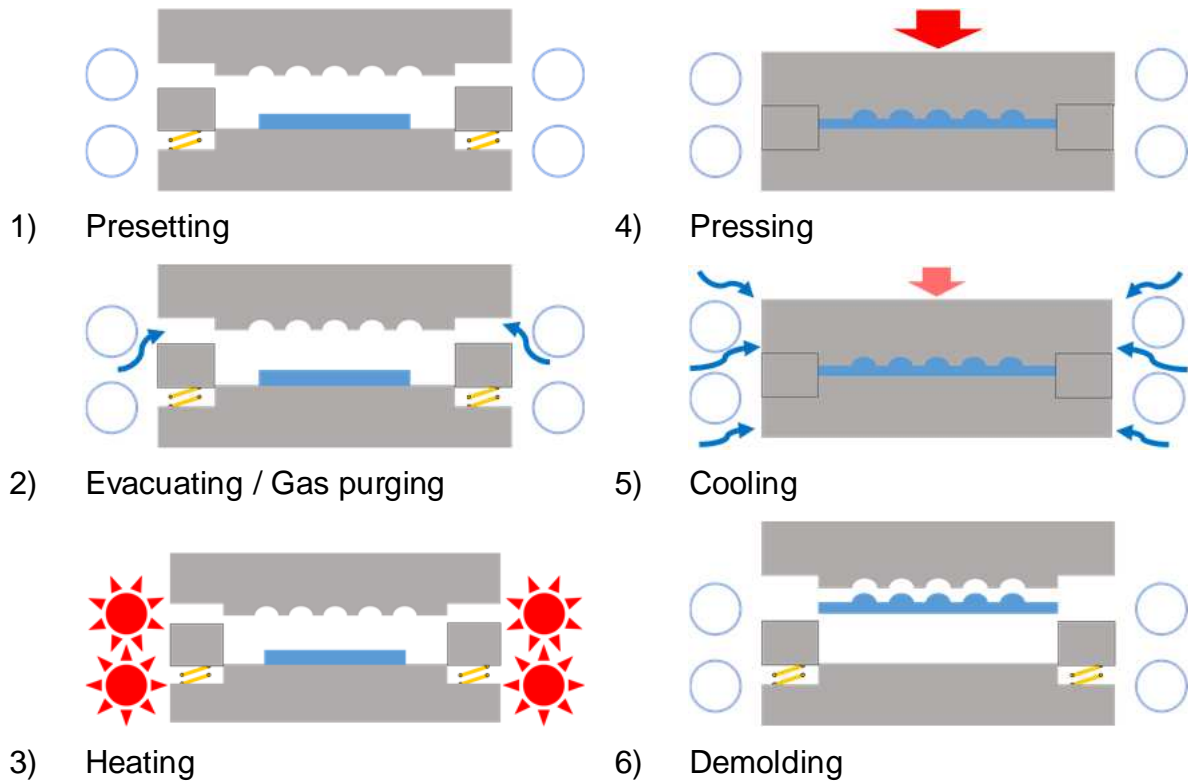


**Figure 5-1: Schematic of compression molding process**

Next, the mold halves are moved together but not fully closed. Depending on the compression press, the processing chamber is either evacuated or an inert atmosphere is created to prevent tool oxidation and accompanying abnormal tool wear. Secondly, gas trapping, diminishing the mechanical and optical part quality, inside the replicated part is prevented.

During heating, the substrate material is brought to or above the glass transition temperature by the heat transfer from the mold. The material softens and is no longer dimensionally stable. With raised temperature  $T$  the viscosity of the material is increased and thus the fluidity improved [10]. On the other side, the decomposition temperature of the plastic must be factored in.

When the optimum temperature is reached, the upper mold is descended to fully close the cavity and the compression force  $P$  is applied. The compression force must be high enough to press the viscous polymer into the micro structures. Inherent stresses are reduced by the applied pressure on the material. However, too high compression pressure can lead to material defects like bursts due to too high compressive stress inside the material as occurred in [10] and shown in Figure 5-2 on the left. Additionally, the mold can be damaged by cracking, especially when brittle materials are used as mold materials [63].

After molding, the entire mold with the therein enclosed part is cooled down below  $T_g$  to cure the material. The cooling is normally performed by supplying a continuous gas stream into the gas chamber. The compression pressure is kept or reduced in the cooling phase. During cooling, the plastic is subjected to shrinkage. The cooling rate must be observed, as too fast cooling rates result in a poor material homogeneity. In addition, if the compression pressure is too low, undesirable defects due to excessive shrinkage occur as shown on the right in Figure 5-2.

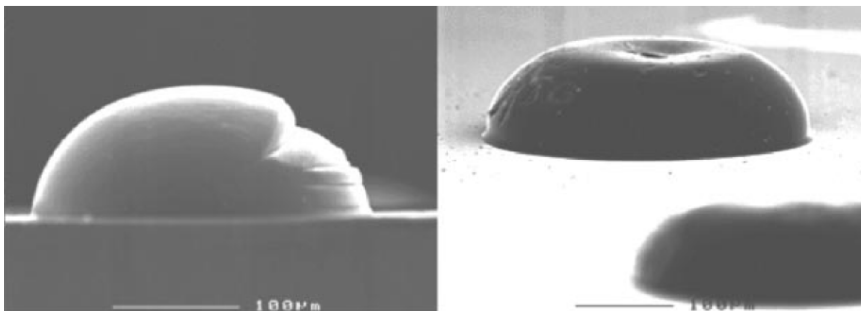


**Figure 5-2: Microlens defects; left: material burst caused by overpressure during the molding and cooling step; right: shrinkage defect in lens center [10]**

The demolding of the components is the most crucial step [29]. The compression pressure is set down to zero, the mold is opened, and the molded part is extracted. Also, in this step the process temperature needs to be chosen carefully. Non-reversible deformation can occur due to the material softness if the part temperature is too close to  $T_g$ . In [37], demolding of HDPE was performed at 80 °C. In [5] and [35] the demolding temperature for PMMA was between 40 °C and 50 °C, whereas Li et. al demolded PMMA at room temperature [68]. Press-molded polycarbonate MLA were demolded at room temperature (26 °C) and occasionally at a temperature of 60°C, too [63]. At 60°C,

the replicated PC MLA tends to stick at the mold micro structure which made demolding difficult to obtain and risky regarding damages of the lens surfaces. One can conclude that the optimum demolding temperature must be determined like the other process parameters for each microstructure, mold and charge material. In industry applications the maximum possible demolding temperature is preferred as cycling times can be shortened.

## **5.2 Compression Presses**

Press-molding is conducted on compression presses in which the necessary pressure is vertically applied on the substrate material to force it into the mold micro structure. Compression presses which can press both glass and polymer are often used. The main elements of a compression press are the compression unit, the heating and cooling system and the gas transfer system [27].

The compression unit carries all the components for the compression step. It is generally built of two vertically aligned chucks on which the mold halves can be clamped. One of the chucks is firmly fixed in the machine while the other one, usually the lower chuck, can be moved up and down towards the other. The movement is actuated by a hydraulic cylinder. The female or cavity mold part is usually fixated on the lower chuck. During mold closing (Figure 5-1, process step 4)), the upper half dips into the lower one. A process chamber isolates the mold from the outside. The gas transfer system is used to create a vacuum inside the process chamber using a vacuum pump. Alternatively, the process chamber can be floated with inert gas, like nitrogen or argon. In this case, a gas supply next to the compression press has to be provided. The heat required to heat the mold and plastic material is supplied by an infrared heating system. To cool down the mold, a gas is either supplied into the chamber again [37] or an external fan is used [35]. All process parameters are measured by sensors and software controlled [27].

Depending on the application, it can be distinguished between semiautomatic or fully automatic compression presses [28]. Semiautomatic molds are used for laboratory applications, in which the press follows a programmed cycle. The material loading and the part demolding is done manually by the operator. In industrial production, all

pressing steps including the material handling are fully automatized [28], [29], [69]. Manually operated compression presses for laboratory applications were additionally mentioned in [28], but publications in which these presses were used were not found during the literature review. This can be explained by an expectedly unstable process and today's safety standards, which are presumably not fulfilled by those setups.

### **5.3 Optical Mold Fabrication**

In difference to macro molding techniques, a separation of the tool from the micro structured mold insert is established in micromolding [29], [70]. The tool parts are mounted on chucks of the press machine, enclose the substrate material and transfer the heat energy to the substrate material during heating or away during cooling. The mold insert contains the microstructure to be replicated into the substrate material. High effort is put into the fabrication of the mold insert to achieve precise geometric dimensions, low tolerances and low surface roughness. Any deviations of the lens-negative from the optical design lead to changes in the optical properties of the compression-molded lenses. Inaccuracies and form deviations of the micro structure cannot be compensated in the later replication process. A low surface roughness is desired to avoid friction of the material during the compression and especially during demolding. A low wear and tear of the micro structures over higher cycling times and process parameters is important for quality and economic reasons. This can be prevented by using hard, ductile materials and a proper micro structural design. However, hard materials are more difficult to machine due to their brittleness. Usual materials for optical molds are aluminum [55], [71], brass [71], [72] or nickel-phosphor coated materials [73]. A wide range of recent optical mold fabrication methods were detailed and compared by M. Roeder et. al [54], summarized in Figure 5-3. UPM methods are often used for mold machining due to their outstanding advantages in terms of precision as described in chapter 4.1.3. However, their limitation on non-ferrous metals as mold materials must be outlined at this point. Although hardened steel is widely used in all fields of engineering, it cannot be diamond cut. Excessive tool wear based on chemical phenomena occur at the diamond tool and the workpiece.

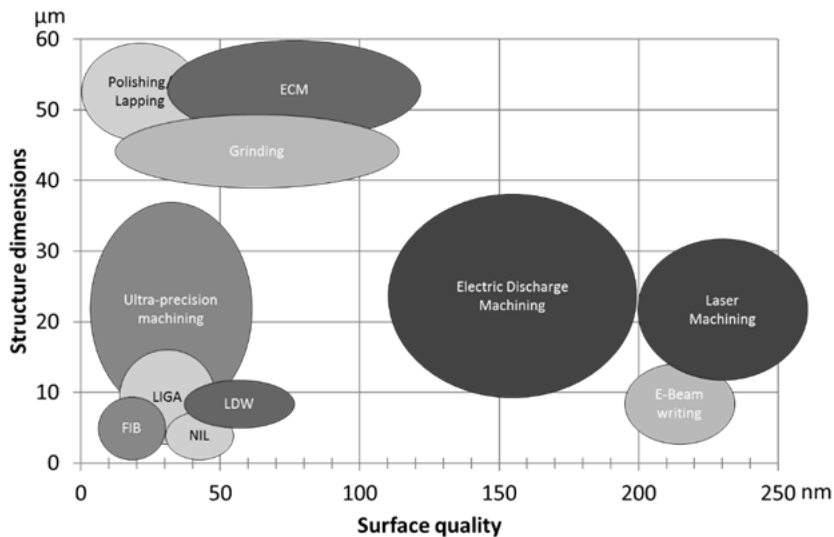


**Figure 5-3: Comparison of different manufacturing techniques for optical molds [54]**

In summary, it can be said that the choice of the manufacturing technology for an optical mold is dependent on several aspects. For each mold, the manufacturing process should be chosen considering the application specific part quality in terms of dimensions and surface quality, the availability of different technologies in a laboratory or company and also economic aspects.

## 5.4 Advantages and Disadvantages of Compression Molding

Today, injection molding has been established for most applications in microtechnology and dominates over compression molding especially because of the fast and efficient production. Nevertheless, compression molding shows some superiority in terms of part quality and process suitability for certain applications.

The great advantage of compression molding is that parts can be easily produced by using preformed blanks which are close to the final part shape [41]. In terms of molded part dimensions, more complex features with aspect ratios >10 and thinner part thicknesses are achievable [43], [59]. In compression molding, the flow paths are generally short. The friction forces between the mold and the lowered material are comparatively low as the material is only heated by the mold but not by an additional heating unit as in injection molding [29]. Due to the lowered friction, the residual stress inside the material is reduced. Compression molding shows therefore a higher suitability for the fabrication of high-quality optical parts [35]. Also, the process

reproducibility is very high. As described in chapter 5.2, the mechanical setup of compression presses is also less complex compared to injection molding machines. Especially the tooling cost can be reduced as the press-molding tools are less complex [41] as there is no sprue and runner system like in injection molding. In this regard, extra material for sprues and runners is firstly not needed and the normally mechanical removal of the residual sprues is not necessary [29].

Disadvantage to injection molding processes is the needed heating of the entire mold to melt the charge material as this results in very long cycling times, especially when the mold has to be cooled down again on low temperatures for demolding. In addition, the mold is charged in an extra process step before the process can be started as there is no continuous material supply. This increases the production costs dramatically, making compression molding less suitable for mass fabrication. On the other side, press-molding is advantageous in laboratory applications, prototyping or low-scale series production [29], [43].

In summary, press-molding is a suitable molding technique when parts of high aspect ratios or in optical quality have to be produced. However, compression molding is time consuming and thus, of higher process costs. Non-complex parts with low aspect ratios can be fabricated more easily by means of injection molding. To combine the advantages of both processes, ICM was introduced in chapter 4.2.3, which is more suitable to produce optical parts in press-molding quality.

## 6 Design of Experiments

The experimental part of this study included

- 1) design and machining of a compression molding tool including the design of the microlens array
- 2) a selection of materials to be pressed
- 3) the press-molding experiments
- 4) and the characterization of the molded parts

The entire setup and the boundaries for the press-molding and characterization of the polymer MLA in this study are described in this chapter.

### 6.1 Design and Fabrication of a Compression Molding Tool

Before starting the press-molding experiments, a tool was designed and machined. For the laboratory experiments, the usual separation between tool parts and mold insert as described in chapter 5.3 was considered not to be necessary and the microlens array was machined directly into the mold.

#### 6.1.1 Mold and Microlens Array Design

A first dimensional design for the mold was provided at the beginning of this study by the UP micro forming group at Yan Laboratory. It is shown in the appendix (1) - (4). The design was based on the fitted dimension of the press-molding machine (chapter 6.2) and molds from previous studies. Crucial manufacturing tolerances, which ensure the later function of the mold, were added as it can be seen from the technical drawings attached in the appendix (5) - (8). A tolerance stack analysis according to [74] in order to calculate the axial guidance length between the Imp 1 and Imp 2 and a tolerance stack analysis for the height of the plunger of the upper mold part was carried out and attached to the appendix (10) and (11). The tool design is shown in Figure 6-1. The mold consists of one *upper mold part*, the *lower mold parts 1 – 3* (Imp 1 – 3), assembly screws and four compression springs (appendix (9)). A simplification of the optical mold was achieved by cutting the MLA directly into the upper mold. The number of



parts was therefore reduced, a tolerance analysis between tool and mold insert was not required and the production time could be shortened. CuZn30 brass material (Japanese material no. C2600) was chosen as mold material.

The upper mold part and the lower mold part 1 were later clamped to the compression press with the upper mold being the fixed part inside the machine. The flat MLA side is formed by the Imp 2 during press-molding. It is inserted into the Imp 3 and mounted by one M4-cylinder head screw. To achieve a good surface quality on the pressed part and an easy demolding, Imp 2 needs to have a low surface roughness. The lower mold part 1 is loaded on four compression springs (part number DC519 by Accurate Inc., Japan) and axially guided by Imp 2 and two M4-low head shoulder screws guided by engineering fits in Imp 3.

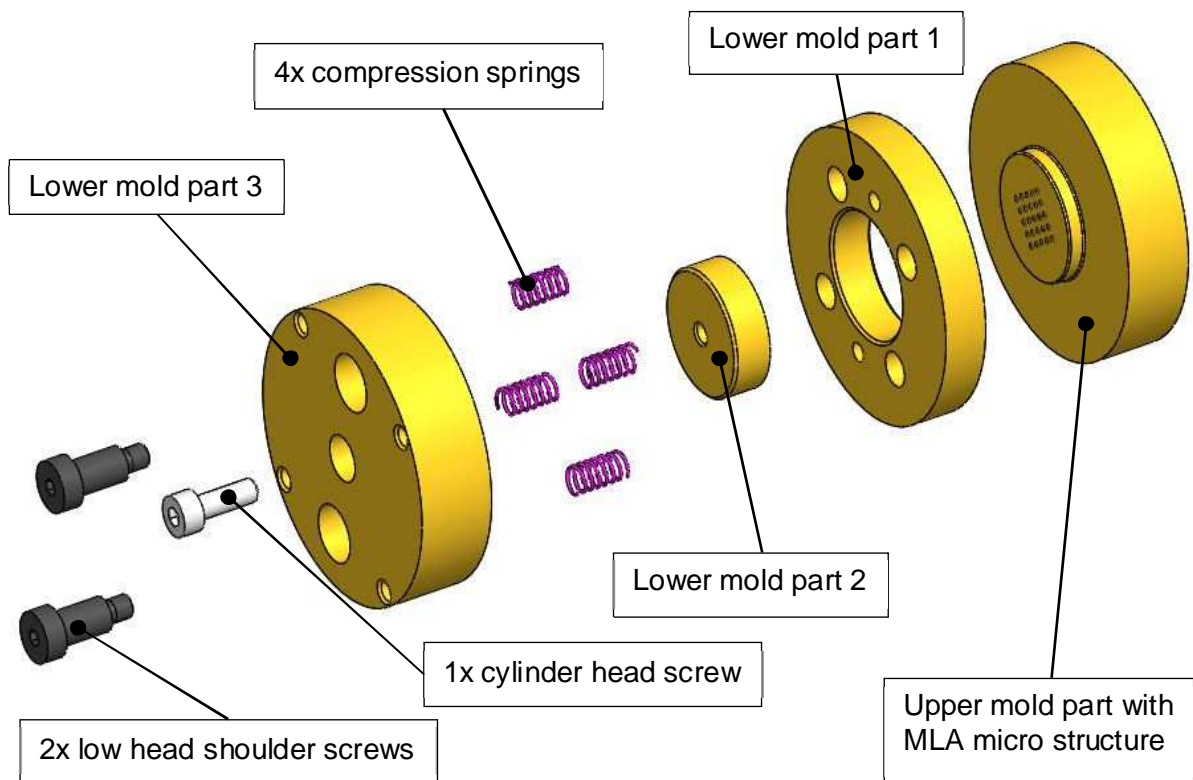


**Figure 6-1: Compression molding tool used in this study (CAD exploded drawing)**

The mold cavity is radially enclosed by Imp 1. The data sheet of the compression springs is attached in the appendix. When closing the mold, Imp 1 is pressed downwards through the upper mold against the spring loads to the stop by the Imp 3. When the mold is opened, Imp 1 is discharged to its initial position by decompression

of the springs. For the temperature sensors, a small hole with a diameter  $\varnothing = 3$  mm and a depth of 6 mm was foreseen in both the upper mold and the lower mold part 3.

The MLA design should be kept simple as the focus of this research lies on the compression molding experiments. Therefore, the mold fabrication process and the latter characterization of the press-molded MLA was less complex and error possibilities caused by mold fabrication or measurement inaccuracies were reduced. The difference between refractive and diffractive lens shapes is already described in chapter 2.1. Due to their more complex shape, DOE were not taken into consideration for the sample MLA design even though the selected material HDPE is generally used for molded DoE in IR applications. The optical design was done according to the common design process for a plano-convex refractive microlens array described in [7] and [24]. The used symbols are according to the ISO 14880 [3]. The cross-sectional profile of this lens shape is described according to [75] by the following formula in which  $K$  represents the conic constant. The conic constant describes the curvature of a lens.

$$h(a) = \frac{1}{R_c} * \frac{a^2}{1 + \sqrt{1 - (K + 1) \frac{a^2}{R_c^2}}} + \text{higher order terms} \quad (6-1)$$

As a simple lens design was desired, the spherical form ( $K = 0$ ) is chosen, so that the higher-order terms were not regarded. The lens diameter was given with  $2a = 1$  mm by the topic. The radius of curvature was set to  $R_c = 5.5$  mm. With these given values, the sag height was calculated to  $h = 22.774$   $\mu\text{m}$ .

$$h = \frac{1}{5.5} * \frac{0.5^2}{1 + \sqrt{1 - (0 + 1) \frac{0.5^2}{5.5^2}}} = 0.022774 \text{ mm} = 22.774 \mu\text{m} \quad (6-2)$$

The lenses were rectangular arrayed in 5 x 5 arrangement with a pitch  $P_{x,y} = 2$  mm. With the pitch  $P_{x,y} >$  lens radius  $a$ , defined boundaries of the lenslets due to the small gaps between two lenslets were generated. This packaging density also facilitated the measurement and evaluation of the lens dimensions. The microlenses were numerated according to Figure 6-2 from 01 - 25 in order to facilitate their location on the substrate and the comparison between individual lenses.

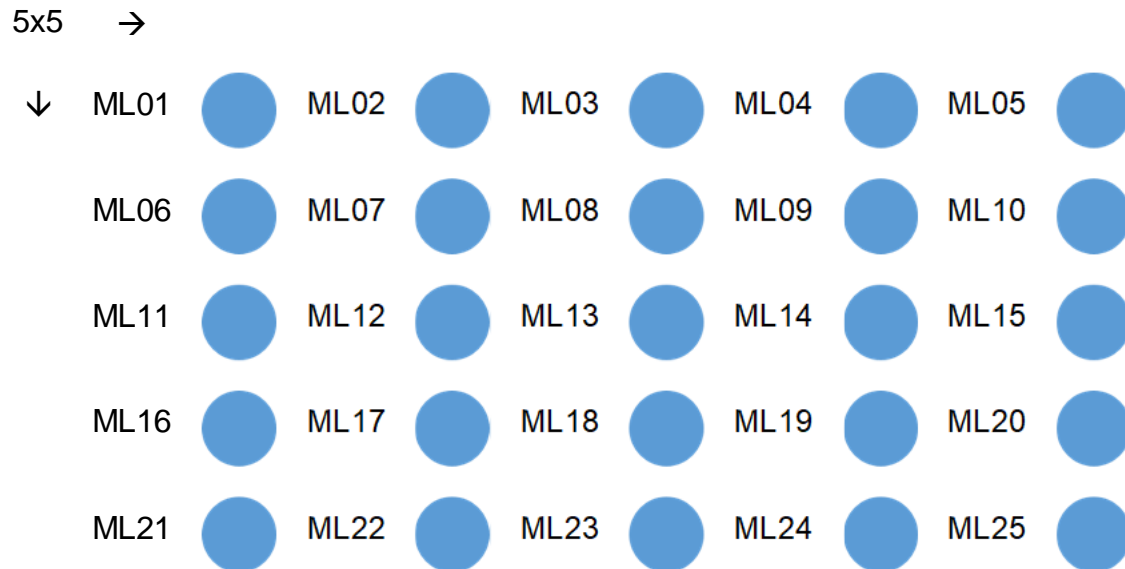


**Figure 6-2: Numeration of microlenses on a substrate in this study**

### 6.1.2 Mold Fabrication

The mold parts were produced in three steps. All mold parts were firstly fabricated by rough machine operations. The machining was carried by the craftsmen of the KEIO manufacturing center. After rough machining, all parts were delivered to the Yan laboratory facility and cleaned ultrasonically in ethyl alcohol (99.5 %) for 10 minutes. The mold parts can be seen in Figure 6-3.



**Figure 6-3: Mold parts (upper mold part already with diamond cut microlens array)**

Further processing was performed on the upper mold and the lower mold part 2. Part areas crucial both for the molding process and the part quality were polished down to achieve a smooth surface. The polishing was carried out on a semi-automatic polishing machine (Dial wrap ML-150P, Maruto Instrument Co. Ltd., Japan) equipped with a swing type drive arm. A soft polishing pad was used for the finish cut on which

diamond polishing powder with grain sizes of 0 - 0.5  $\mu\text{m}$  and a grit size of 60000 was continuously dispensed.

Single-point diamond cutting was used to cut the MLA into the upper mold. Ultra-precision cutting is a main research field of the Yan Laboratory, which is why the MLA cutting was carried out in the context of the research from Yan Laboratory. The entire experimental setup is shown in Figure 6-4. For the single-point diamond cutting process, a four axes CNC ultra-precision lathe (Nanoform X, AMETEK Precitech Inc., Keene, NH, USA) was used. This machine is equipped with an aerostatic high-speed spindle (C-axis). The maximum spindle speed is 10.000 rpm with a position accuracy of  $\pm 1$  arcseconds. The driving units (AC linear motors) for the motions in the x- and z-axis are placed on linear hydrostatic slideways. The position feedback resolution is 8  $\mu\text{m}$ . The workpiece was attached to the spindle by a vacuum chuck. The cutting tool was mounted on the tool post which is driven in STS configuration. Lubrication oil was sprayed on the workpiece during the entire cutting process.

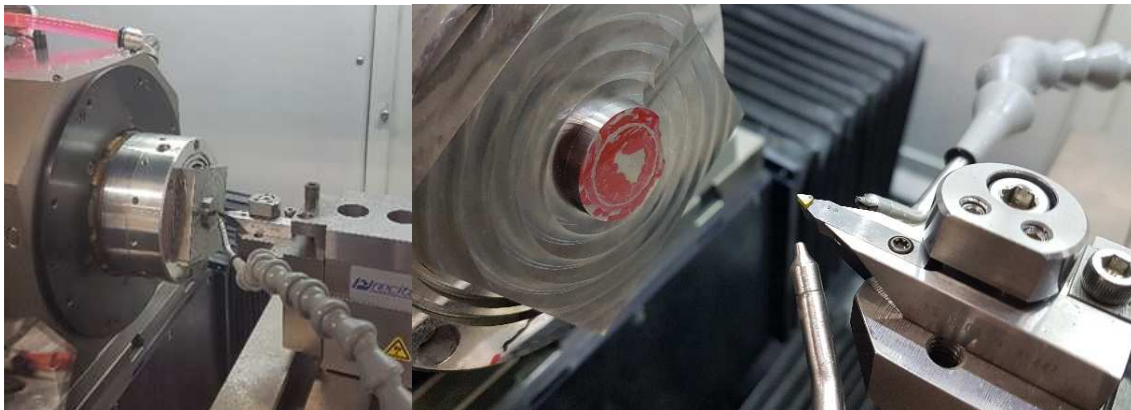


**Figure 6-4: Ultra-precision diamond cutting of the microlens array**

A diamond tool was used to cut the MLA into the brass material. The applied cutting and tool parameters are in Table 6-1. All cutting sequences were performed at a room temperature of 23  $^{\circ}\text{C}$ . After the ultra-precision machining, the mold parts were cleaned again in the ultrasonic bath in ethyl alcohol (99.5 %) for 10 minutes.

Tool material / tool radius [mm]	Depth of cut [ $\mu\text{m}$ ]	Feed rate $f$ [ $\mu/\text{min}^{-1}$ ]	Spindle speed [rpm]
Diamond / 0.5	10	20	20
	10	20	20
	4	10	20
	1	5	20

**Table 6-1: Process parameters and tool geometry for the ML diamond cutting of mold2**

Based on the tolerances of the mold parts, the minimum theoretical cavity volume was  $V_{\text{cavity,theo}} = 380.35 \text{ mm}^3$ . However, due to the polishing and the facing before the microlens diamond cutting, the cavity volume was increased. In order to determine the exact needed amount of material for one press-molding cycle, the cavity volume had to be determined experimentally in a first test series by using granule material.

## 6.2 Press Molding Machine at Yan Laboratory

A Toshiba GMP211 compression press (Toshiba Machine Co. Ltd., Japan) (Figure 6-5) was used to carry out the compression molding experiments. This machine was originally designed for glass molding, but also polymer-based materials can be pressed. The technical setup of the machine is shown in Figure 6-6. Each mold halve was fixed on a mounting plate which was then mounted into the processing chamber. The upper mold half remains fixed during press-molding. The lower mold, which is charged with the material to be pressed in the later molding process, is motioned by an AC servomotor in the Z-axis towards the upper mold for molding and away for demolding. The mold position is measured by an encoder with a measurement resolution of  $0.1 \mu\text{m}$ . The compression press is not equipped with an evacuation system. Instead, each press-molding cycle is started with a purging sequence in which argon gas is flooded into the processing chamber to avoid oxidation of the mold caused by the high temperatures. A silica glass tube encloses the argon gas inside the processing chamber. The argon gas is supplied from gas bottles with a volume of  $7 \text{ m}^3$ . The silica glass tube is surround by an IR lamp heating system which radiates heat energy towards the mold. As the compression press was designed for glass molding,

temperature up to 800 °C can be reached. The temperature of the upper and lower mold is sensed by a thermocouple with a  $\pm 1$  °C accuracy. The temperature probes of the thermocouples were inserted into the  $\varnothing = 3$  mm-holes inside the Imp1 and the upper mold part. Once the adjusted heating temperature is sensed by the thermocouples, the press-molding step is initialized. A force gauge (load cell type) placed beneath the lower axis senses the pressing load with a resolution of 0.1 N. The applicable pressing force ranges from 0.2 kN to 20 kN with a resolution of 0.98 N. After pressing, the mold is cooled down to the demolding temperature by injecting argon gas again. When the demolding temperature is reached, the mold is opened. The default demolding temperature is 80 °C. For this temperature it can be more or less said that three samples can be compression molded with one argon gas bottle. This is a limiting factor for the variation of the demolding temperature.



**Figure 6-5: Compression molding press GMP211 (Toshiba Machine Corp., Japan)**

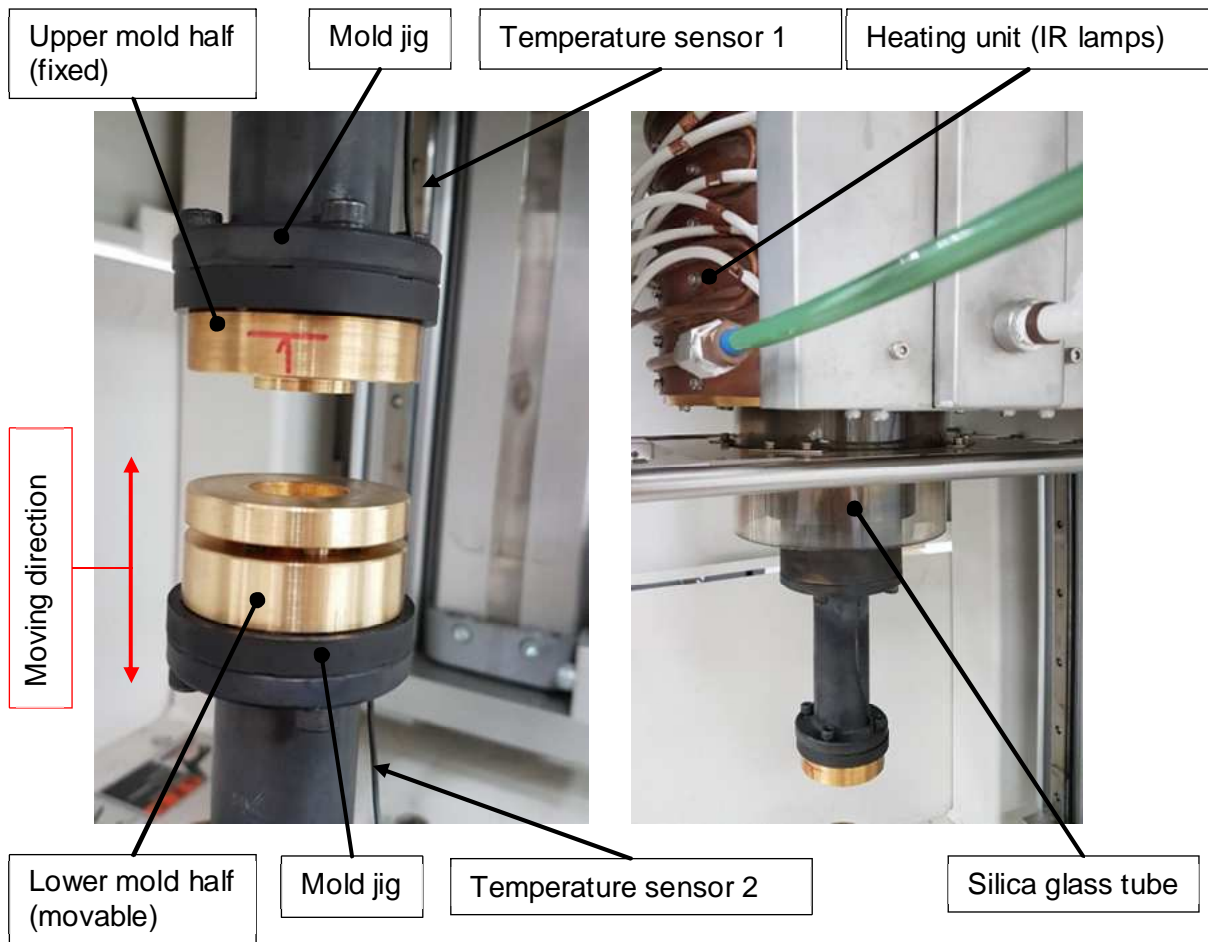


**Figure 6-6: Machine setup for compression molding process**

The heating temperature is not controlled in a closed-loop by the machine. After initializing a press-molding sequence, the amount of thermal energy supplied to the system must be raised manually in percentage increments for the upper and lower mold until the set heating temperature is measured by the temperature sensors. As soon as the heating temperature is reached, the heat input is set down to 0 %. The setting for the upper and lower tool is done in each case via a display. Figure 6-7 shows the adjustment of the thermal energy in percent exemplarily for a heating temperature of 128 °C.

Six different types of parameter with a total of 19 values can be set on the Toshiba GMP211 compression molding machine. Dependent on the pressing step, the AC servomotor position  $Z$  [mm], the cylinder motion speed  $V$  [mm/min], the compression force  $P$  [kN], different temperatures  $T$  [°C] and different time durations  $t$  [s] can be adjusted individually. Figure 6-8 shows the parameter to be

adjusted for one compression molding sequence at the GMP211 compression press. A full description of each parameter is given in the experiment documentation sheet template attached in the appendix (15). In this study, the values for temperature, compression force and the time were varied while the cylinder motion speed and the temperature gradients were fixed. The lower mold position was set to  $Z = 48$  mm. This position is kept during evacuating and heating, before the mold is moved towards the upper mold and fully closed to conduct the pressing.



Figure 6-7: Manual adjustment of the amount of thermal energy supplied by the IR lamps; left: display for lower mold; right: display for upper mold

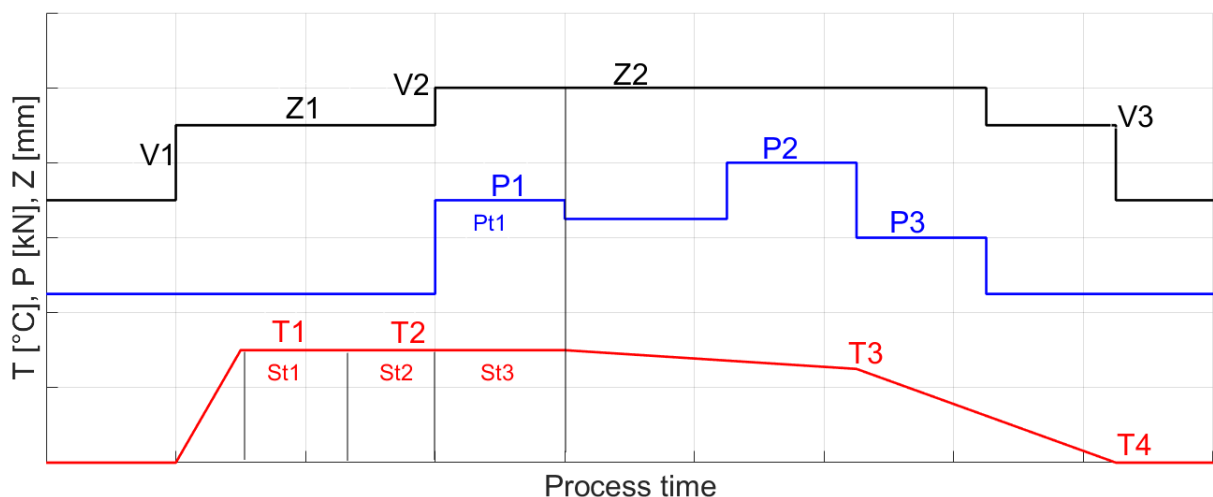


Figure 6-8: Toshiba GMP211 compression molding process



### 6.3 Selection of Optical Polymers

Three different plastic materials were selected for the compression molding experiments. Polycarbonate (PC) and polymethylmethacrylate (PMMA) were chosen as optical polymers. As third material high-density polyethylene (HDPE) was selected. The properties of the selected polymers are presented in the previous chapter 3.2. The initial conditions of the materials as well as the chosen parameters for the experiments described. Since there was no personal experience with the three materials and their press-molding behavior at the beginning of this study, the publications [55] and [63] were used as reference for HDPE and PC.

Four test series were conducted in this study. To distinguish between the test series, each sample is described in the following by a number for the conducted test series containing a number for the molded sample within the test series. The naming convention is described by Figure 6-9. The last two digits describe the microlens number on the array. If only a sample within a test series is described, the last two digits are replaced by xx. This naming convention is followed throughout this study.

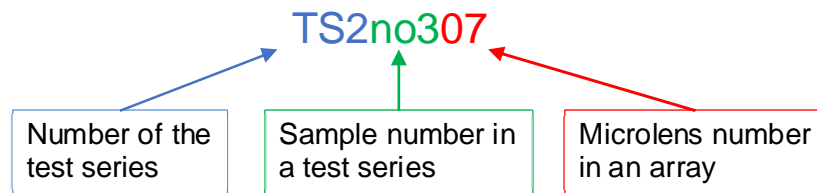


**Figure 6-9: Naming convention in this study to describe the test series, a sample within a test series or a ML within an array**

#### 6.3.1 High-Density Polyethylene

High-density polyethylene was used in previous researches conducted at Yan Laboratory to press Si-HDPE hybrid lenses [55]. Hence, first reference values for the heating temperature and the pressing force were available. The used HDPE material is LINKLON HM600A (Mitsubishi Chemical Holdings Corporation) and was supplied in a cylindrical granule form. The grain size is  $\varnothing$  3 mm x 3.5 mm<sup>2</sup>. Process relevant properties are given in Table 6-2.

Material properties [unit]	Value
Density [g/cm <sup>3</sup> ]	0.955
Glass transition temperature [°C]	125
Decomposition temperature [°C]	133
Refractive Index	1.5

**Table 6-2: Material properties of LINKLON HM600A [37]**

A first trial and error test series with the HDPE was chosen for first machine operations and to determine the exact mold cavity volume based on the  $V_{cavity,theo} = 380.35 \text{ mm}^3$  and the density of the LINKLON HM600A. With these two values, the theoretical charge mass is calculated in equation (6-3).

$$m_{charge,theo} = V_{cavity,theo} * \rho_{HDPE} = 0.955 \frac{g}{cm^3} * 0.38035 \text{ cm}^3 = 0.363 \text{ g} \quad (6-3)$$

Starting with the calculated charge mass  $m_{charge,theo}$ , the amount of material was continuously increased by adding HDPE grains with every process sequence. The used process parameters are given in Table 6-3. The temperature was kept stable at 131 °C as this temperature was found as optimum temperature in previous experiments at Yan Laboratory [55]. The compression force was set to 1.0 kN. The process times were firstly set to Pt = 350 s and St3 = 20 s but were prolonged during carrying out the experiment. In addition, the process times St1 and St2 were set during this first test series. The machine opened the mold at a demolding temperature of 80 °C and the parts were removed at 60 °C. The experimental results for test series 1 are described in detail in chapter 7.2.

Sample no.	Temperature [°C]				Compression force [kN]			Process times [s]			
	T1	T2	T3	T4	P1	P2	P3	Pt1	St1	St2	St3
<b>TS1no1xx</b>	131	131	131	80	1.0	1.0	1.0	350	0	0	20
<b>TS1no2xx</b>	131	131	131	80	1.0	1.0	1.0	350	0	0	20

Sample no.	Temperature [°C]				Compression force [kN]			Process times [s]			
	T1	T2	T3	T4	P1	P2	P3	Pt1	St1	St2	St3
TS1no3xx	131	131	131	80	1.0	1.0	1.0	410	10	10	10
TS1no4xx	131	131	131	80	1.0	1.0	1.0	410	20	20	20
TS1no5xx	131	131	131	80	1.0	1.0	1.0	410	20	20	20
TS1no6xx	131	131	131	80	1.0	1.0	1.0	410	30	20	20

**Table 6-3: Press molding parameters for test series 1 - HDPE**

Six samples were molded in test series 3. The process parameters of test series 3 are given in Table 6-4. For the first three samples the heating temperatures were varied in a range between 125 °C and 131 °C in order to find out the best heating temperature. The heating temperature was then kept stable again at 131 °C and the compression force was varied between 0.8 kN and 1.4 kN. The demolding temperature was set for all samples to the default demolding temperature of 80 °C and for which good experiences were made for HDPE in previous studies.

Sample no.	Temperature [°C]				Compression force [kN]			Process times [s]			
	T1	T2	T3	T4	P1	P2	P3	Pt1	St1	St2	St3
TS3no1xx	125	125	125	80	1.0	1.0	1.0	410	60	60	20
TS3no2xx	128	128	128	80	1.0	1.0	1.0	410	60	60	20
TS3no3xx	131	131	131	80	1.0	1.0	1.0	410	60	60	20
TS3no4xx	131	131	131	80	0.8	0.8	0.8	410	60	60	20
TS3no5xx	131	131	131	80	1.2	1.2	1.2	410	60	60	20
TS3no6xx	131	131	131	80	1.4	1.4	1.4	410	60	60	20

**Table 6-4: Press molding parameters for test series 3 - HDPE**

### 6.3.2 Polycarbonate

The polycarbonate material and the raw form was specified by the research topic. The PC was supplied under the supplier by C.I. TAKIRON Corporation in sheet form with a size of 10 x 10 mm<sup>2</sup> and a thickness of  $t = 2$  mm. The most important molding properties of the chosen PC are given in Table 6-5. The Japanese data sheet with an English translation is attached to the appendix (12).

Material properties [unit]	Value
Density [g/cm <sup>3</sup> ]	1.2
Glass transition temperature [°C]	150
Decomposition temperature [°C]	240
Linear expansion coefficient [°C <sup>-1</sup> ]	$6.5 \times 10^{-5}$
Refractive Index	1.587
Transmission [%]	min. 87 ( $t = 3$ mm)

**Table 6-5: Material properties of polycarbonate by C.I. TAKIRON Corporation [76]**

Before test series 2 was conducted, the polycarbonate had to be cut into cylindrical sheets of a defined diameter. The material thickness  $t = 2$  mm was given by the raw material dimensions. The experimentally determined HDPE mass in test series 1 was between 0.442 g and 0.456 g. The mean value of  $m_{HDPE} = 0.449$  g is therefore used to calculate the diameter of the polycarbonate sheets in the following

$$V_{cavity} = \frac{m_{HDPE}}{\rho_{HDPE}} = \frac{0.449 \text{ g}}{0.955 \frac{\text{g}}{\text{cm}^3}} = 0.470157 \text{ cm}^3 = 470.157 \text{ mm}^3 \quad (6-4)$$

$$V_{PC,sheet} = \frac{\pi}{4} d_{PC,sheet}^2 * t_{PC} \quad (6-5)$$

$$d_{PC,sheet} = \sqrt{\frac{4 * V_{PC,sheet}}{\pi * t_{PC}}} = \sqrt{\frac{4 * 470.157 \text{ mm}^3}{\pi * 2 \text{ mm}}} = 17.301 \text{ mm} \quad (6-6)$$

From equation (6-6) it can be seen that cylindrical sheets with a diameter of 17.301 mm were needed to carry out the press-molding experiments with polycarbonate. The sample sheets of the calculated diameter were milled in the KEIO manufacturing center as shown in Figure 6-10. The milling was performed on a Makino KE-55 CNC-machine (Makino Inc., Japan). The calculated diameter and a roundness tolerance of 0.050 mm was achieved. After milling, the samples were ultrasonically cleaned in purified water and weighed. The weight of the milled samples varied between 0.548 g and 0.553 g.



**Figure 6-10: Preparation of cylindrical polycarbonate sheets; left: milling of samples; right: Diameter measurement using a micrometer**

Six samples were molded in test series 2. The process parameters of test series 2 are given in Table 6-6. Like for the HDPE press-molding experiments, the heating temperature was varied for the first three samples applying the compression force steadily at 1.0 kN. In [63], the best heating temperature for embossing PC was found to be 182 °C. This temperature was used as reference value for sample TS2no2xx. In the following, the heating temperature was then kept at 182 °C and the compression force was varied between 0.8 kN and 1.4 kN. The demolding temperature was set for all samples to the default demolding temperature of 80 °C.

Sample no.	Temperature [°C]				Compression force [kN]			Process times [s]			
	T1	T2	T3	T4	P1	P2	P3	Pt1	St1	St2	St3
TS2no1xx	175	175	175	80	1.0	1.0	1.0	410	60	60	20
TS2no2xx	182	182	182	80	1.0	1.0	1.0	410	60	60	20

Sample no.	Temperature [°C]				Compression force [kN]			Process times [s]			
	T1	T2	T3	T4	P1	P2	P3	Pt1	St1	St2	St3
TS2no3xx	189	189	189	80	1.0	1.0	1.0	410	60	60	20
TS2no4xx	182	182	182	80	0.8	0.8	0.8	410	60	60	20
TS2no5xx	182	182	182	80	1.2	1.2	1.2	410	60	60	20
TS2no6xx	182	182	182	80	1.4	1.4	1.4	410	60	60	20

**Table 6-6: Press molding parameters for test series 2 – Polycarbonate**

### 6.3.3 PMMA

PMMA was chosen as third test material for the press-molding experiments. Extruded PMMA sheets of a size of 10 x 10 mm<sup>2</sup> and a thickness of  $t = 2$  mm were supplied under the brand name COMOGLAS™ by Kuraray Co., Ltd. The most important molding properties of COMOGLAS™ are given in Table 6-7. The Japanese data sheet with an English translation is attached to the appendix.

Material properties [unit]	Value
Density [g/cm <sup>3</sup> ]	1.19
Glass transition temperature [°C]	110
Decomposition temperature [°C]	220
Linear expansion coefficient [°C <sup>-1</sup> ]	$7 \times 10^{-5}$
Refractive Index	1.49
Transmission [%]	93

**Table 6-7: Material properties of COMOGLAS™ [77–79]**

The cylindrical PMMA sheets had to be cut out of a supplied material as previously done for the polycarbonate. As PMMA can be laser cut, this process was chosen due to its ease of use and its very short process time. The cutting was performed on a laser

engraver Speedy 300 (Trotec Laser GmbH, Austria). The cutting parameters were predefined by the machine software for the type and thickness of the material. The diameter of the PMMA sheets was set to the same size as the polycarbonate sheets. However, the achieved diameter of the 20 samples was  $\varnothing = 17.214$  mm with a roundness of 0.100 mm. In addition, it was observed that the material was heated up by the laser's heat input into the working table. Thus, in all PMMA samples the honeycomb structure of the working table was found to be locally replicated with void formation around the marks. The laser cutting and a microscope image of the laser cut PMMA sheet is shown in Figure 6-11.



**Figure 6-11: Preparation of cylindrical PMMA sheets; left: laser cutting; right: image of marks and void formation caused by heat input of the laser machine on the substrate (100x-magnification)**

Six samples were molded in test series 4. The process parameters of test series 4 are given in Table 6-8. The heating temperature was varied for the first three samples applying the compression force steadily at 1.0 kN. The glass transition temperature of PMMA varies in a wider temperature range compared to HDPE and PC as it can be seen in Table 3-1. Since no paper in which a PMMA with the glass transition temperature of COMOGLAS™ was found during the paper review, the heating temperature was firstly varied between 130 °C, 140 ° and 150 °C. In the following, the heating temperature was then kept at 182 °C and the compression force was varied between 0.8 kN and 1.4 kN. The demolding temperature was set for all samples to the default demolding temperature of 80 °C.

Sample no.	Temperature [°C]				Compression force [kN]			Process times [s]			
	T1	T2	T3	T4	P1	P2	P3	Pt1	St1	St2	St3
<b>TS4no1xx</b>	130	130	130	80	1.0	1.0	1.0	410	60	60	20
<b>TS4no2xx</b>	140	140	140	80	1.0	1.0	1.0	410	60	60	20
<b>TS4no3xx</b>	150	150	150	80	1.0	1.0	1.0	410	60	60	20
<b>TS4no4xx</b>	140	140	140	80	0.8	0.8	0.8	410	60	60	20
<b>TS4no5xx</b>	140	140	140	80	1.2	1.2	1.2	410	60	60	20
<b>TS4no6xx</b>	140	140	140	80	1.4	1.4	1.4	410	60	60	20

**Table 6-8: Press molding parameters for test series 4 – PMMA**



## 6.4 Measuring Equipment

A full evaluation of the MLA fabrication process by means of compression molding can only be done, if all process relevant parameters and the dimensions of both the optical mold dimensions and the replicated lenses are known. In this study all ML properties were measured with contactless, optical measurement techniques. It must be mentioned that the measurement of transparent, micro structured objects is generally challenging to obtain with light-based measuring devices as the focus point is hard to spot [80]. An overview of the measured dimensions and the measuring machines is given in Table 6-9. A balance was used to weigh the amount of needed material for one compression molding sequence.

ML Properties	Dimension	Measuring machine
Geometrical	ML lens diameter	Scanning probe microscope OLYMPUS OLS4100
	Sag height based on cross-sectional lens profile	Optical non-contact profilometer MITAKA NH-3SP
	Surface roughness Ra, Rq	Scanning probe microscope OLYMPUS OLS4100 / Optical non-contact profilometer MITAKA MLP-3
	Form accuracy based on cross-sectional lens profile	Optical non-contact profilometer MITAKA NH-3SP

**Table 6-9: Measuring machines used to measure the mold and microlens arrays**

### 6.4.1 Balance SHIMADZU TW323N

A Shimadzu TW323N balance measures weight in a range from minimum 0.02 g up to maximum 320 g in steps of 0.001 g. It was deployed to determine the amount of material required for one press-molding sequence. Its accuracy is  $\pm 0.002$  g.

### 6.4.2 Scanning Probe Microscope OLYMPUS OLS4100

The Olympus OLS4100, shown in Figure 6-12, is a scanning probe microscope (SPM). It was used to measure the ML diameter  $2a$  and the surface roughness both of the mold and of the replicated MLA. With a stage of 100 x 100 mm in X- and Y-direction

and a Z focusing unit stroke of 10 mm, all provided samples in this study could be measured.

The movement resolution in Z is 10 nm. As a light source either a white LED or a 405 nm laser can be chosen. Three magnifications were used for the measurement to be carried out in this study. The provided sample were inspected visually with the 5x- and the 10x-magnification. The 10x magnification (NA = 0.30, WD = 11.00 mm) was used in the following to measure the ML diameters. The line surface roughness was measured with the 50x- and 100x-magnification (both NA = 0.95, WD = 0.35 mm). It must be said that the measured surface roughness strongly depends on the set measuring boundaries.

To receive meaningful and comparable results, the line surface roughness measurements in this study were carried out according to instructions given in the standard ISO 4288 [81]. Five line surface roughness measurements per microlens were carried out over a sampling length  $l_r$ . It was measured perpendicular to the tool marks. The length of  $l_r$  was determined by an assumed value for the  $RS_m$  surface roughness for periodic profiles or the  $R_a$  surface roughness for aperiodic profiles. Each measured surface profile was filtered with a cut-off wavelength  $\lambda_c$  equal to the chosen sampling length [82]. The microlens curvature was mathematically removed. Finally, the mean  $R_a$  and  $R_q$  values of the five measurements were calculated as these were identified in chapter 2.2 as the most crucial surface parameters to determine and compare a lens surface quality.



**Figure 6-12: Olympus OLS4100**

### 6.4.3 Digital Microscope KEYENCE VH-Z100UR

A Keyence VH-Z100UR digital microscope was selected beside the Olympus OLS4100 for the visual inspection of the molded parts as it provides an easy adjustment of the magnification. Magnifications in a range from 100x up to 1000x can be achieved. The working distance (WD) is 25 mm.

### 6.4.4 Laser Probe 3D Measuring Instrument MITAKA Series

Two laser probe 3D measuring devices by Mitaka Kohki Co., Ltd. were employed in this study. Both instruments are shown in Figure 6-13. The MITAKA NH-3SP provided by the Yan Laboratory was taken to measure the sag heights of the press-molded lens. The surface roughness measurements were partially conducted with the MITAKA MLP-3 available at the IFM.



**Figure 6-13: Laser probe 3D measuring instrument [83]; left: MITAKA NH-3SP; right: MITAKA MLP-3**

The MITAKA NH-3SP is an optical non-contact profilometer to measure lens profiles, optical molds and other optical microstructures both in two or three dimensions. The possible measuring range in the x- and y-direction is 150 mm with a scale resolution of 0.01  $\mu\text{m}$ . The measuring range in the z-direction is maximum 10 mm with a scale resolution of 0.001  $\mu\text{m}$ .

The MITAKA NH-3SP is equipped with each a 10x-, 50x- und 100x-magnification objective. The 10x-magnification was used to align the ML substrate in x- and y-direction. The 100x-magnification objective (NA = 0.70, WD = 6.5 mm) was used for

cross-sectional profile measurements of the mold and the polyethylene along the x-axis. The 50x-magnification objective (NA = 0.55, WD = 10.1) was used to measure the PC and PMMA samples. Before each measurement was started, several settings had to be defined as it can be seen in Figure 6-14. The machine was adjusted to align itself to the ML center by measuring the change of lens height over a pre-defined distance with a pre-defined measurement pitch of 1 μm in the positive and negative x- and y-direction. With finishing a measurement, the lens profile is displayed in the machine software, in which several adjustments like tilt compensation or a cut-off filtering of the profile could be carried out.

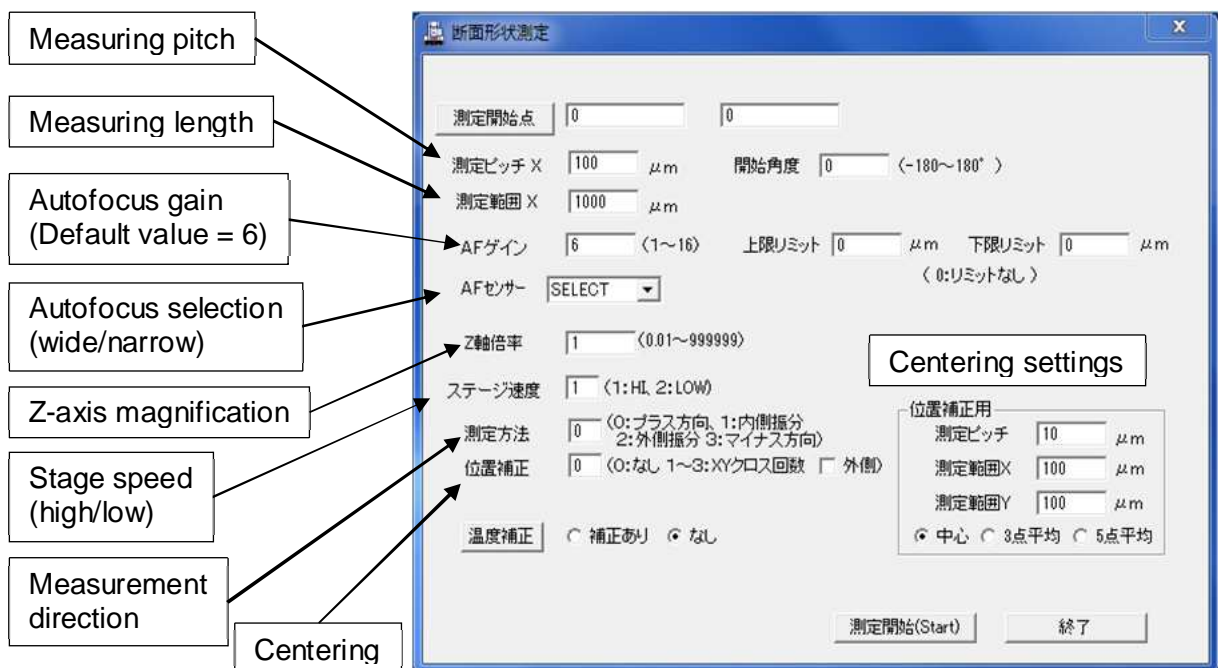


**Figure 6-14: MITAKA NH-3SP Lens measuring settings**

The operating principle and the handling of the MITAKA-MLP3 is identical to MITAKA NH-3SP. The measuring range in X and Y is 120 mm and in Z 130 mm. The scale resolution is 0.1 μm in all directions. The MLP3 is equipped with a 5x- and a 100x-magnification objective (NA = 0.15, WD = 20 mm and NA = 0.80, WD = 20 mm). After having conducted one measurement, the measured data are loaded into the Mitaka Map software in which different calculations can be carried out.

#### **6.4.5 Scanning Electron Microscope**

An Inspect™ scanning electron microscope (SEM) (FEI Company, USA) was used in this study to take the large-area images of the microlens array. As the press-molding materials were polymers, the samples were coated with an osmium layer of 7 nm by using chemical vapor deposition (HPC-20, Vacuum Device Co., Ltd., Japan).

### **6.5 Experimental Documentation**

The conditions and the used process parameters were documented in an experiment documentation sheet. The documentation sheets for the test series 2,3 and 4 are attached in the appendix (16) - (33).

MATLAB was used to evaluate and to plot the measured microlens profiles. The measured data were loaded into MATLAB in which a tilt compensation of the lens profiles was carried out by using the MATLAB polynomial curve fitting function *polyfit*. A falsification of the measurement results due to an incomplete flatness of the tool and the pressed substrates could thus be minimized.

## 7 Experimental Results and Discussion

In the following the experimental results for the obtained design of experiments of this study are presented and discussed.

As the replicated lens quality is dependent on the mold microstructure, the microstructure in the mold was measured after the diamond cutting. The measured values were evaluated by comparing them with the theoretical lens profile. Based on this comparison, the expected quality of the molded MLA can be determined. In this regard, each microlens profile in a molded array can be compared with the respective mold profile to evaluate the effect of the press-molding parameters on the replication quality.

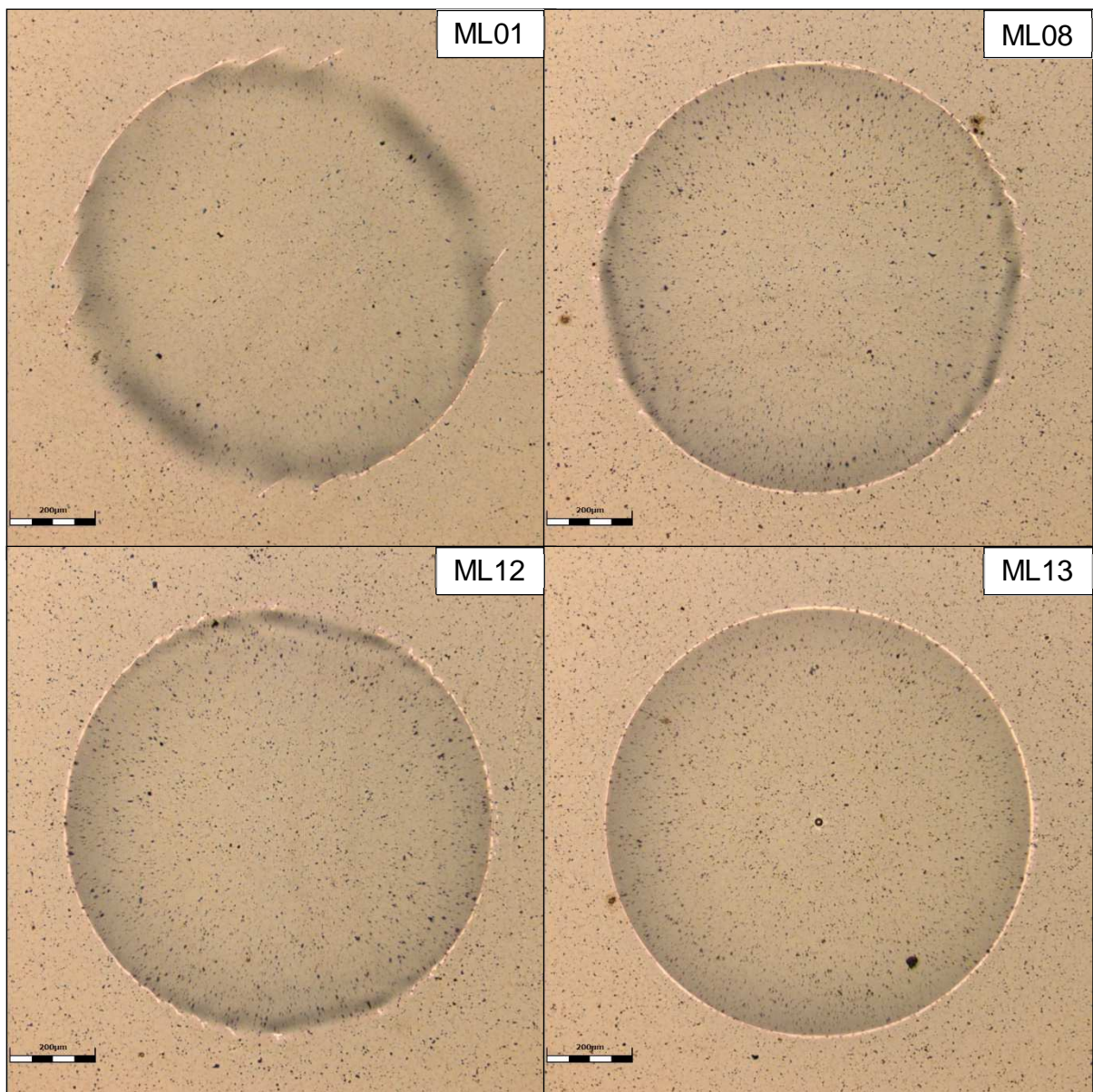
### 7.1 Mold Dimensions Before Compression Molding

The ultra-precision cutting microlens array is shown in Figure 7-1. After machining, the microlens structure in the mold was measured. The ML diameter  $2a$ , the sag height  $h$  and the lens profile including its form accuracy of each lens was measured to have comparable values for the later replicated lens profiles. The surface roughness was measured for five microlenses.

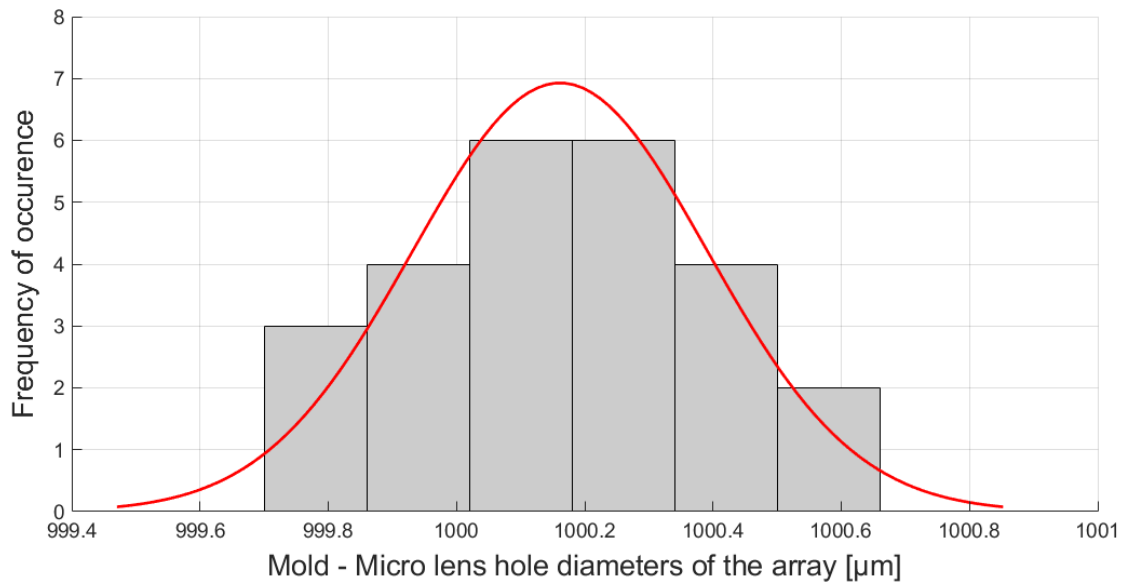


**Figure 7-1: Ultra-precision machined microlens array**

A first observation of the lens appearance was done with the Olympus OLS4100 before the lens dimensions were measured. The cut ML01, ML08, ML12 and ML13 are shown in Figure 7-2. In the following, the diameters of all 25 microlenses were measured. The measured best fit diameter was 1000.00  $\mu\text{m}$  (ML12). The measured minimum and maximum diameters were 999.72  $\mu\text{m}$  (ML15) and 1000.62  $\mu\text{m}$  (ML05). The mean diameter was calculated to 1000.16  $\mu\text{m}$ . All collected diameters are frequency distributed in Figure 7-3, which shows an even distribution of the measured values over the entire value range.



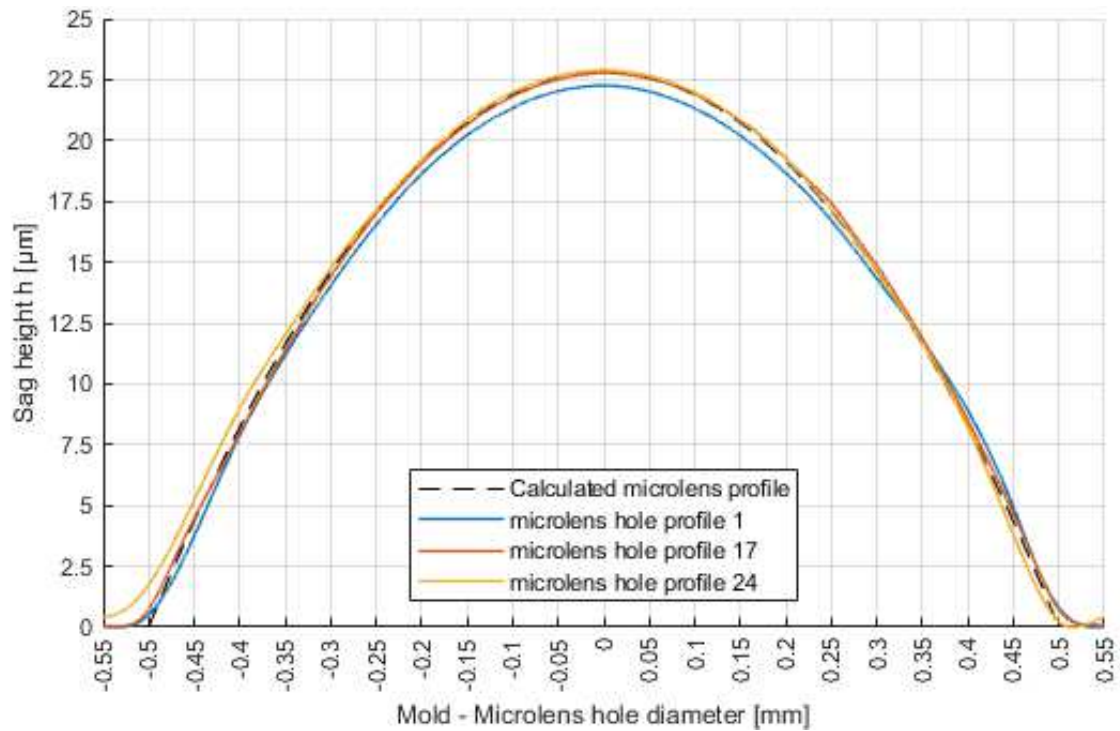
**Figure 7-2: Mold microlenses at 10x magnification; upper left: ML01; upper right: ML08; lower left: ML12; lower right: ML13**



**Figure 7-3: Frequency distributed microlens diameters in the mold**

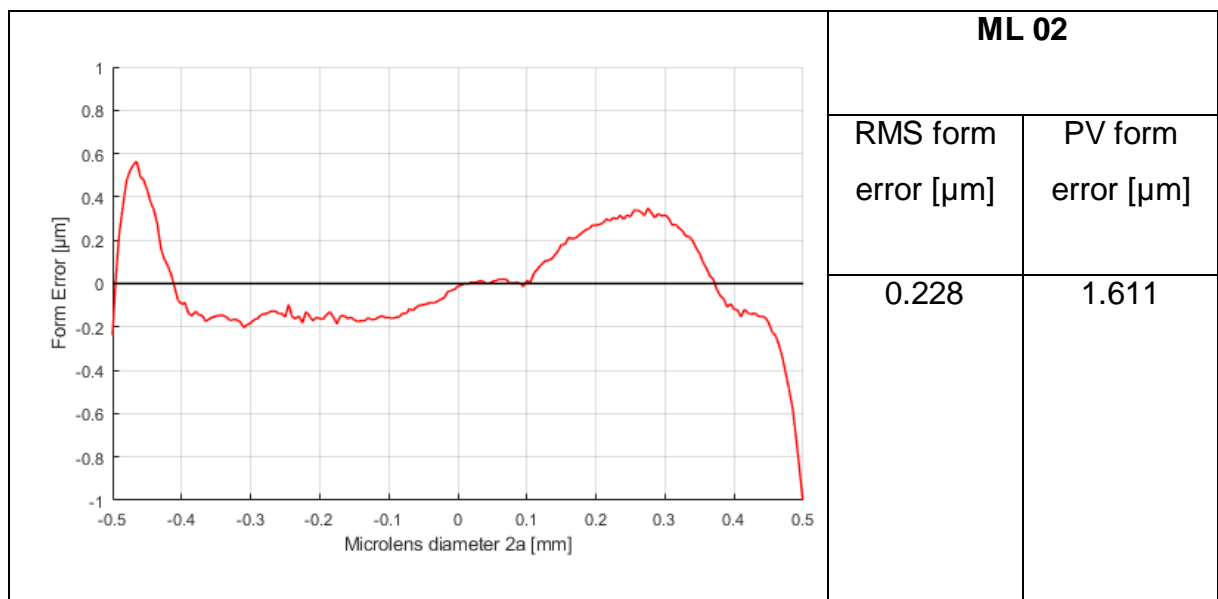
The cross-sectional profiles along the x-axis of each lens were measured with the MITAKA NH-3SP. The exact center point of each lens was respectively calculated by three calibration measurements in the x- and y-direction over a distance of 200 μm and a measuring pitch of 1 μm. The microlenses were then measured in the x-direction from the determined center over a range of -650 μm to 650 μm. The measurement pitch was set to 0.25 μm resulting in a total of 5201 measured points. The measured profiles were filtered afterwards with a cut-off wavelength of  $\lambda_c = 0.08$  mm in the instrument's software. As previously mentioned in chapter 6.5, MATLAB was used to determine the depths of the ML which represent the sag heights of the replicated ML. 4483 points in total were measured, which is equivalent to a measured length of 1120.75 μm. The first and last 75 points measured of this length were fitted by a linear regression. The measured mold profile was then fully tilt compensated by rotating all measured profile points by the angle between the horizontal axis and the created order fit. After that the measured profiles were set into comparison to the calculated lens profile from equation (6-1). The best approximation to the calculated height is shown by ML17 with a depth of 22.779 μm. ML01 showed the smallest value with 22.260 μm, whereas ML24 was the deepest with 22.890 μm. The profiles of ML01, ML17 and ML24 are compared to the theoretical lens profile in Figure 7-4.





**Figure 7-4: Comparison of microlens hole profiles with the theoretical lens profile**

The form error was analyzed for the measured microlens profiles along the x-axis. Using the Mitaka, the form error was each wise calculated for the ML diameter range from -0.5 – 0.5 mm and the radius of curvature. The maximum PV form error was found for ML 02, the minimum PV form error was found for ML 12. The form error increased from the ML in the array center to the outer edge of the microlenses. The form error profiles are plotted in Table 7-1.



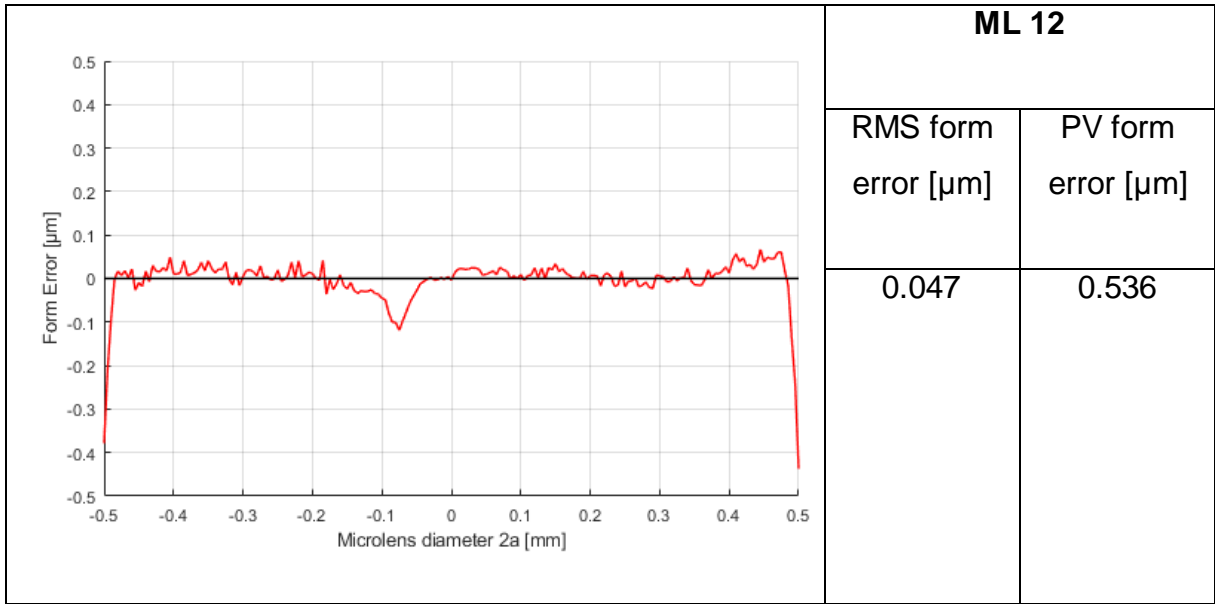


**Table 7-1: RMS and PV form error of ML hole 2 and 12**

The line surface roughness was measured following the steps in [81] as mentioned in chapter 6.4.2. As the ML microstructure was diamond cut, a periodic surface topography with the smallest mean groove spacing  $RSm \leq 0.04$  mm was assumed. For  $RSm \leq 0.04$ , the sampling length  $l_r$  and the cut-off wavelength  $\lambda_c$  was set to 0.08 mm. The surface roughness of ML 01 – 05 was measured five times. The mean  $R_a$  and  $R_q$  values of the 5 measurements are given in Table 7-2. From these values, the mean surface roughness for the mold microstructure was calculated to be  $R_a = 18.2$  nm and  $R_q = 25.8$  nm. The surface roughness values of the measured ML showed a good homogeneity, for which reason it was decided to reduce the roughness measurements to three ML distributed over the array for the later molded microlens arrays.

	<b>ML01</b>	<b>ML02</b>	<b>ML03</b>	<b>ML04</b>	<b>ML05</b>
<b><math>R_a</math> [nm]</b>	17	19	17	19	19
<b><math>R_q</math> [nm]</b>	24	28	23	27	27

**Table 7-2: Ra and Rq surface roughness values of the mold microlenses**

However, as it can be seen in Figure 7-5, occasional material imperfections were found in the microlens holes, which were suspected to be replicated in the molded microlens arrays. The microfractures may be caused by inhomogeneous material and by too high cutting forces during ultra-precision machining of the micro structure.

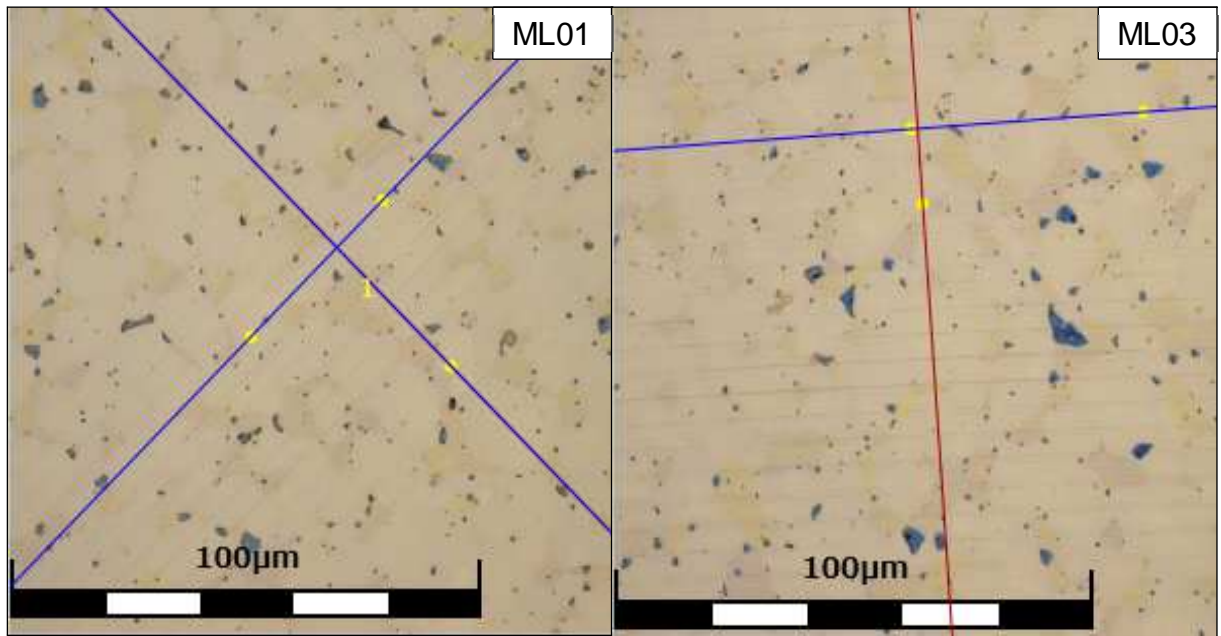


**Figure 7-5: Surface roughness measurement perpendicular to cutting tool marks; left: ML hole 01; right: ML03**

To reduce the surface roughness and thus to decrease frictional forces between the mold and the charge material, the lower mold part 3 was polished as it can be seen in Figure 7-6. The achieved surface roughness  $Ra$  was 17 nm.

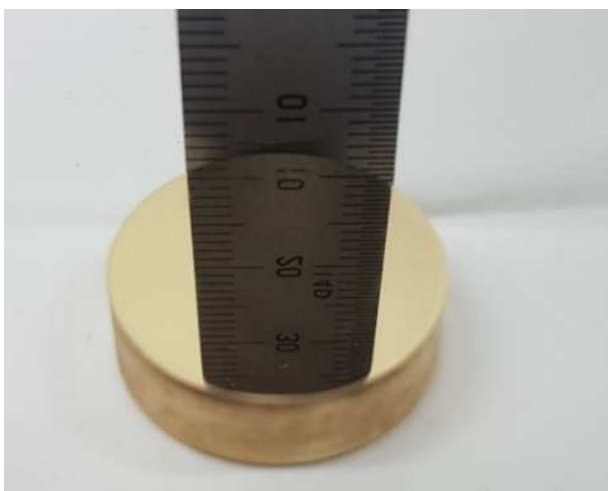


**Figure 7-6: Polished lower mold part 3**

It can be concluded that the cutting results of the mold were sufficient for the planned compression molding experiments. The ML diameters and sag height showed a sufficient uniformity throughout the entire array. Nevertheless, a surface roughness  $Ra$  of 19 nm is high for an optical mold as surface roughness  $Ra \leq 10$  nm are normally achieved by diamond cutting and required for optical applications. Considering the Rayleigh and Maréchal criterion for the form error, the measured form error values are too high for visible light, but sufficient for wavelengths in the IR range from 8 – 14  $\mu\text{m}$ . An improvement of the MLA quality, especially of the surface roughness and form error is expected by using a tool with a smaller tool nose radius, and by lowering the feed rate.

Since the above outlined ML represent the minimum, mean and maximum measurement results in terms of dimensions, form error and surface roughness, it was decided to compare the press-molded MLA from the upcoming test series 2 – 4 with the measured mold dimensions by means of

- the microlens diameter of ML05, ML12, ML15 including the microlens diameter of ML01, ML17, ML24
- the sag heights of ML01, ML17, ML24
- the PV form error of ML02, ML12
- the line surface roughness of ML01, ML17, ML24.

## 7.2 Compression Molding of Test Series 1 – HDPE

Test series 1 was carried out in trial and error to determine the needed amount of material to fill the mold cavity. Starting with a charge mass 0.361 g calculated in equation (6-3), the charge mass was increased for every sample until the cavity was completely filled. The process parameters were set according to Table 6-3. The weighted amount of HDPE used for every sample is given in Table 7-3.

	Sample 1	Sample 2	Sample 3	Sample 4	Sample 5	Sample 6
Charge mass [g]	0.361	0.411	0.411	0.421	0.442	0.456

**Table 7-3: Used charge mass of every sample in test series 1 - HDPE**

From sample 1 until sample 5 an incomplete filling of the cavity was observed after press-molding, hence the samples were porous. In addition, the material was not melted completely for sample 1 and sample 2 resulting in clearly visible weld lines between the single grains after pressing. For this reason, the time parameters St1 and St2 were set for the upcoming samples in order to increase the time for the heat conduction from the outer mold surface to the material inside and thus, to plasticize the material more effectively. However, the same charge mass as for sample 2 was used again to mold sample 3, since the molding process of sample 2 stopped during the cooling phase due to a lack of argon gas. St1 and St2 were increased until a far-reaching fusion of the grains was detected. From sample 5 to sample 6 it was seen that too much material was employed. The excess material was pressed into the guidance gaps between Imp 2 and Imp 3 and between the upper and the lower mold, forming a polymer flash around the MLA edge as shown in Figure 7-7.

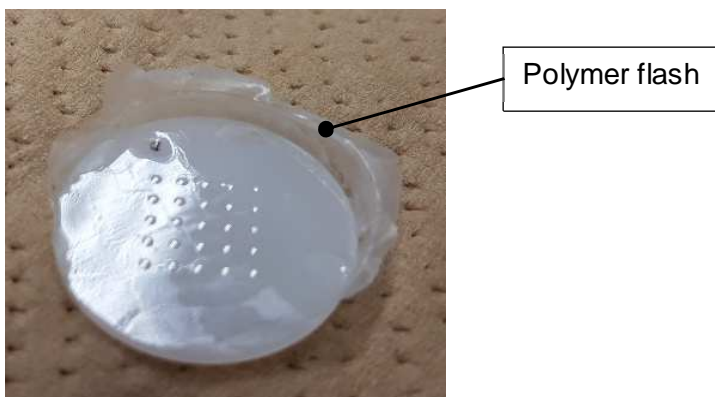


**Figure 7-7: Polymer flash caused by excess material**

The test series showed that finding the needed amount of material to fill a cavity is difficult but needed to assure the quality of the molded parts. The needed charge mass of HDPE was between 0.442 g and 0.456 g, which was a difference of one HDPE grain. In result, the exact cavity volume laid between 0.462 cm<sup>3</sup> and 0.478 cm<sup>3</sup>.

In addition, it was observed that the incremental heat supply has to be adjusted carefully. Heat inputs over 10 % and a too late reduction down to 0 % of the incremental heat supply before the heating temperature was reached led to a too fast and unstable increase of the mold temperature. In result, the charge mass was either not completely melted or an increase of the heating temperature while the pressing step has already been initialized was sensed by the thermocouples. These effects could be explained by the two following reasons. For the used compression press Toshiba GMP211, the heating temperature is not directly measured inside the mold cavity but at the outer mold surface as it can be seen in Figure 6-6. Since the pressing step is initialized at the GMP211 when the thermocouples measure the set heating temperature, it could occur that the mold cavity is not yet fully heated up when the pressing is started due to the needed time for the heat transfer from the outer mold surface to the cavity. Secondly, a too fast increase in the incremental heating led only to an early recognition of the set temperature by the thermocouples, but the heat energy was insufficiently transferred to the mold cavity. These effects could be prevented by a reduction of the heat input for both molds down to incremental values  $\leq 10\%$  at a temperature of 20 °C below the set heating temperature. Following this procedure, an unstable overheating of the mold could be prevented.

### 7.3 Compression Molding of Test Series 3 – HDPE

The measurement results of test series 3 are presented in this chapter. A SEM picture of one of the molded HDPE MLA is shown in Figure 7-8. Due to organizational reasons, test series 3 was performed before test series 2.

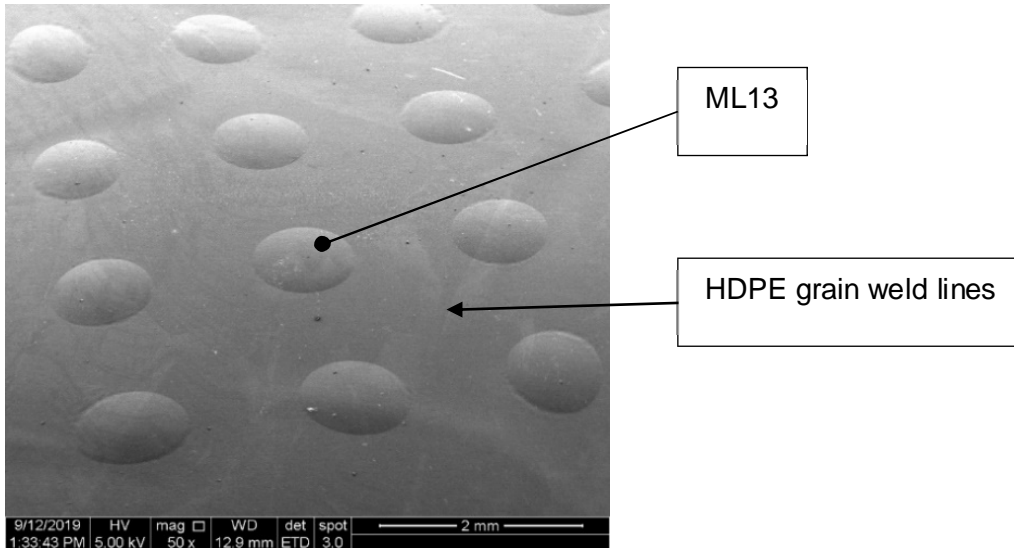


**Figure 7-8: Compression molded HDPE microlens array**

On basis of the results for the needed charge mass in chapter 7.2, a HDPE grain was split for each molded sample. Nevertheless, the charge masses varied still between 0.445 g and 0.448 g as it was difficult to cut the grains in steps of 1 mg. No clear burrs were detected for 0.446 g, for which reason this mass can be defined as the needed amount of HDPE material to fill the mold cavity.

The microlens diameters of ML1, ML5, ML12, ML15, ML17 and ML24 were measured for all samples. The measured values are set into comparison with the measured mold diameters in Table 7-4. To determine the difference in the sag height between the mold and the replicated HDPE microlenses, the 2D profiles of ML1, ML17 and ML24 were measured along the x-axis of each sample. The settings for the profile measurements were equal to the setting used for the microlens hole measurements of the mold, presented in chapter 7.1, but the centering was only carried out two times. The comparison of the measured profiles and sag heights is summarized in the following tables 7-4 to Table 7-10. Table 7-11 contains the measured PV form errors of test series 3.

For the line surface roughness measurement, a surface roughness of  $R_a \leq 0.02 \mu\text{m}$  was assumed as previously done for the mold. The first measurement was therefore done over a sampling length  $l_r = 0.08 \text{ mm}$  by filtering the measured surface profile with a cut-off wavelength of  $\lambda_c = 0.08 \text{ mm}$ . First measurements showed a line roughness of  $R_a \geq 0.02 \text{ nm}$ , which is why the measurement parameters had to be increased according to [81] to  $l_r = 0.250 \text{ mm}$  and  $\lambda_c = 0.250 \text{ mm}$ . The 50x-magnification objective had to be used as the sampling length could not be covered with the 100x-magnification. The set step height was  $0.010 \mu\text{m}$ .

	<b>Microlens diameter 2a [<math>\mu\text{m}</math>]</b>					
	<b>ML01</b>	<b>ML05</b>	<b>ML12</b>	<b>ML15</b>	<b>ML17</b>	<b>ML24</b>
<b>Mold</b>	1000.12	1000.62	1000.00	999.72	1000.34	1000.37
<b>TS3no1xx</b>	975.03	966.64	975.27	971.75	969.545	981.23
<b>TS3no2xx</b>	976.29	975.28	974.26	976.22	974.75	983.48
<b>TS3no3xx</b>	981.02	978.14	978.42	973.97	982.35	981.85
<b>TS3no4xx</b>	970.24	961.50	964.80	962.15	967.80	971.47
<b>TS3no5xx</b>	973.10	973.90	972.38	972.57	977.83	973.96
<b>TS3no6xx</b>	965.31	971.11	970.91	976.92	973.95	981.42

**Table 7-4: Microlens diameters of test series 3**



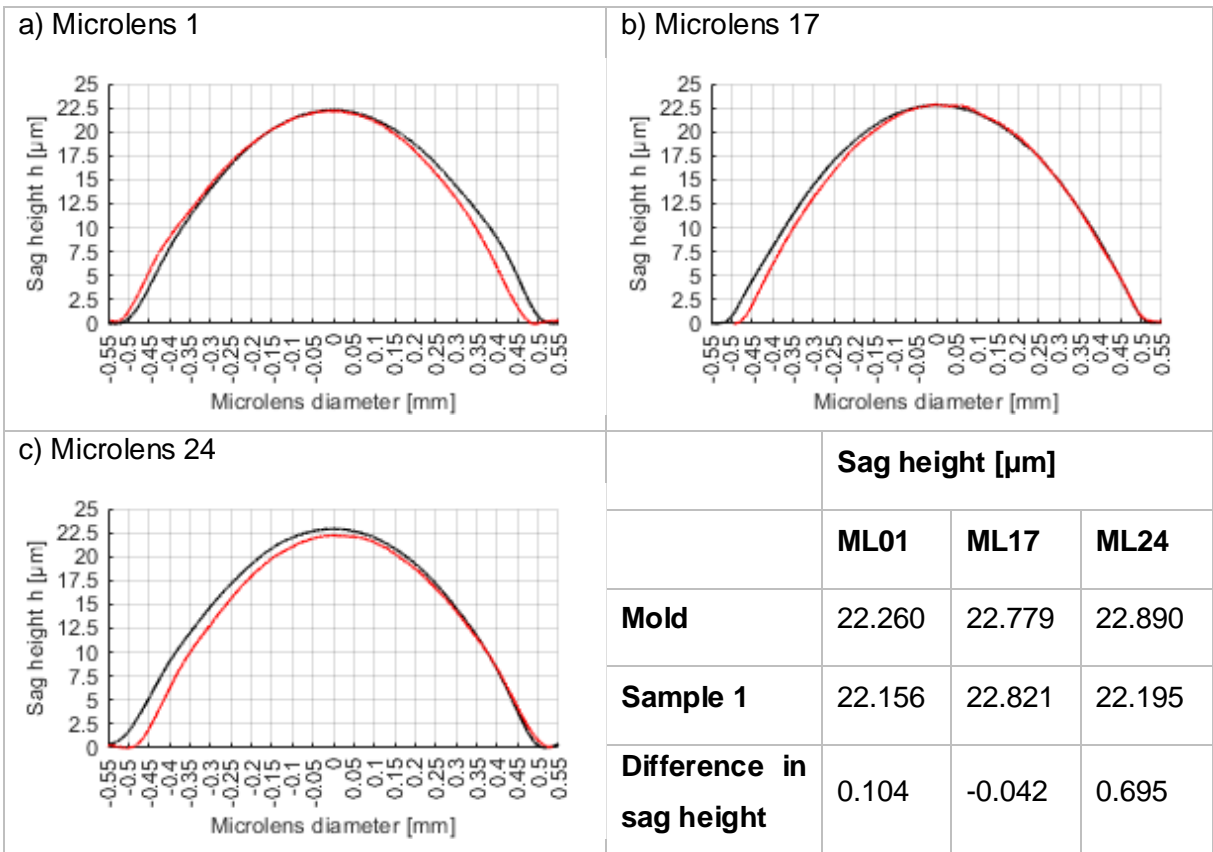


**Table 7-5: Microlens sag height of TS3no1xx**

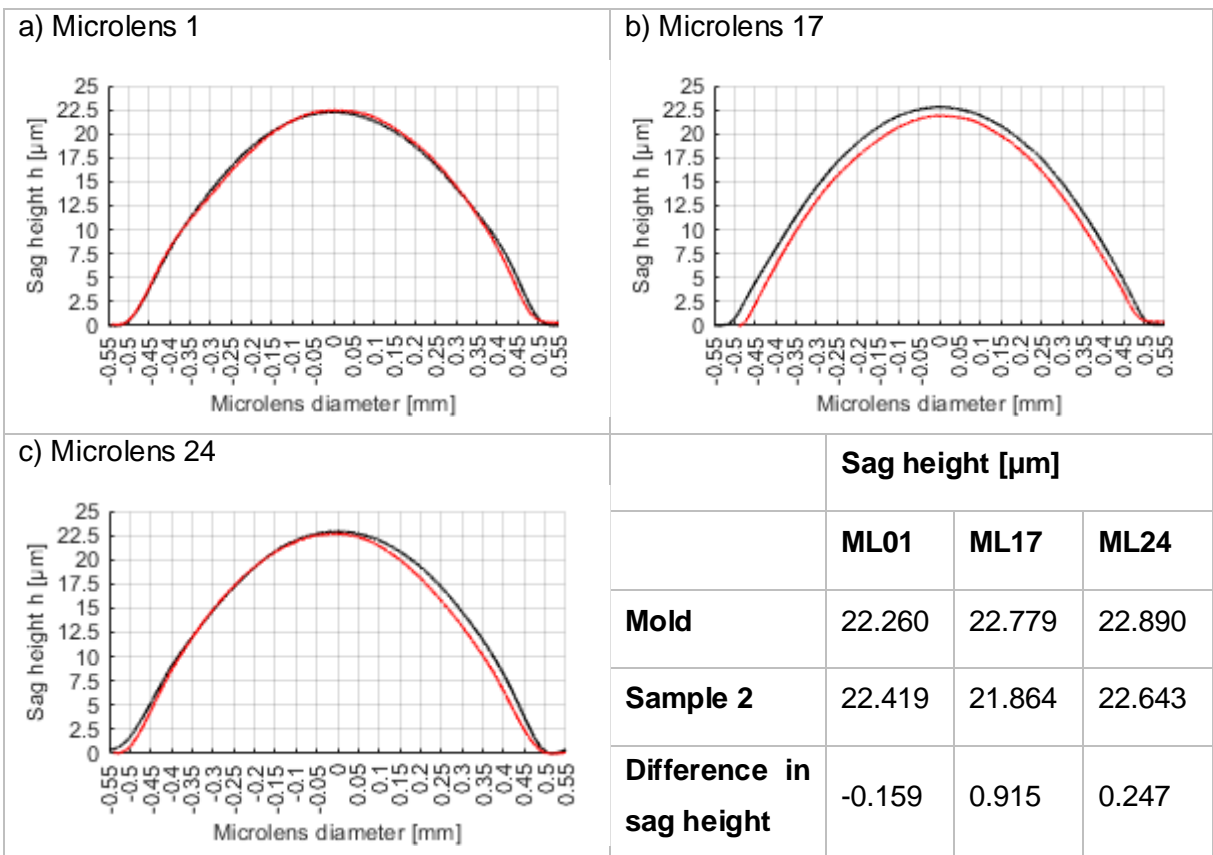


**Table 7-6: Microlens sag height of TS3no2xx**

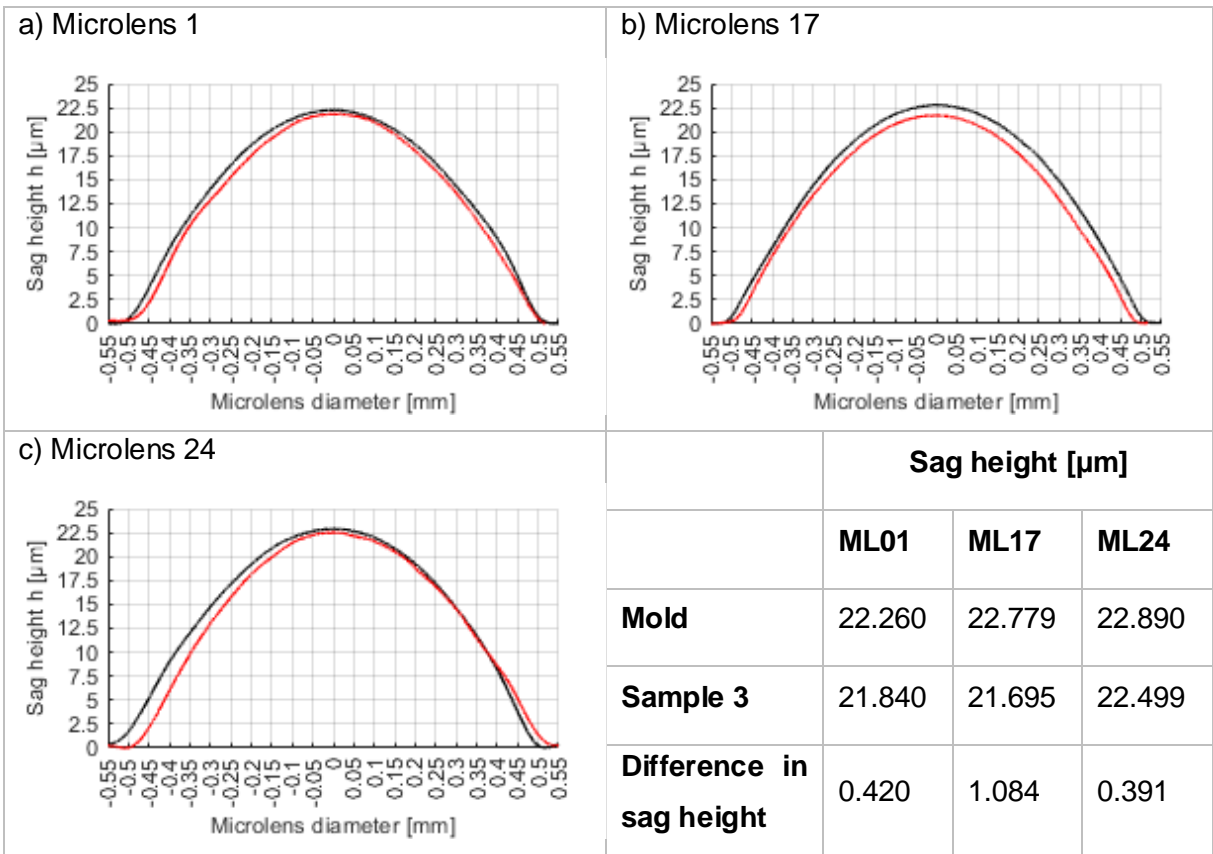


**Table 7-7: Microlens sag height of TS3no3xx**

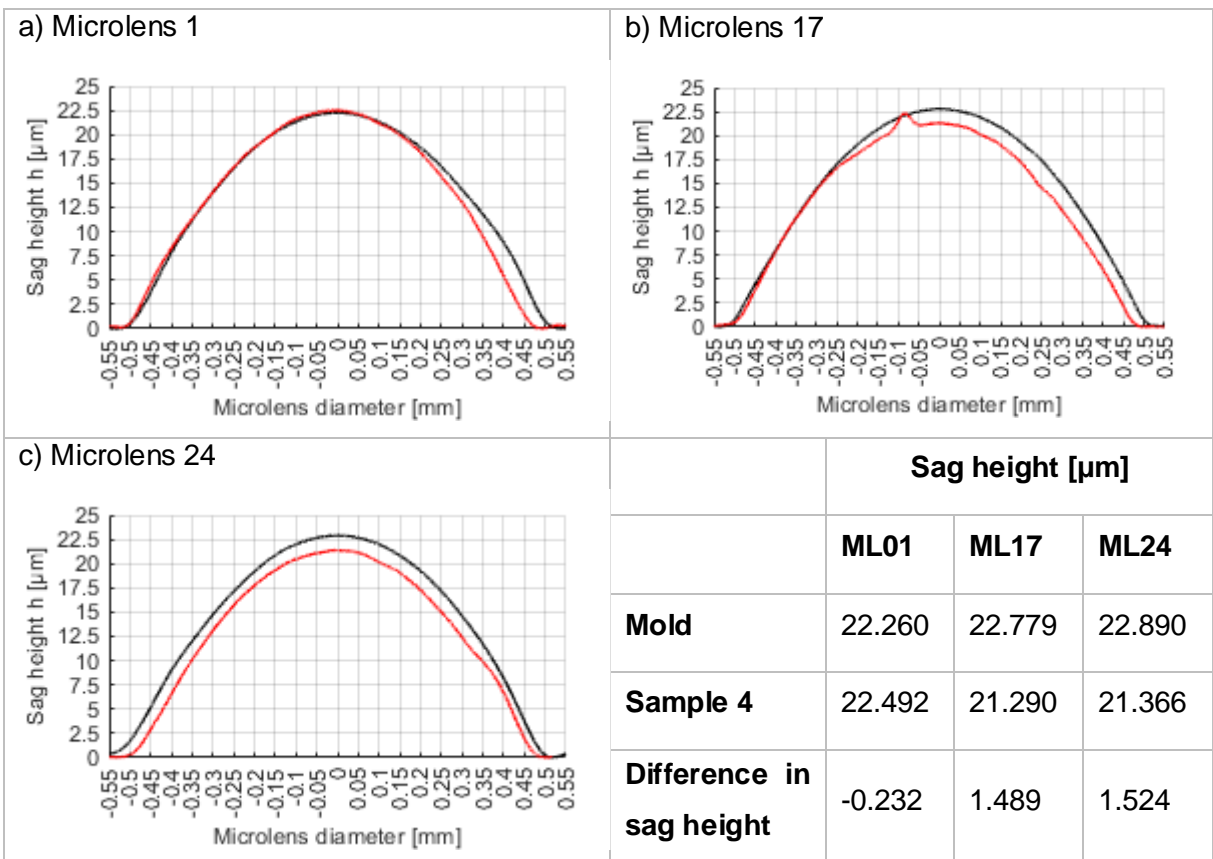


**Table 7-8: Microlens sag height of TS3no4xx**

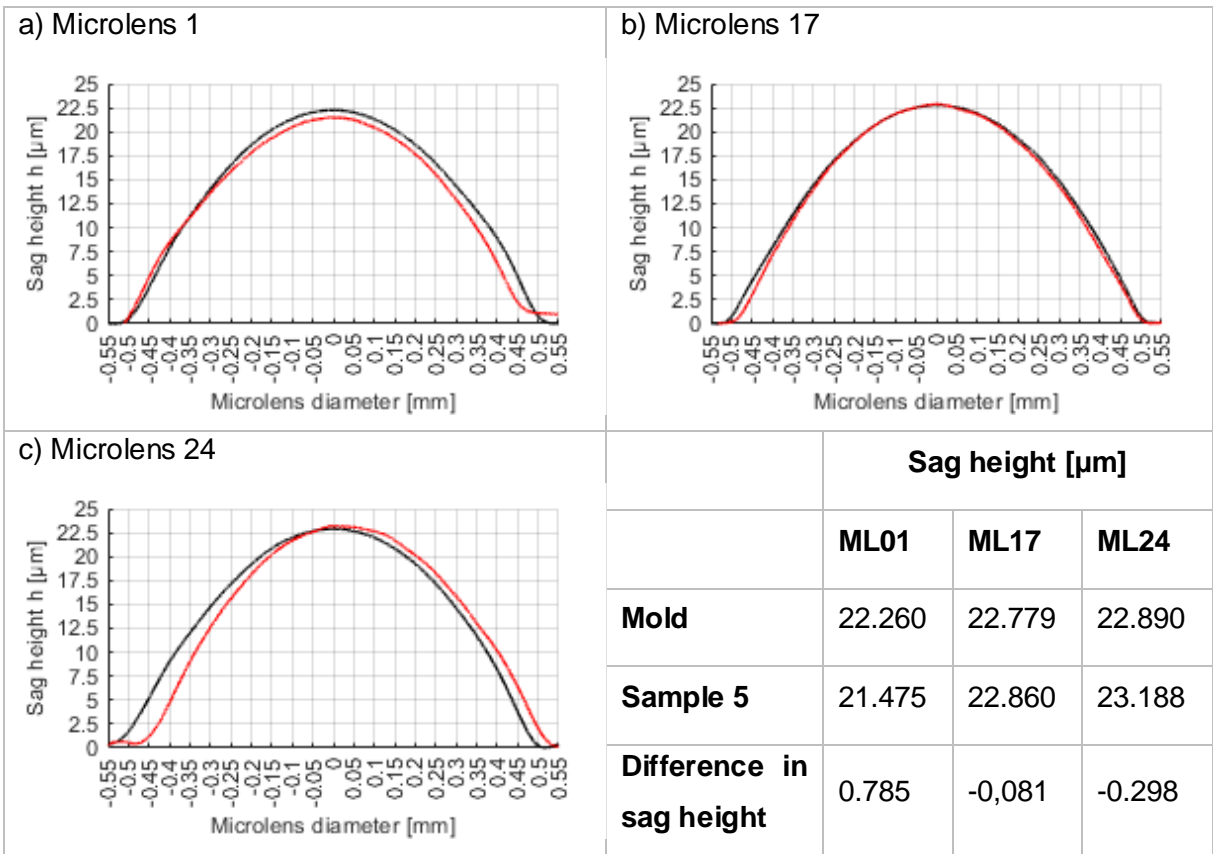


**Table 7-9: Microlens sag height of TS3no5xx**

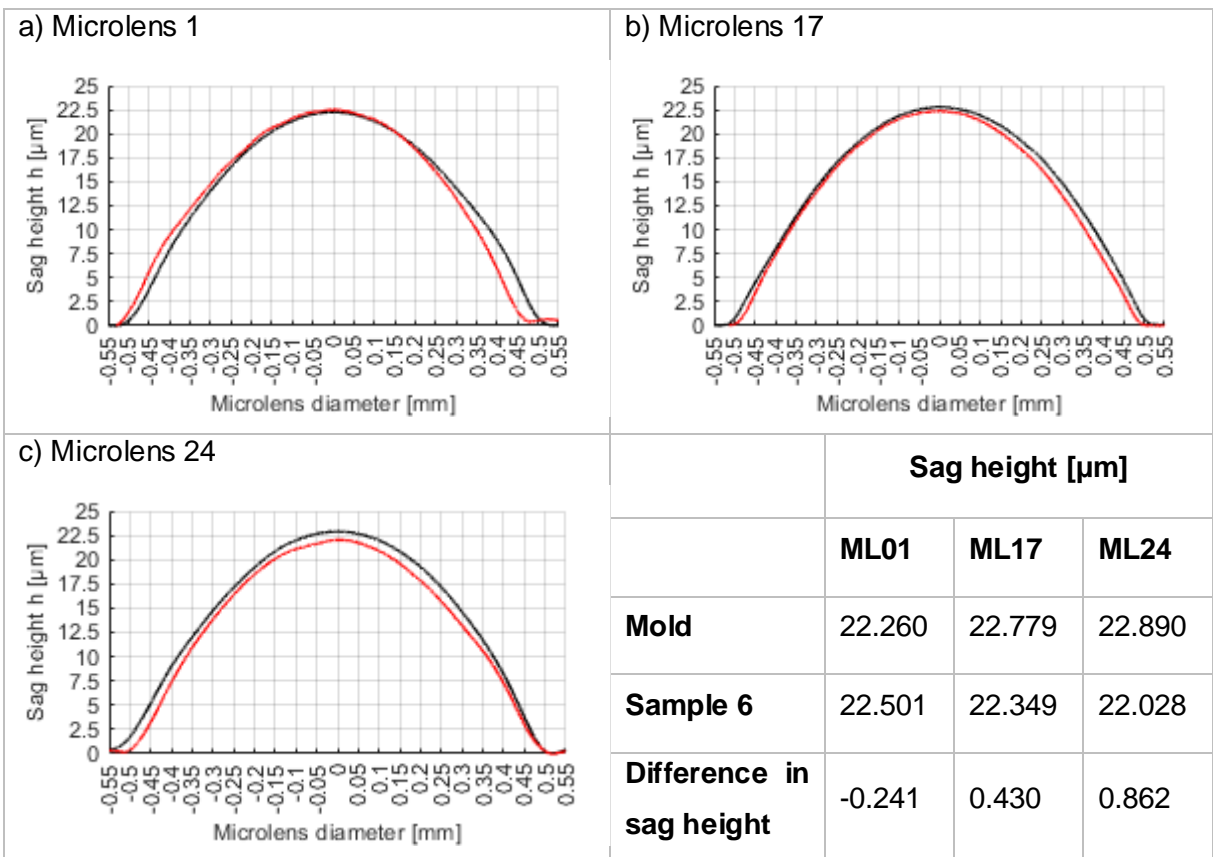


**Table 7-10: Microlens sag height of TS3no6xx**

	PV form error [ $\mu\text{m}$ ]					
	TS3no1xx	Ts3no2xx	TS3no3xx	TS3no4xx	TS3no5xx	TS3no6xx
ML02	2.074	3.337	1.633	2.383	2.316	2.333
ML12	2.258	1.701	1.480	1.761	1.297	1.755

Table 7-11: PV form error results of test series 3

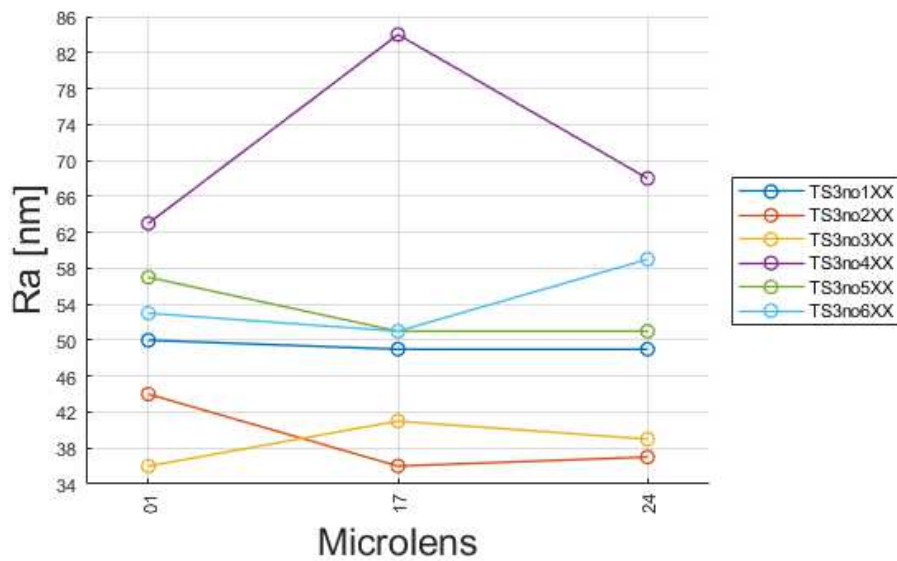


Figure 7-9: Surface roughness Ra of the press-molded samples in test series 3

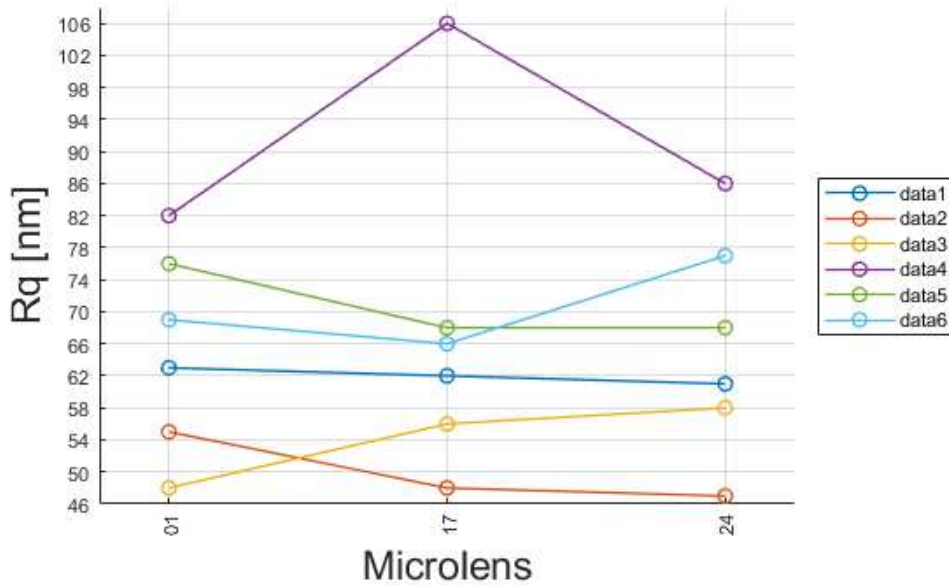
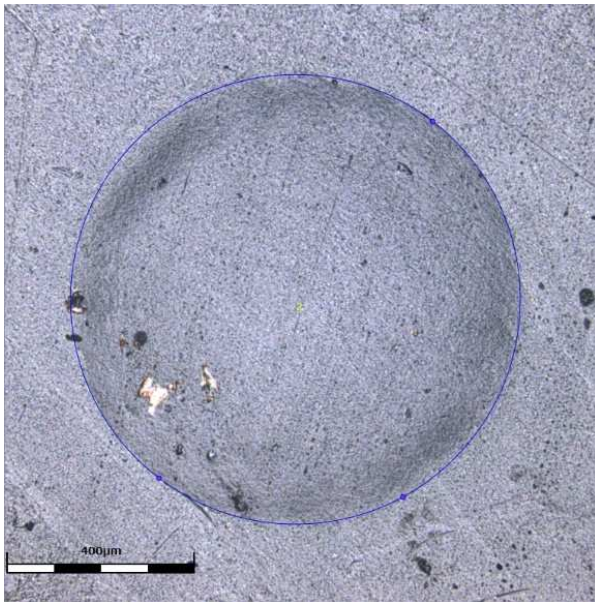


Figure 7-10: Surface roughness Rq of the press-molded samples in test series 3

During the measurements with the OLYMPUS OLS4100, small brass particles were found in the replicated MLA parts. As it can be seen in Figure 7-11, the particles were deposited sporadically in the lens geometry. It is assumed that frictional force between the melt polymer and the mold caused the abrasion of the found particles, which were then distributed in the samples by the polymer flow.



**Figure 7-11: Brass particle found in TS3no405**

The results of this test series are discussed in the following. Table 7-4 indicates that the measured ML diameters range from 961.50 μm to 983.48 μm. In result, the shrinkage in the lens diameter was smaller than 4 % compared to mold for all measured microlenses. The diameter measurement with the Olympus OLS4100 is very subjective. A clear correlation between the varied HDPE press-molding parameters and the measured diameters cannot be seen for single microlenses as the measured minimum and maximum diameter values are distributed over all molded samples. However, when the mean diameter values of all microlenses on an array are compared, an increase in the mean can be found with increasing the heating temperature. The mean diameter was 973.24 μm for a heating temperature of 125 °C (TS3no1xx), 976.71 μm for 128 °C (TS3no2xx) and 979.29 μm for 131 °C (TS3no3xx). The latter sample also showed the highest mean lens diameter regarding the varied compression forces.

A defined correlation was also not determined for the sag heights when the individual microlenses were compared for different parameters. The overall shrinkage in the sag height was less than 5 %. For some microlenses a higher sag height than the sag height of the corresponding lens in the mold was measured. This could be explained by uncertainties in the measurement, for example by the alignment of the MLA in the Mitaka NH-3SP, as well as in the data preparation in MATLAB. The unstable results for the measured lens diameter and the sag height could be explained with the heating process of the Toshiba GMP211 compression press. In this respect and taking the temperature sensor accuracy of  $\pm 1$  °C into account, an experimental heating temperature difference of 3 °C from sample to sample is relatively small.

As introduced in chapter 2.2, the form error of a lens can be evaluated by the Rayleigh criterion. HDPE was considered in this study for its optical properties in the thermal IR range from 8  $\mu\text{m}$  – 14  $\mu\text{m}$ . Thus, the PV form error should be less than 2  $\mu\text{m}$  for a wavelength of  $\lambda = 8$   $\mu\text{m}$  and less than 3.5  $\mu\text{m}$  for  $\lambda = 14$   $\mu\text{m}$ . For ML02, the Rayleigh criterion for the thermal IR wavelength range was fulfilled for a compression force of 1.0 kN (TS3no3xx) as the form error was smaller than 2  $\mu\text{m}$ . The Rayleigh criterion was fulfilled for all measured ML12 except TS3no1xx. Furthermore, a reduction of the form error both of ML02 and ML12 was observed at higher temperatures as it was also shown for the Si-HDPE Fresnel lens press-molded at the Yan Laboratory [55]. The best form deviation results were achieved for ML02 at 131 °C and a pressing force of 1.0 kN and for ML12 at a pressing force of 1.2 kN. The highest form error results were found for the lowest compression force of 0.8 kN (ML02) and for the lowest heating temperature (ML12). In accordance with the observations made in [10] and shown in Figure 5-2, it can be concluded that a too low compression force compensates shrinking effects insufficiently, especially during the cooling phase and a deterioration of the profile occurs.

The measured surfaces roughness values are plotted in Figure 7-9 and Figure 7-10. The lowest  $R_a$  and  $R_q$  roughness were achieved for TS3no2xx and TS3no3xx. A reduction of the roughness values was observed in general for increasing heating temperatures. This might be caused by the lowered viscosity of the melted polymer at higher temperatures and thus, by limited frictional forces between the brass material and the HDPE. Similar to the form error results, the highest surface roughness was

measured for a compression force of 0.8 kN. This could be explained by an incomplete filling of the micro cavities. The  $R_q$  surface roughness was measured to evaluate the scattering proneness of the MLA. The scattering of light was introduced in chapter 2.2 by equation (2-2). Total integrated scattering of an optical surface is desired to be as small as possible but should not exceed 2 % of the incident light. To cover the entire wavelength range from  $\lambda = 8 \mu\text{m}$  to  $\lambda = 14 \mu\text{m}$ , the  $R_q$  surface roughness should be smaller 90 nm. In this regard, all samples except sample TS3no4xx are within the TIS tolerance of 2 %.

The brass particles, found in the replicated MLA samples, could be explained by a non-sufficient cleaning of the mold after the MLA diamond cutting and by too high frictional forces between the mold material and the HDPE during pressing.

## **7.4 Compression Molding of Test Series 2 - Polycarbonate**

The measurement results of test series 2 are presented in this chapter. A SEM picture of a press-molded PC sample is given in Figure 7-13.

As previously observed in test series 1, the manual adjustment of the heating temperature had to be obtained carefully as a too late decrease or a decrease in too small incremental steps lead to unstable temperature conditions during pressing. To determine the effect of the manual heat input on the melting behavior of the PC plate material, a pre-series of 5 samples was molded before test series 2 was started. Using the experimental parameters of TS2no2xx, the incremental heat supply was reduced to  $\leq 5 \%$  from a heating temperature of 170 °C downwards to 150 °C. For a too fast reduction of the heat supply at a temperature of 170 °C, gas trapping was clearly visible with the naked eye. The created voids are shown in Figure 7-12. For a heat supply reduced down to 2 % at a temperature of 150 °C, gas trapping was not clearly visible anymore. For this reason, test series 2 was carried out by setting the heat input down to 2 % from a temperature of 150 °C.

The pressed samples were inspected using the Keyence VH-Z100UR digital microscope. Micro gas trappings, creating flow lines, were found at the microlens

boundaries in TS2no1xx. As it can be seen in Figure 7-14, the flow lines were diminished with increasing the temperature from TS2no1xx to TS2no3xx.

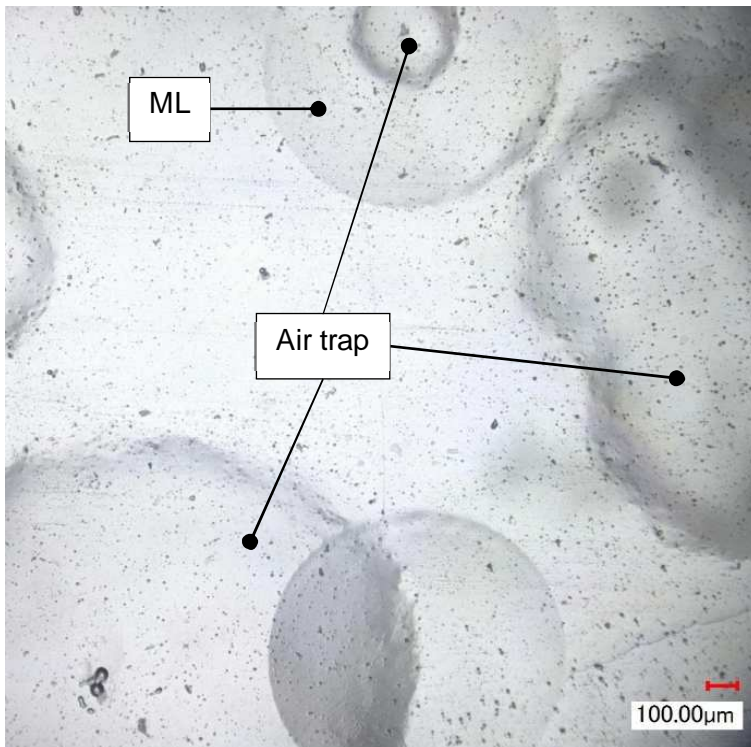


Figure 7-12: Air trapping in a press-molded PC sample

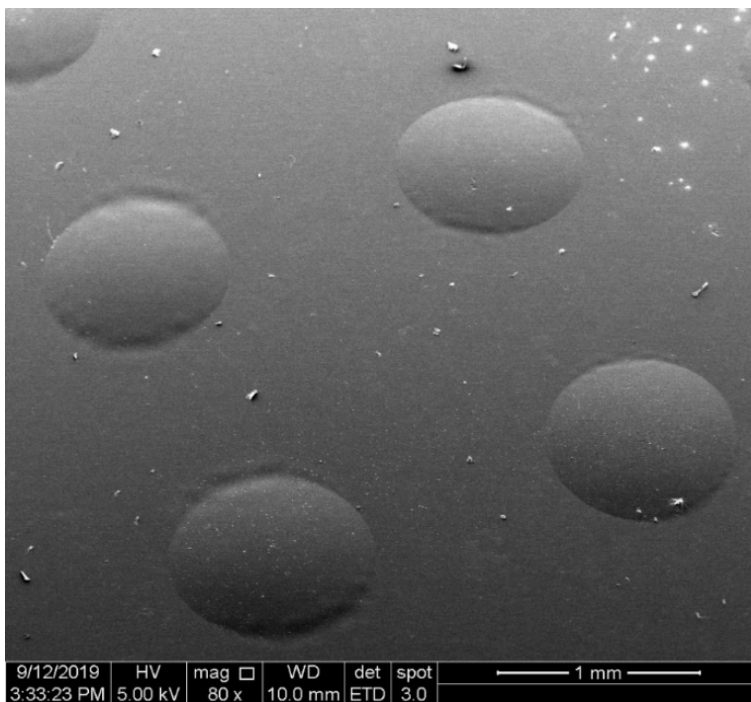
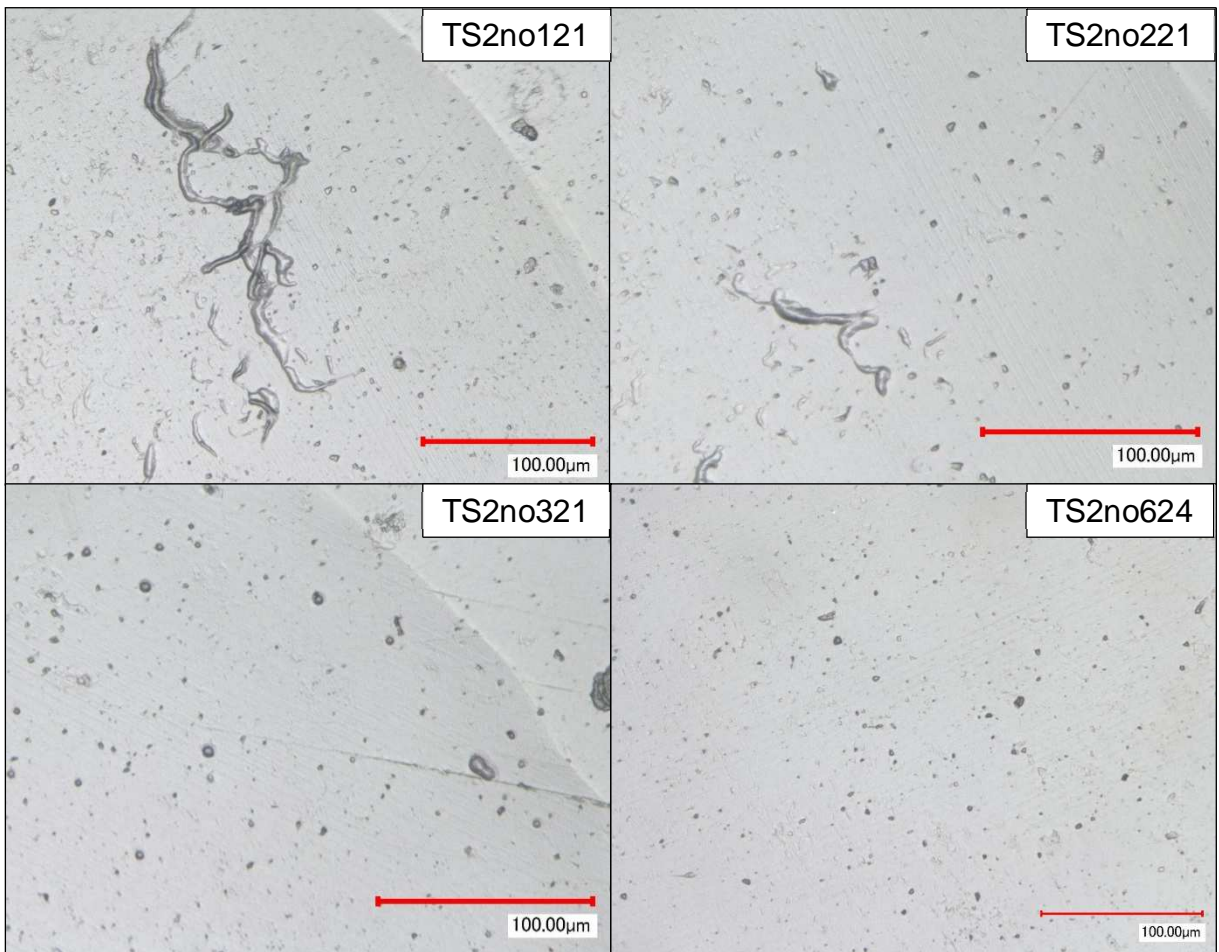


Figure 7-13: SEM picture of a compression molded polycarbonate MLA





**Figure 7-14: Flow lines with entrapped gas (900x-magnification)**

The MLA TS2no1xx, TS2no2xx and TS2no5xx stuck to the mold after demolding. The part sticking effect is shown in Figure 7-15. Following the procedure in [63] in order to prevent a damage of the MLA, it was waited until the mold and the MLA attached were cooled down to temperatures lower 30 °C before the MLA was taken out.



**Figure 7-15: PC sample sticking to the mold after demolding**

The measurement of the transparent samples was difficult to obtain with the light-based measuring devices as they struggled to find a focus point. The measurement of the diameter was conducted as planned with the Olympus OLS4100 at the 10x- magnifications. The lens diameter results are given in Table 7-12. For magnifications higher 10 it was seen that the focus drifted away. A line surface roughness measurement as conducted for the mold and test series 3 was therefore not possible. Also for the Mitaka NH3-SP, it was hard to find the focus point. To measure the sag height and the form error of the samples, the 50x-magnification objective was used, since for a higher magnification the drift of the focus point was too high and the measurements were non-reproducible. The measurement was conducted over a length of 650  $\mu\text{m}$  in both x-directions with a pitch of 1  $\mu\text{m}$ . The autofocus sensor mode was set to use a narrow area for a more precise measurement. The autofocus speed and stage speed were set to the “low mode”. The measured sag heights are given from Table 7-13 to Table 7-18. The line surface measurements were conducted at the IFM in Stuttgart. The cross-sectional profiles were measured along the x-axis with the Mitaka MLP-3. The surface roughness was calculated in the Mitaka Map software for a cut-off wavelength and sampling length of 0.250 mm. The results are visualized in Figure 7-17 and Figure 7-18.

	<b>Microlens diameter 2a [<math>\mu\text{m}</math>]</b>					
	<b>ML01</b>	<b>ML05</b>	<b>ML12</b>	<b>ML15</b>	<b>ML17</b>	<b>ML24</b>
<b>Mold</b>	1000.12	1000.62	1000.00	999.72	1000.34	1000.37
<b>TS2no1xx</b>	975.03	968.64	975.26	971.74	969.53	981.22
<b>TS2no2xx</b>	976.29	975.27	974.25	976.11	974.74	983.48
<b>TS2no3xx</b>	981.01	978.14	978.42	973.96	982.34	981.85
<b>TS2no4xx</b>	970.23	961.49	964.80	962.14	967.79	971.46
<b>TS2no5xx</b>	973.09	973.89	972.37	972.56	977.82	973.95
<b>TS2no6xx</b>	965.31	971.10	970.90	976.92	973.94	981.41

**Table 7-12: Microlens diameters of test series 2**

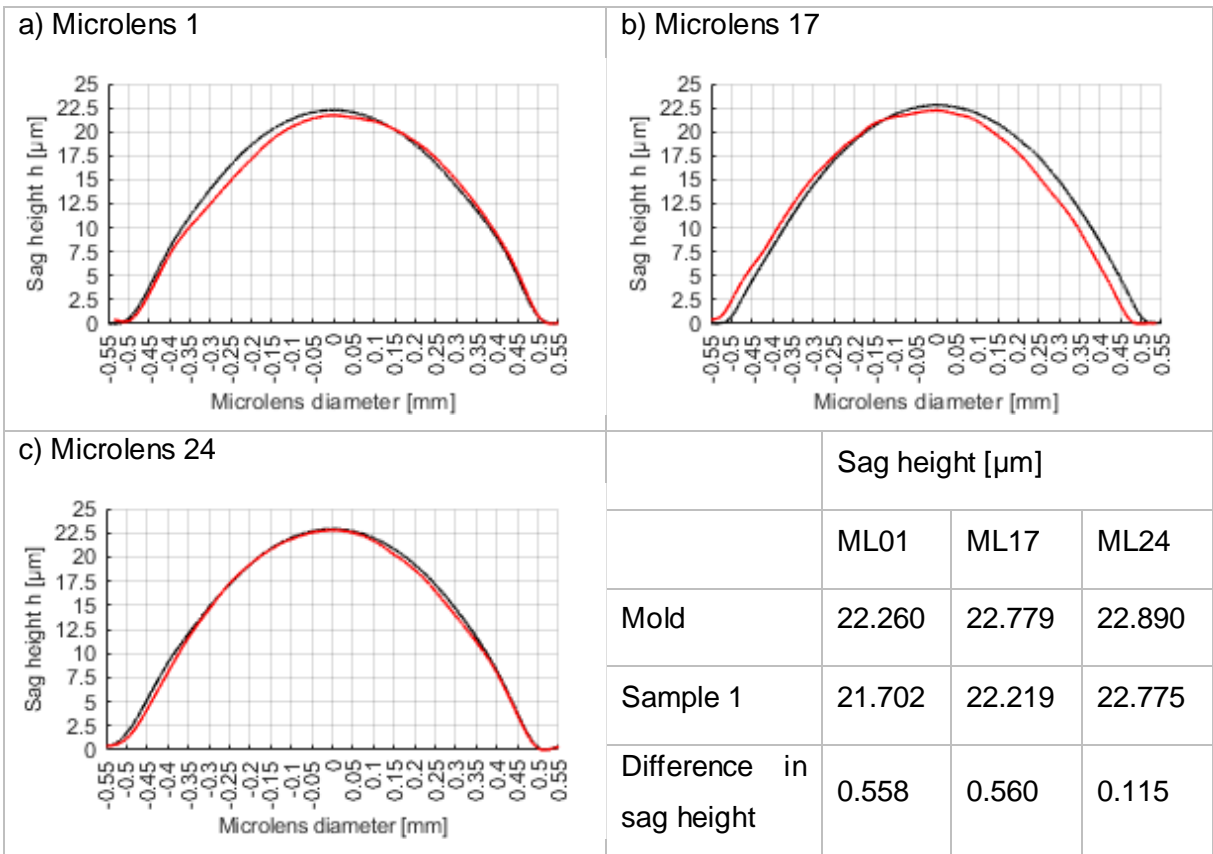


**Table 7-13: Microlens sag height of TS2no1xx**

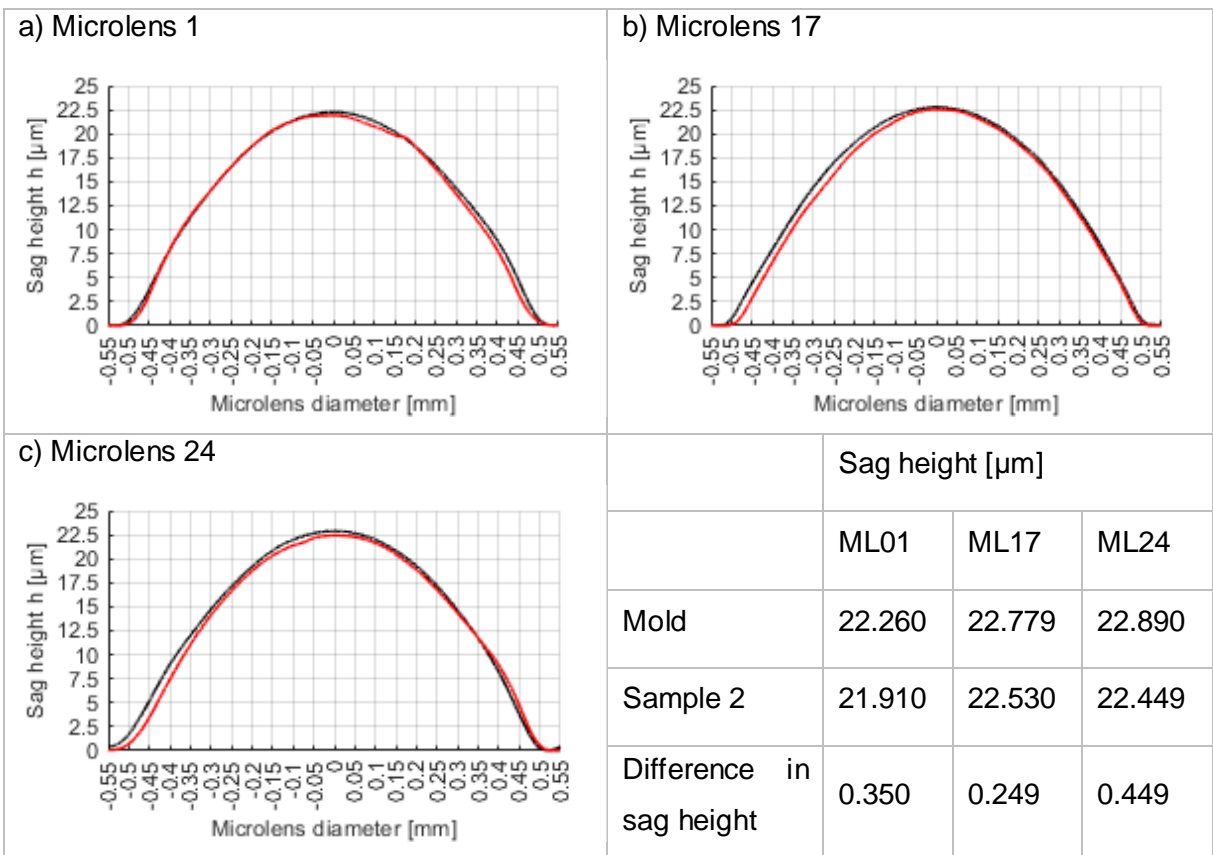


**Table 7-14: Microlens sag height of TS2no2xx**

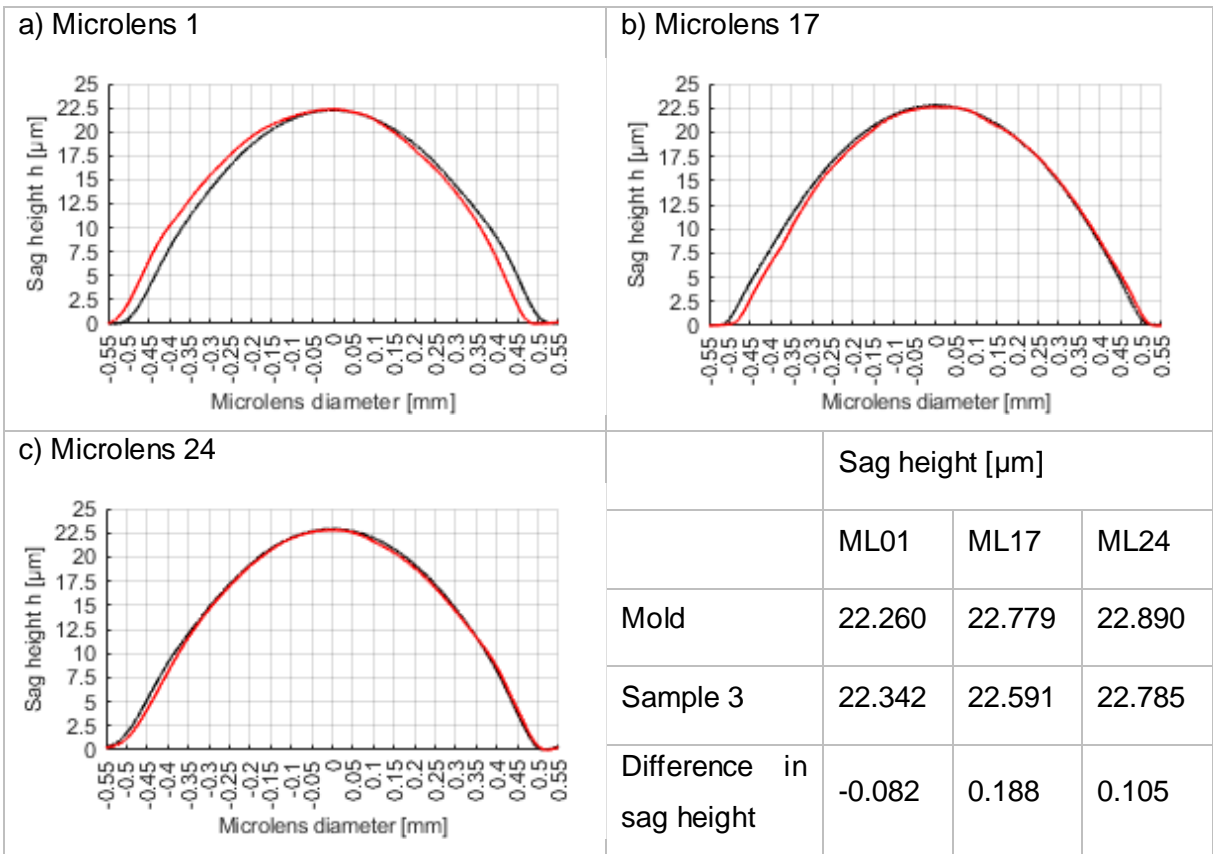


**Table 7-15: Microlens sag height of TS2no3xx**

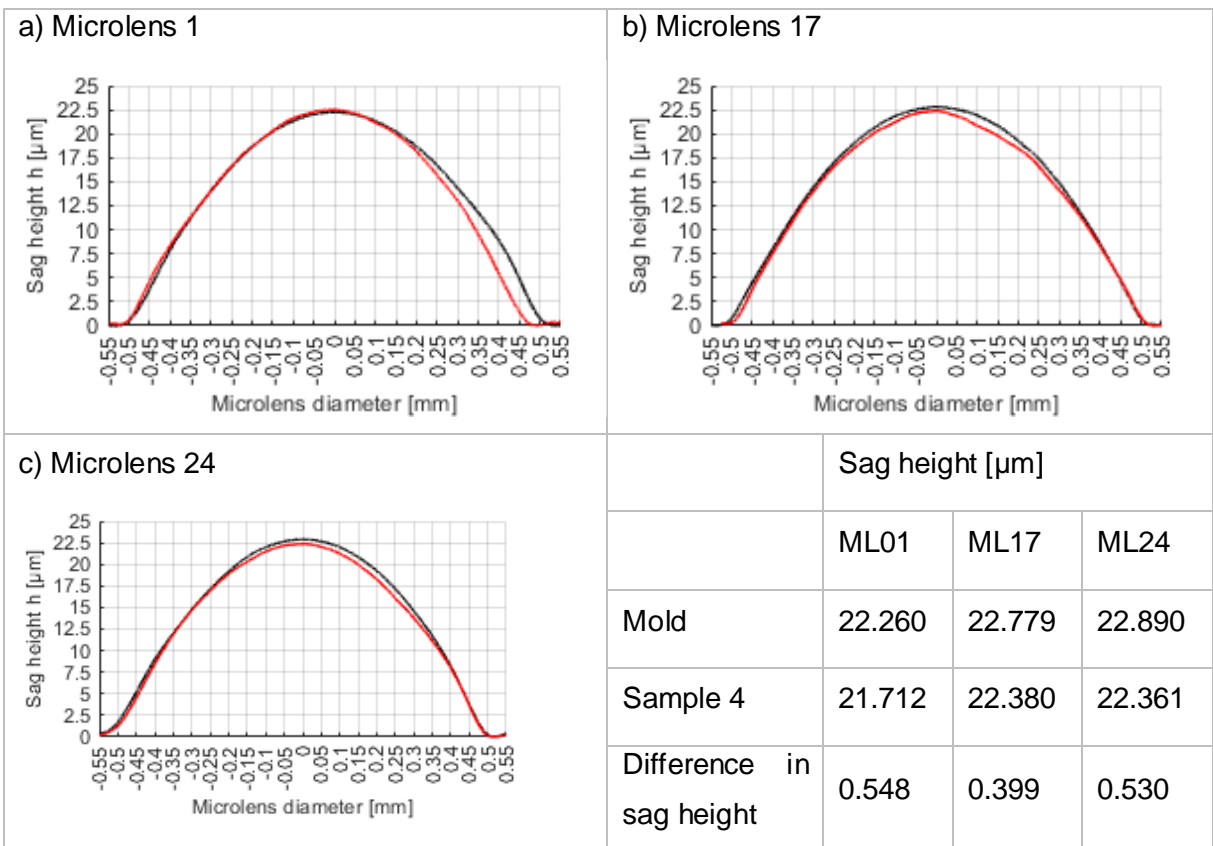


**Table 7-16: Microlens sag height of TS2no4xx**

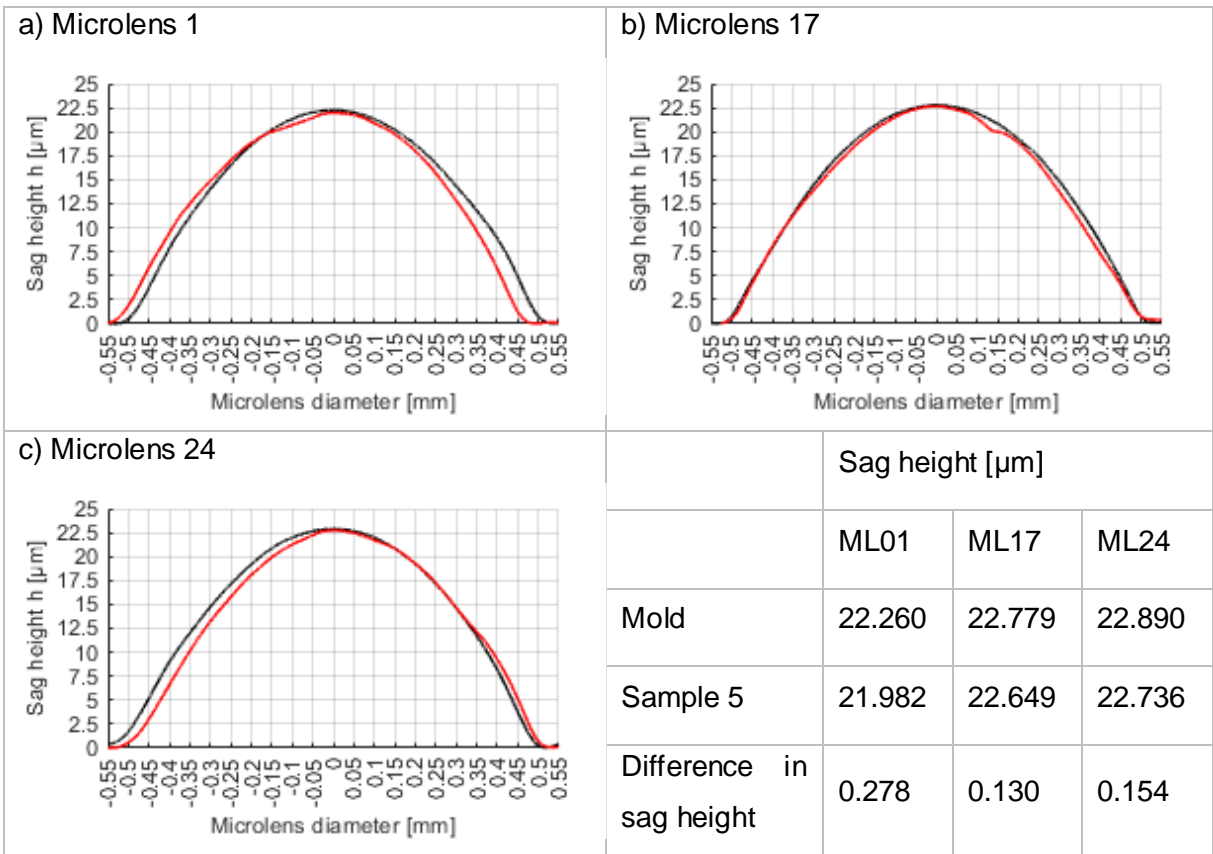


**Table 7-17: Microlens sag height of TS2no5xx**

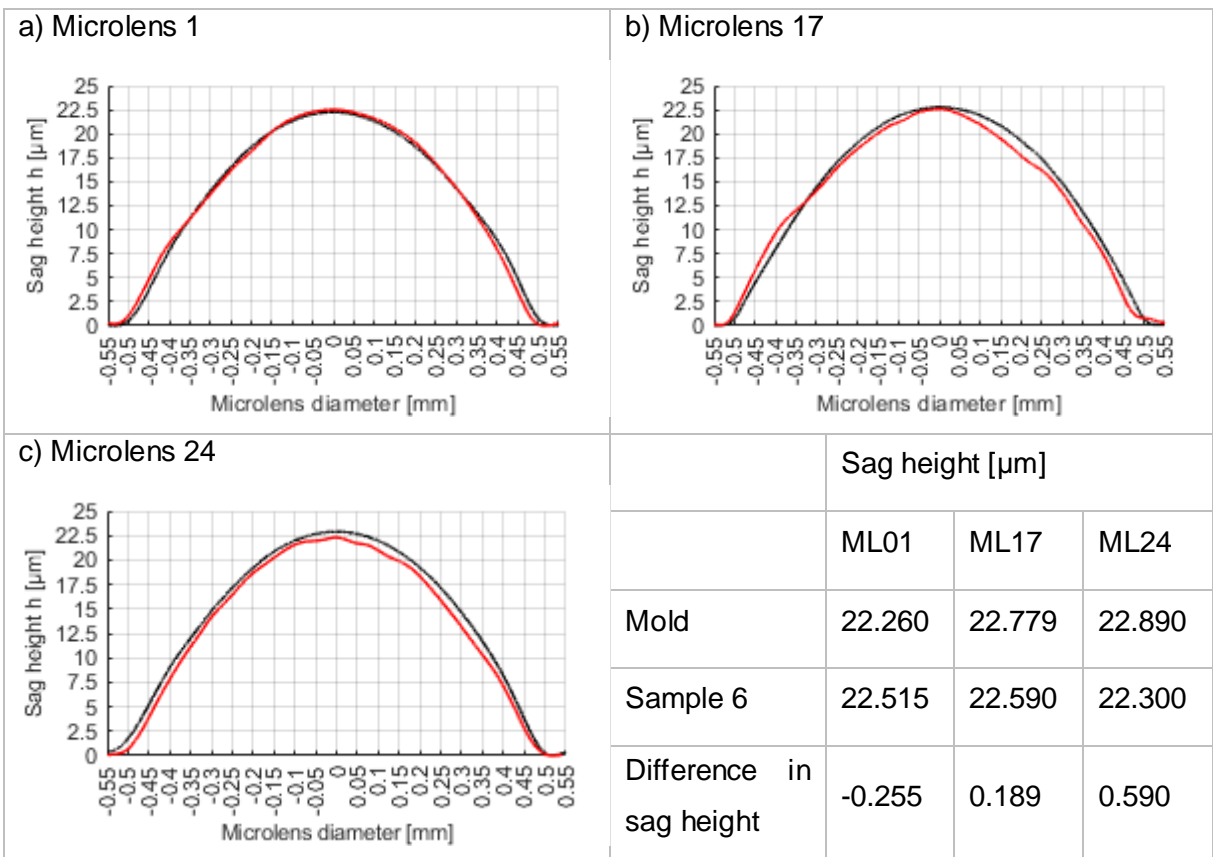


**Table 7-18: Microlens sag height of TS2no6xx**

	PV form error [ $\mu\text{m}$ ]					
	TS2no1xx	Ts2no2xx	TS2no3xx	TS2no4xx	TS2no5xx	TS2no6xx
ML02	1.675	1.643	1.590	1.690	1.659	1.438
ML12	1.026	0.782	1.904	1.458	0.808	1.093

Table 7-19: PV form error results of TS2noxx

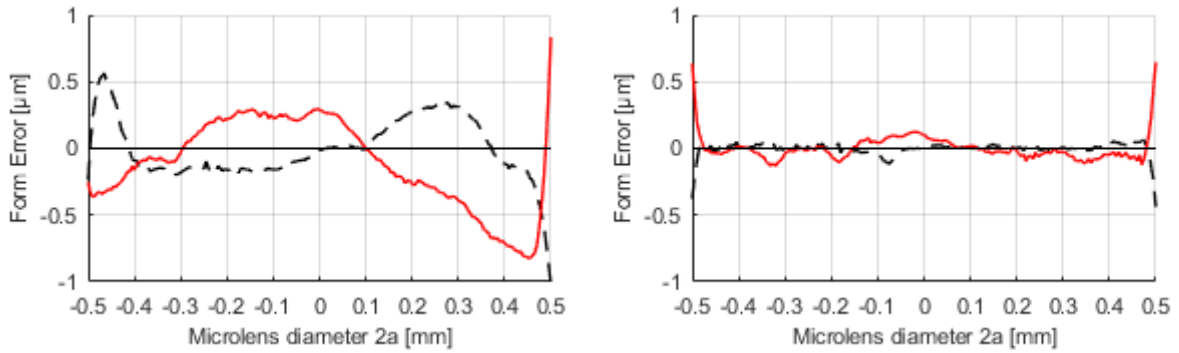


Figure 7-16: Form error of test series 2 left: TS2no202; TS2no212

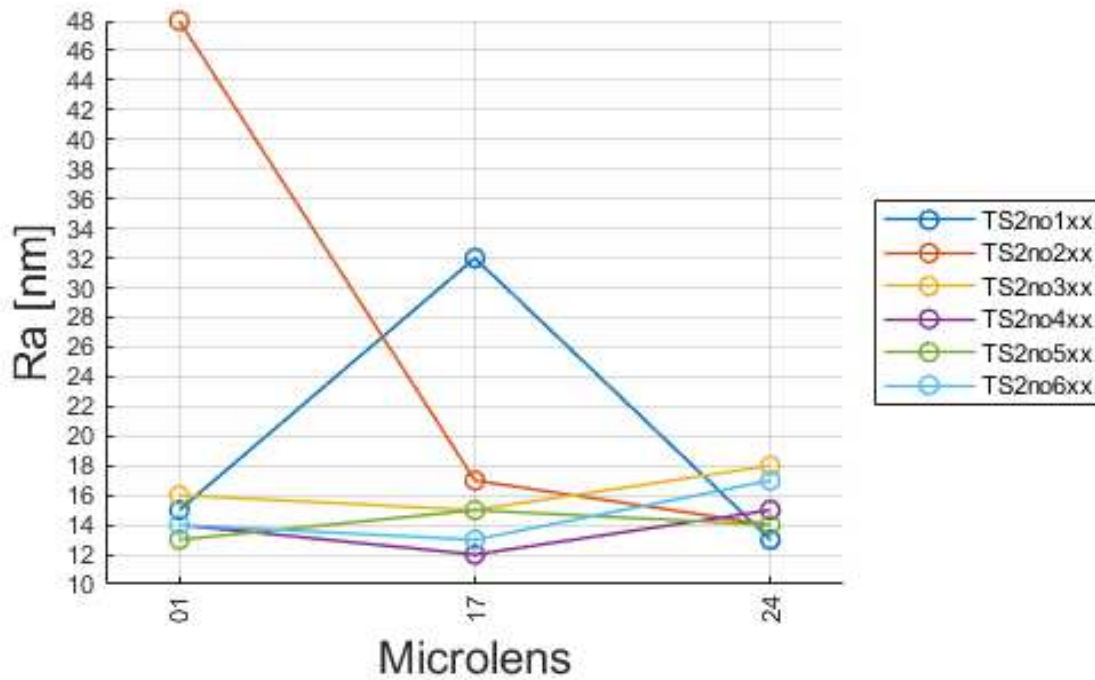
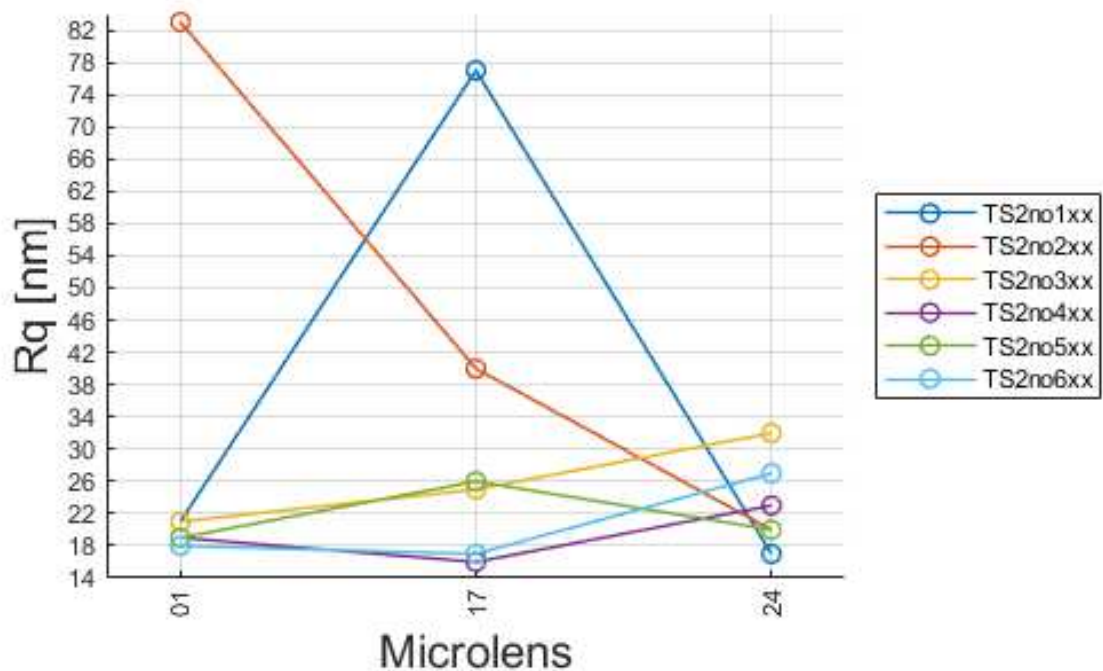


Figure 7-17: Surface roughness Ra of the press-molded samples in test series 2



**Figure 7-18: Surface roughness Rq of the press-molded samples in test series 2**

The results of this test series are discussed in the following. In comparison to the used granule material in the previous test series, the use of plate material was advantageous. While weld lines from the melting grains were still present in the HDPE samples after molding (Figure 7-8), such effects did not occur within this test series.

Micro gas traps in form of flow lines were presented in Figure 7-14 for the heating temperatures 175 °C, 182 °C and 189 °C. With increasing the heating temperature, the gas traps were reduced for the plano-convex lens shape, which is in accordance with the results made in [84]. It is assumed that present gas inside the cavity is better displaced with increased heating temperature due to better flow characteristics of the polymer. However, micro gas voids are still present at the highest temperature and for a compression force of 1.4 kN (TS2no624 in Figure 7-14). The influence of these micro voids on the optical performance should be determined by optical measurements, for example wave aberration measurements with a Mach-Zehnder-interferometer or imaging performance tests. In addition, a further diminishing of gas trapping could be accomplished by the use of an evacuating tool to create a vacuum inside the process chamber.

The variation of the lens diameters for the press-molding parameters is given in Table 7-12. The diameters range from 961.49  $\mu\text{m}$  to 983.48  $\mu\text{m}$ . The overall shrinkage in the lens diameter is smaller than 4 % compared to the mold. Comparing the results for the varied heating temperatures, higher ML diameters can be observed for higher press molding temperatures. Exemplarily shown for ML17, the lens diameter was 969.53  $\mu\text{m}$ , 974.74  $\mu\text{m}$  and 982.74  $\mu\text{m}$  respectively for 175 °C, 182 °C and 189 °C. Thus, the material shrinkage was lowered with increasing the heating temperature, which is similar to the HDPE pressing results. The ML diameters for a pressing force of 0.8 kN were the smallest which could be explainable with an incomplete filling of the mold microstructures. For the samples TS2no2xx, TS2no5xx and TS2no6xx a correlation between the ML diameter and the compression force cannot be seen for individual lenses. Inaccuracies in the measurement results could also be due to the subjectivity of the measurement method.

In difference to the HDPE test series, a correlation between the pressing parameters and the lens sag height results was observed. The difference in the sag height was less than 1  $\mu\text{m}$  for all measured ML. The overall shrinkage was smaller than 3 %. Equal to the results for the lens diameters, the shrinkage in the sag height was prevented with increasing the heating temperature. The difference in the sag height for ML17 molded at 175 °C was 0.560  $\mu\text{m}$ , while it was only 0.118  $\mu\text{m}$  at 189 °C. A reduction of the sag height difference and thus of the shrinkage is also seen when the compression force is increased from 0.8 kN up to 1.2 kN. The smallest sag heights and therefore the highest shrinkage was found for the compression force of 0.8 kN. Comparing the sag heights of ML01, the sag height difference was 0.548  $\mu\text{m}$  for 0.8 kN, decreasing to 0.350  $\mu\text{m}$  for 1.0 kN and down to 0.278  $\mu\text{m}$  for 1.2 kN. For 1.4 kN, the sag height difference was increased again for ML17 and ML24. Due to the waviness of the lens profiles, shown in Table 7-18, a destruction of the profile burst by overpressing could have occurred. On the other side, this explanation is not consistent with the measured form errors of the samples press-molded with the same compression force. The decrease in the sag height difference for higher compression forces is in accordance with the results presented in the publication [63], which was used as a reference for the polycarbonate design of experiments. The improvement of the sag height at higher pressing forces might be due to a better displacement and hence a better filling of the microcavities. Since the pressing force was kept during cooling, it is



secondly assumed that higher pressing forces have a positive influence on the shrinkage as long as the compressive strength of the polymer is not exceeded.

To corroborate these two statements, the form error values should be considered here, too. Comparing all measured values in Table 7-19 with each other, the form errors of TS2no2xx showed the best results. Its form deviation over the lens diameter is plotted in Figure 7-16. The measured form errors of ML12 for all samples were closed to the ML form errors of the mold. The form errors of ML02 were comparatively high in comparison with the mold. However, similar to the HDPE measurements, the form error of ML02 decreased for increased temperatures. For ML12 the form error decreased from TS2no1xx to TS2no2xx. Since all measured values were higher than the form error of the mold, the Rayleigh criterion was not fulfilled for visible light. A respective PV form error smaller than 95 nm and 184 nm was necessary for a wavelength  $\lambda = 380$  nm and  $\lambda = 740$  nm.

A comparison of the shrinkage between the test series conducted with HDPE and PC materials shows that the PC material shrinkage was slightly smaller than in the case of the HDPE. This result was expected, since the macromolecular chains of semi-crystalline polymers start to crystallize during cooling [85].

The measured surfaces roughness values are plotted in Figure 7-17 and Figure 7-18. With exception of the  $R_a$  values of TS2no117 and TS2no201, the individual ML show a uniform characteristic for the varied press-molding parameters. It is assumed that TS2no1xx and TS2no2xx were deteriorated by scratching the mold surface as these samples stuck to the mold after demolding and had to be removed manually. Although the improvement in the surface roughness with increased heating temperature and thus, lowered polymer viscosity was expected due to the results made in [63] and in the HDPE test series, a conclusion about this relationship cannot be drawn here for the molded PC samples. Surprisingly the best  $R_a$  roughness values down to 12 nm were achieved with TS2no4xx. For the HDPE MLA, the comparatively high form errors and differences in sag height of the PC samples pressed at 0.8 kN were explained with an insufficient filling of the microcavities. Eventually, the improved roughness is caused by surface tensions effects as they occur in the thermal reflow process, presented in chapter 4.1.1. However, the roughness values of the other samples were only

marginally higher. With exception of TS2no117 and TS2no201, all measured  $R_a$  values were  $\leq 18$  nm. Considering 50 nm as maximum  $R_a$  surface roughness according to the chapter 2.2, all press-molded MLA were suitable for optical applications. Specifying 2 % as the maximum amount of scattered light according to equation (2-2), a surface roughness  $R_q = 8.7$  nm respectively  $R_q = 4.3$  nm was desired for  $\lambda = 740$  nm and  $\lambda = 380$  nm. In result, the  $R_q$  surface roughness of all press-molded MLA was too high.

As mentioned in chapter 7.1, an improvement of the MLA quality, especially in terms of the form error and the surface is to be aimed at.

As explained in chapter 5.1, a sticking of parts to the mold after demolding is critical in terms of quality. Especially the replicated microstructures are sensitive to damaging. Adhesion effects between the CuZn30 brass and the polycarbonate could be the reason for the part sticking in this test series. The effects could be caused by chemical or physical bonding of the parts, but above all by the relatively high surface roughness of the mold resulting in a mechanical bonding between the two materials. In order to avoid these effects in further studies, the mold surface roughness should be firstly improved followed by an in-depth research about finding an optimum demolding temperature. Demolding at 80 °C seems to be unfavorable for the material combination CuZn30 brass and PC. At last it should be mentioned that mold particles were found again in some substrates. As the mold was cleaned again before this test series was conducted it is assumed that the mold material is not a proper material for press-molding in terms of hardness.

## 7.5 Compression Molding of Test Series 4 – PMMA

The manual adjustment of the heating temperature was carried out in the same way as previously done for the polycarbonate test series. At a temperature of 110 °C and thus, 20 °C lower than the set heating temperature for the first sample, the heat supply was decreased down to 2 %. After demolding, the MLA TS4no3xx, TS4no4xx, TS4no5xx and TS4no6xx stuck to the mold and had to be detached from the mold.

The measurements were conducted following the proceedings of the previous test series with optical polymers. The Olympus OLS4100 was used to measure the microlens diameters which are given in Table 7-20. The sag heights and form errors measured with the Mitaka NH-3SP are given from Table 7-21 to Table 7-27. Finding the focus point on the PMMA substrates with the Mitaka NP-3SP was more difficult to obtain compared to the previous PC measurements. This could be explained with the 6 % higher transparency of the COMOGLAS™ PMMA than the polycarbonate. The line surface roughness was measured at the IFM with a cut-off wavelength  $\lambda_c = 0.250$  mm over a sampling length of the same amount.

	Microlens diameter 2a [ $\mu\text{m}$ ]					
	ML01	ML05	ML12	ML15	ML17	ML24
<b>Mold</b>	1000.12	1000.62	1000.00	999.72	1000.34	1000.37
<b>TS4no1xx</b>	994.12	995.01	993.14	991.16	995.16	994.21
<b>TS4no2xx</b>	994.55	994.46	993.58	992.86	994.18	993.86
<b>TS4no3xx</b>	992.65	994.75	994.49	992.57	994.37	994.00
<b>TS4no4xx</b>	993.65	995.20	992.97	993.10	994.59	994.10
<b>TS4no5xx</b>	992.78	995.75	993.94	992.50	994.59	995.40
<b>TS4no6xx</b>	993.31	994.81	992.10	992.30	992.64	994.37

**Table 7-20: Microlens diameters of test series 4**

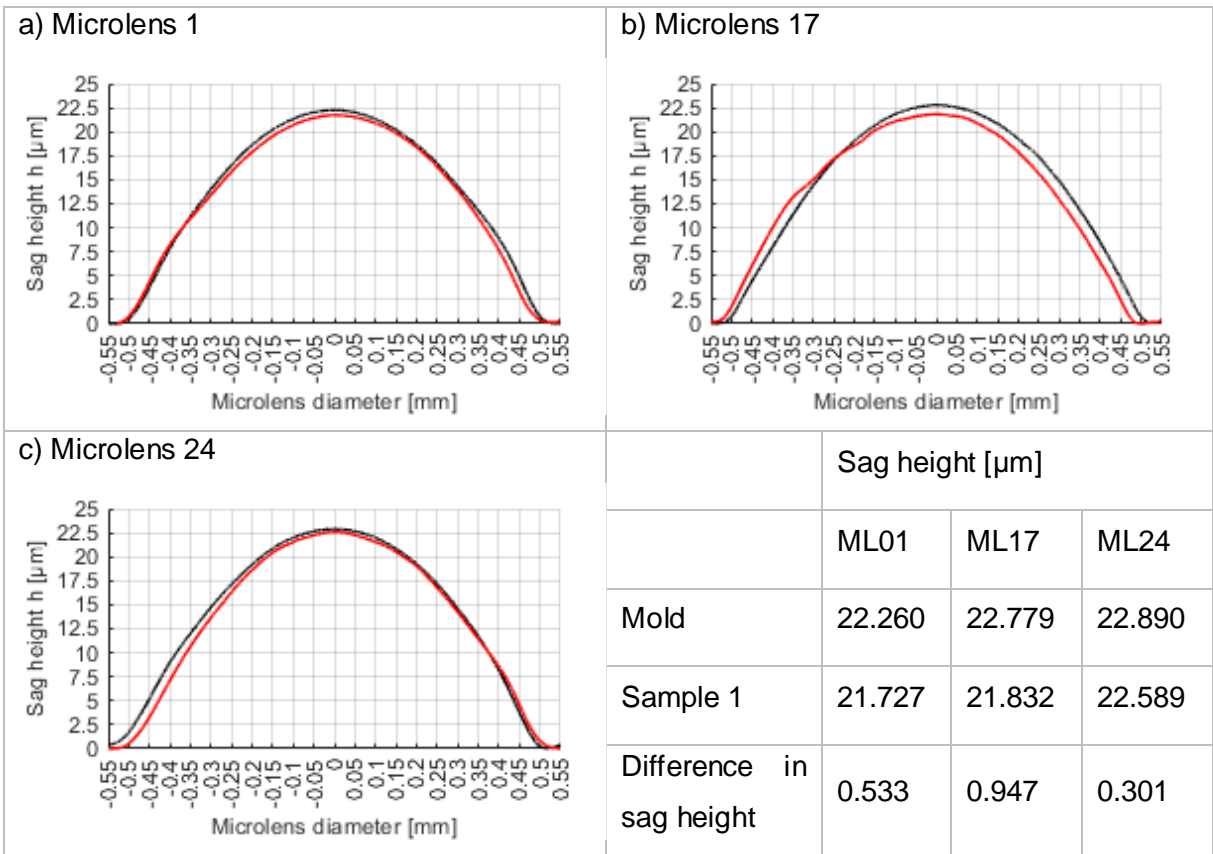


**Table 7-21: Microlens sag height of TS4no1xx**

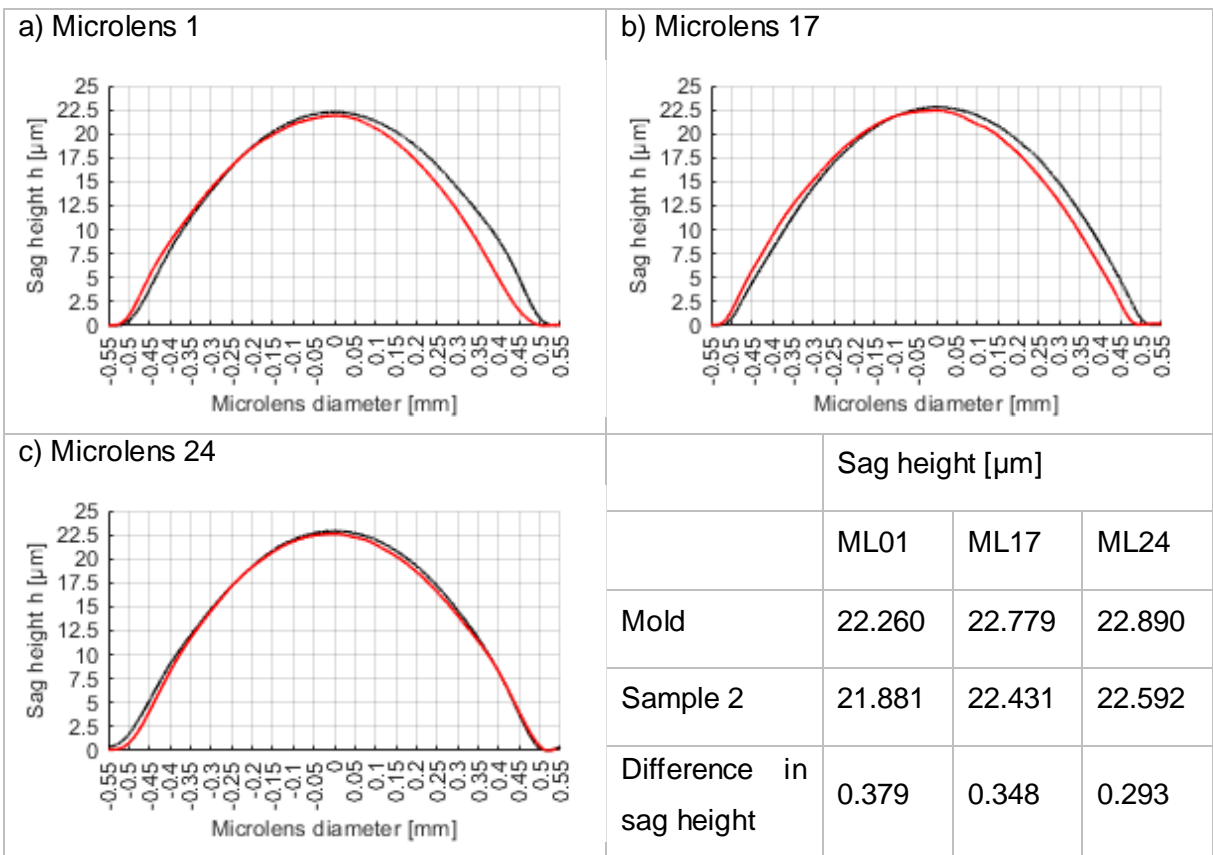


**Table 7-22: Microlens sag height of TS4no2xx**

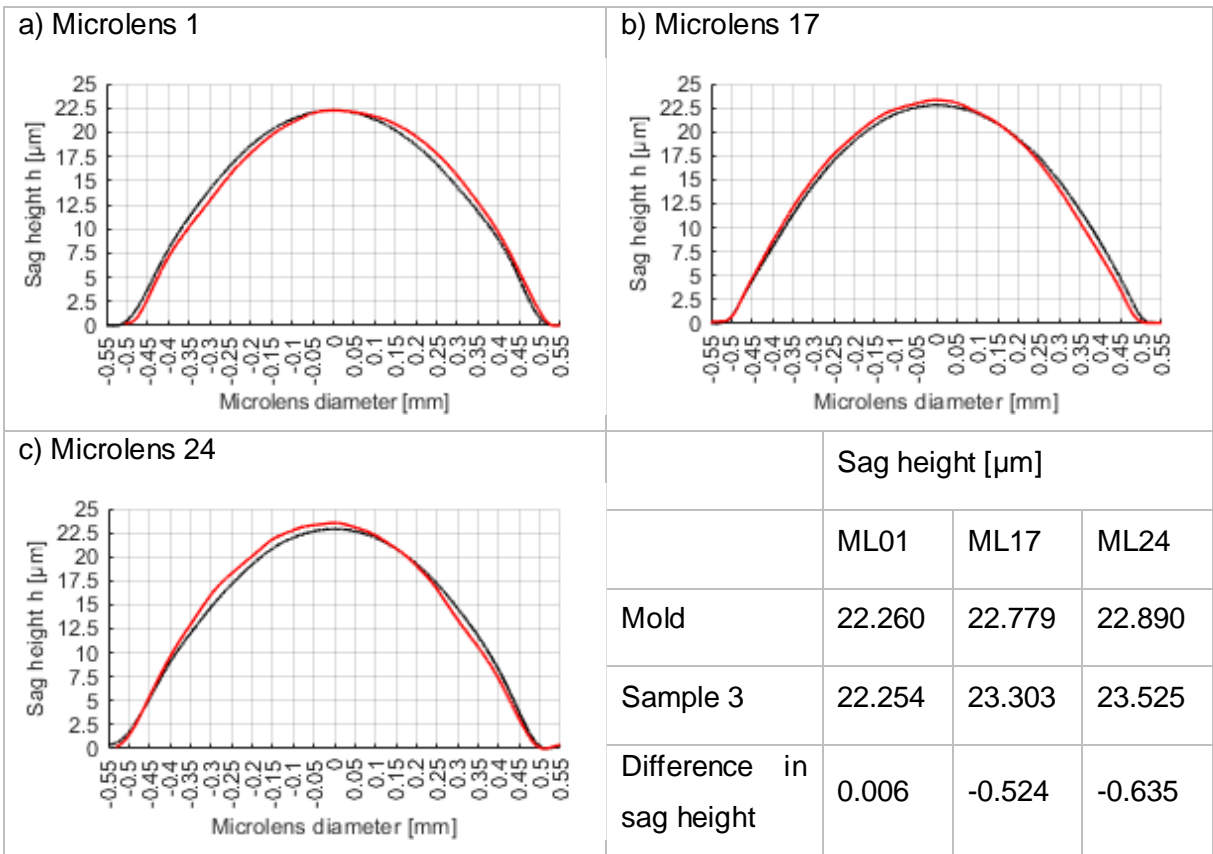


**Table 7-23: Microlens sag height of TS4no3xx**

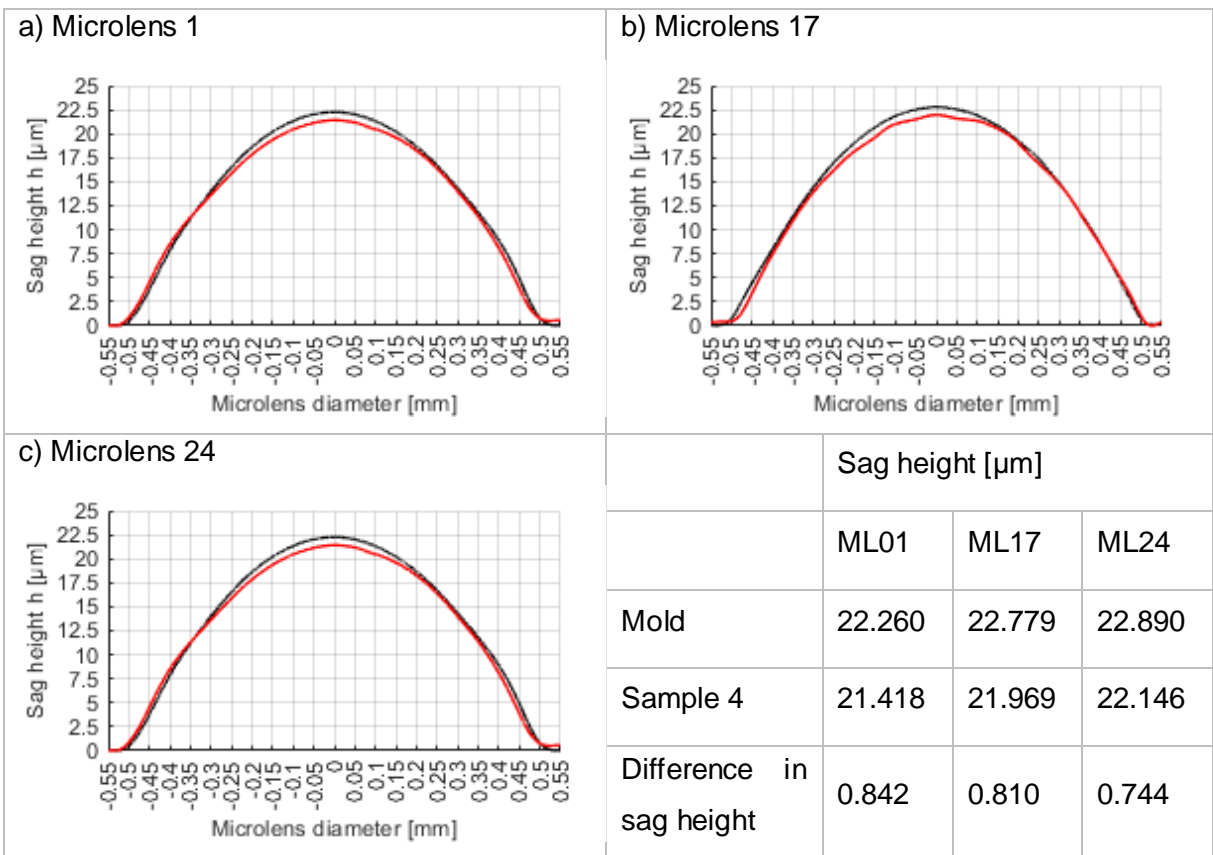


**Table 7-24: Microlens sag height of TS4no4xx**

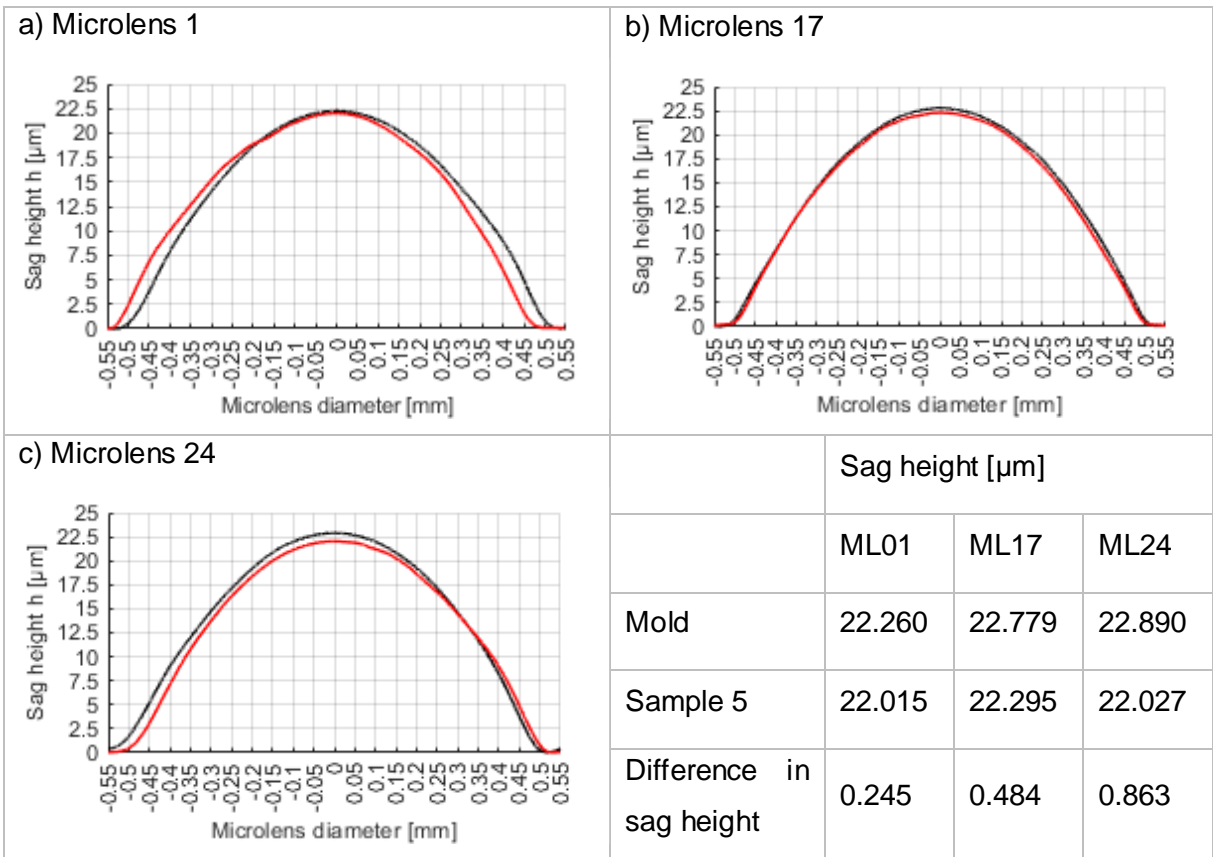


**Table 7-25: Microlens sag height of TS4n05xx**

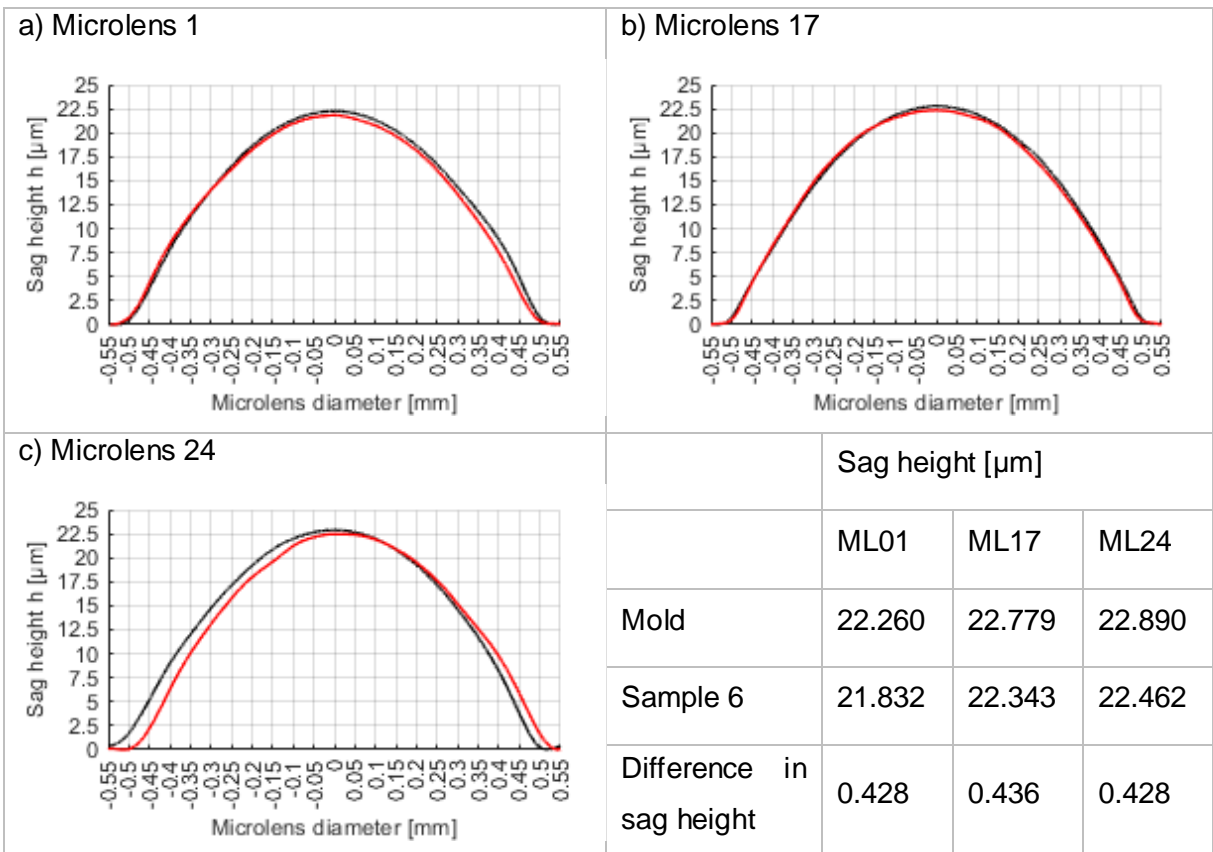


**Table 7-26: Microlens sag height of TS4n06xx**

	PV form error [ $\mu\text{m}$ ]					
	TS2no1xx	Ts2no2xx	TS2no3xx	TS2no4xx	TS2no5xx	TS2no6xx
<b>ML02</b>	1.865	1.403	1.670	1.281	1.497	1.290
<b>ML12</b>	0.801	0.899	0.986	1.050	0.888	1.435

**Table 7-27: PV form error results of test series 4**

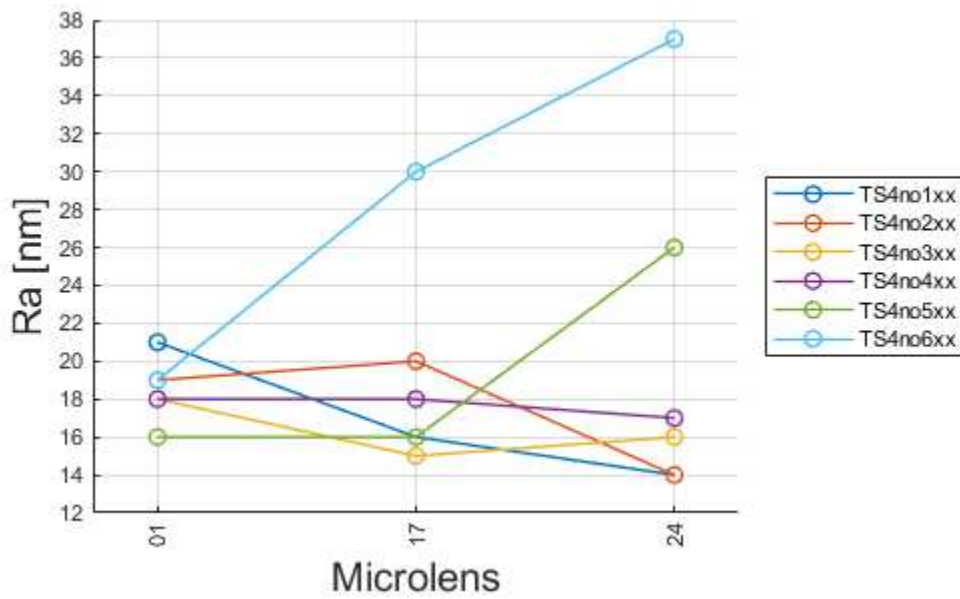


**Figure 7-19: Surface roughness Ra of the press-molded samples in test series 4**

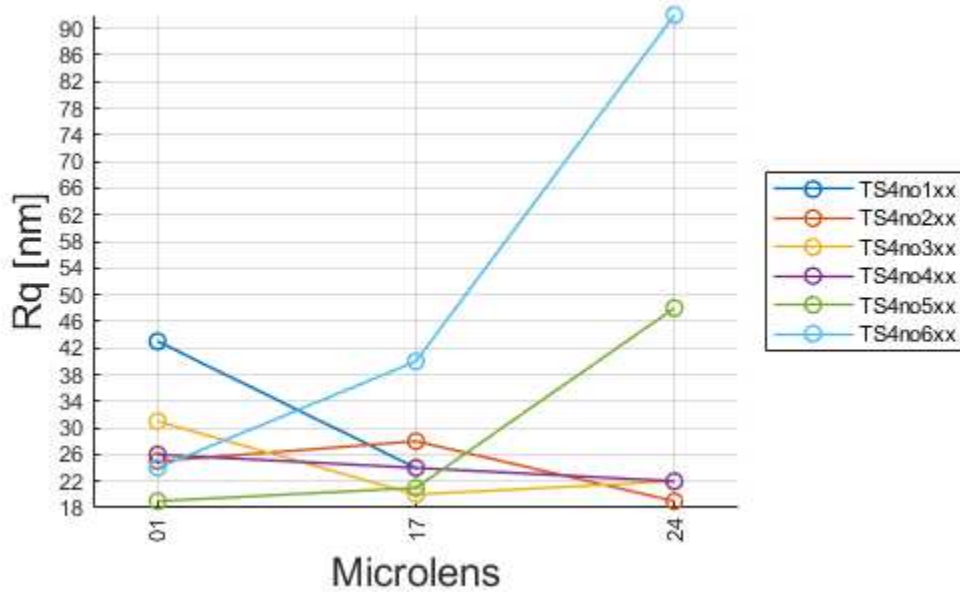


**Figure 7-20: Surface roughness Rq of the press-molded samples in test series 4**

The results of this test series are discussed in the following. The ML diameters vary over all samples from 991.16  $\mu\text{m}$  up to 995.75  $\mu\text{m}$ . Comparing the minimum diameter to the mold, the calculated shrinkage in the diameter is  $\leq 1\%$ .

Equivalent to the PC samples, the shrinkage in the sag height was smaller than 1  $\mu\text{m}$  for all samples. Also in this test series the sag heights increased for higher temperatures. The difference in the sag height of ML01 was 0.533  $\mu\text{m}$  at a heating temperature of 130  $^{\circ}\text{C}$ , decreasing down to 0.379  $\mu\text{m}$  at 140  $^{\circ}\text{C}$  and only 0.006  $\mu\text{m}$  at 150  $^{\circ}\text{C}$ . ML17 and ML24 on TS4no3xx have a higher sag height compared to the mold ML which can be explained by measuring inaccuracies which were already mentioned in the discussion of the results for the HDPE. As observed for HDPE and PC, the sag heights of the ML pressed at 0.8 kN were the smallest resulting in the maximum shrinkage of 3.8 %. The incomplete filling of the microstructures during pressing should be given here as possible explanation again. The smallest sag height difference was shown for all ML on TS4no2xx, pressed at 1.0 kN, whereas for higher pressures, TS4no5xx and TS4no6xx, the sag height slightly decreases again. Eventually the plano-convex microlenses on the array were lengthened due to adhesion effects as these two MLA stuck to the mold after demolding [63].

The form error results are plotted in Table 7-27. Equal to the molded PC MLAs, the Rayleigh criterion is not fulfilled for visible wavelength. The PV form errors of ML12 were all higher than the PV form error of 536 nm of the mold ML. In contrast, the measured PV form errors of TS2no202, TS4no402, TS2no502 and TS2no602 were lower than the respective ML with PV form error of 1.611  $\mu\text{m}$ . An explanation for this characteristic is not found yet as the PV form error results are contradictory to the results made in the previous two test series. The results could be caused by the occurred focus point drifting during the profile measuring as the Mitaka NH-3SP was pushed to its boundaries.

A slight improvement of the  $R_a$  surface roughness on average with increased heating temperatures can be assumed from Figure 7-19, verifying the results discussed before. The surface finish of TS4no5xx and TS4no6xx were obviously deteriorated due to the mold sticking after demolding. Though all measured  $R_a$  values were below 50 nm and



the samples therefore suitable for optical applications, the TIS tolerance of 2 % was not fulfilled for all samples as it can be seen in Figure 7-20.

Possible reasons for the MLA sticking to the molds were already mentioned in the discussion of the results for the PC test series. The same phenomena can be assumed to become effective for the PMMA material. For this reason, discussable avoidance measures should not be mentioned here again.

## 7.6 Mold Microstructure After Compression Molding

During the press-molding experiments, the mold material was exposed to temperatures from room temperature until 189 °C and frictional forces between the mold material and the polymer. After conducting the last press-molding experiments with the PMMA, the mold microstructures and the Imp 3 were observed using the Olympus OLS4100 without prior cleaning.

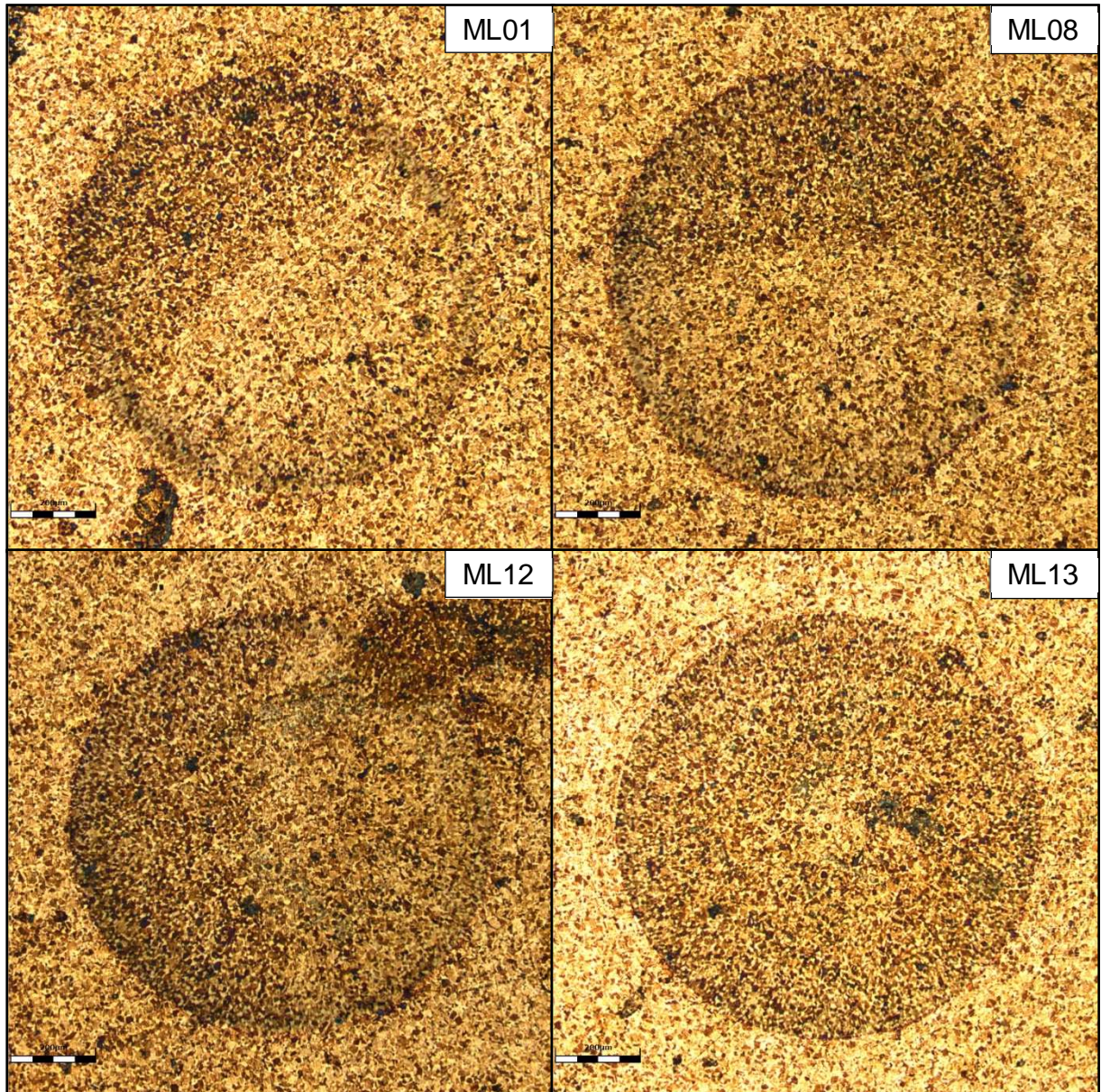


**Figure 7-21: Mold microstructures after the press-molding experiments at 10x magnification; upper left: ML01; upper right: ML08; lower left: ML12; lower right: ML13**

Around 30 samples were compression molded within this study. Comparing the mold in Figure 7-21 after the press-molding experiments with the mold before the press-molding experiments as shown in Figure 7-2, a clear deterioration of the microlens dimensions can be seen. The defined edges created by the diamond cutting process are found rounded and blurred after the experiments. The surface roughness was controlled with the Mitaka MLP-3. The results are given in Table 7-28. With measured  $R_a$  values between 26 nm up to 39 nm, the surface roughness was up to two times higher compared to the initial condition. The  $R_q$  surface roughness showed a similar deterioration.

	<b>ML01</b>	<b>ML17</b>	<b>ML24</b>
<b><math>R_a</math> [nm]</b>	26	29	39
<b><math>R_q</math> [nm]</b>	33	39	55

**Table 7-28:  $R_a$  and  $R_q$  surface roughness values of the mold microlenses after the compression molding experiments**

The tool marks created by the UP turning were still visible as it can be seen in Figure 7-22. Even more recognizable is that the grains of the alloy components of the brass material became clearly visible at a 10x-magnification. The tool wear can be clarified with occurring abrasion caused by excessive frictional forces between the mold and polymer material during the pressing. The changed surface finish is also an indication for the hypothesis that the brass particles found in the molded MLA were abraded during the pressing. Beside the worsening of the surface roughness, residual PMMA fragments were found in the microstructures (Figure 7-22). The residual polymer is probably caused by adhesive wear between polymer and mold material. While the abrasive wear is expected to occur during pressing, the adhesive wear assumingly occurs during the demolding. After the cooling step, the solidified polymer and the brass might adhere to each other due to adhesion effects. The supposed reasons for the occurring adhesion effects were already discussed in chapter 7.4. When the lower mold is moved downwards to open the cavity, the molded MLA is ripped off the upper mold. Due to sliding forces between both materials, the polymer material is locally ruptured and keeps adhered to the brass.

Figure 7-23 shows the tarnishing of the lower mold part 3 after the compression molding experiments. Tarnishing is mostly caused by oxidation of the outermost layer of a surface. During the experiments, the brass material was exposed to fast heating and cooling cycles between room temperature up to 189 °C. The effect of the tarnished surface was not further investigated during this study.

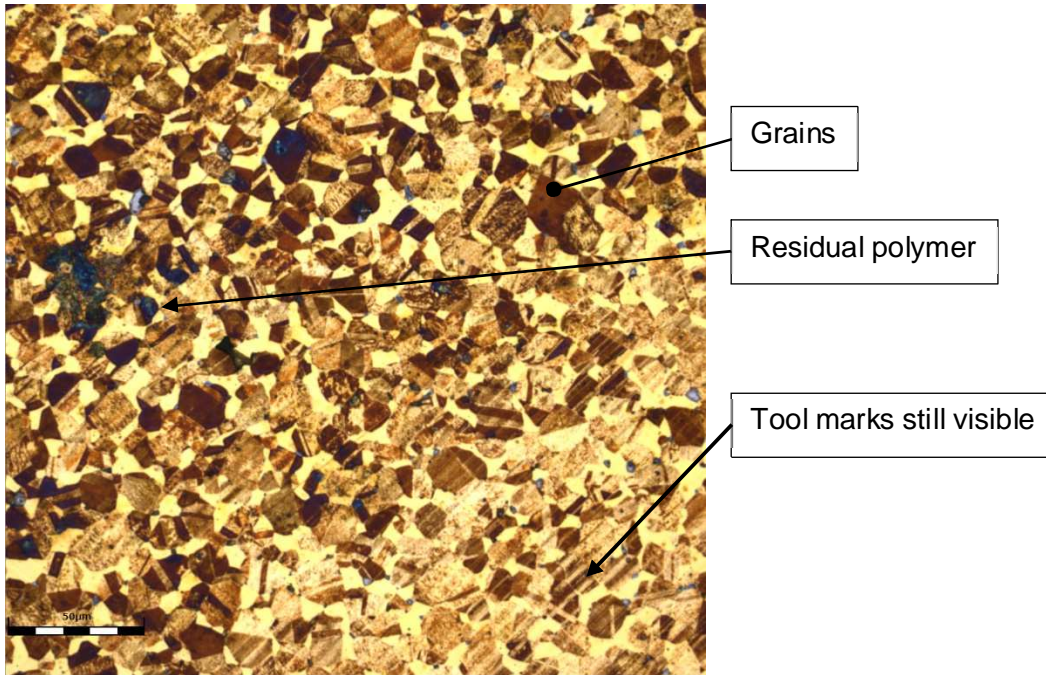


Figure 7-22: Microlens in the mold after pressing in 50x-magnification.

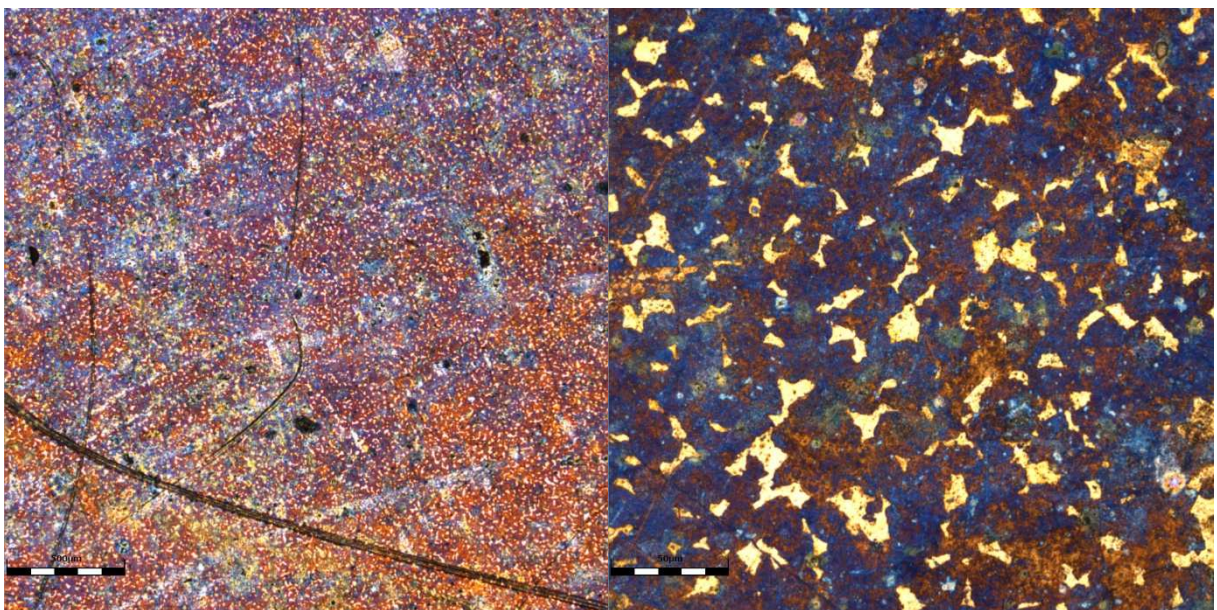


Figure 7-23: Thermal oxidation of the lower mold part 2 after the compression molding experiments

## 8 Summary

In this study the *fabrication and characterization of press-molded polymer microlens arrays* was investigated theoretically and experimentally.

To introduce into the topic, the fundamentals about microlenses, microlens arrays and optical polymers were exemplified. Direct and indirect fabrication methods were identified in the following and the respective state of research was pointed out. Compression molding with a focus on microlenses was further emphasized in chapter 5 to lead over into the experimental part of this study. The objective of the experimental part was the compression molding and the subsequent characterization of MLA made of HDPE, PC and PMMA. Prior to the molding experiments, a mold was designed and fabricated by machine operations. The microlens array was diamond turned and the lenses were characterized by the microlens diameter, sag height, form error and surface roughness. A sufficient uniformity in the microlens diameter and sag height was achieved for the molded array. The form error of the lenses was sufficient for wavelengths in the thermal IR range but too high for visible light. The surface roughness on the microlens apex was comparatively high for optical applications. In result, the mold quality was suitable for the experiments and the intermediate goal of the experimental part, the precision machining of a mold, was achieved. The press-molding experiments were conducted, and the molded MLA were characterized by means of the same dimensions as the mold. Finally, the MLA results were set into comparison to the mold microstructure dimensions and discussed in chapter 7. In result, all needed measures to fulfill the objective of this study were realized.

The first test series was conducted in order to determine the needed amount of material to fill the cavity and to investigate the effect of the incremental heat supply on the heating of the mold charge. It was determined that the heat supply had to be set carefully for each material for the Toshiba GMP211 compression press by adjusting the incremental heat input and the heating time. The parameters temperature and compression force were varied in the upcoming test series 1 – 3. The results of these experiments can be summarized as follows:

- An increased heating temperature had a positive effect on the part shrinkage. The diameters and sag height deviated less from the respective mold for higher heating temperatures.
- The compression force in the range 1.0 – 1.2 kN had a positive effect on the part shrinkage. The diameters and sag height deviated less from the respective mold the most for a compression force of 0.8 kN.
- The form error of the ML pressed at a low pressure of 0.8 kN was higher than the form errors of the ML pressed at higher pressures of 1.0 kN and 1.2 kN. For 1.4 the form error increased for some ML again.
- The Rayleigh criterion, used to characterize possible wavefront aberration, was only fulfilled for the HDPE microlens arrays in the thermal IR wavelength range. The Rayleigh criterion was not fulfilled for the PC and PMMA microlens arrays in the visible wavelength range.
- The heating temperature is assumed to have a positive effect on the surface roughness due to a decreased viscosity of the polymer. The surface roughness of the HDPE and PMMA samples was improved for increasing temperatures. This effect could not be shown for the PC samples.
- All molded HDPE MLA, except the one pressed at 0.8 kN were within the tolerance of 2 % for total integrated scattering. The  $R_q$  surface roughness of the PC and PMMA samples was found too high to prevent TIS.
- Part sticking to the mold after demolding is assumed to be caused by adhesion effects. In addition, residual polymer was found after detaching the samples which is assumingly caused by adhesive friction.
- Micro gas trapping was diminished at the used compression press for increasing the heating temperature
- Brass mold material particles were partially found in molded samples.

As it was seen in chapter 7.6, a deterioration of the mold surface occurred during the experiments. The microlens edges were found blurred, the surface roughness was increased and an oxidation of the brass material was observed.

Some of the created results are directly related to the mold. Future research could focus on finding a more suitable mold material by comparing the quality of parts molded from different mold materials or coatings. In this regard, the quality of the diamond turned microlenses should be improved in terms of the surface roughness and the form error. Furthermore, as some parts stuck to the mold after demolding, a further study could concentrate on finding the best suitable demolding temperature for the pressed materials. The compression molding results for the materials could be further validated by a molding simulation.

## List of Cited Literature

- [1] UNIVERSITY OF STUTTGART: *Institute for Micro Integration - Institut*.  
URL <https://www.ifm.uni-stuttgart.de/en/institute/>. - abgerufen am 2019-08-26
- [2] YAN LABORATORY, KEIO UNIVERSITY: *Yan Laboratory for Precision Machining and Nano Processing (PMNP) Research*.  
URL <http://www.yan.mech.keio.ac.jp/research/index.html?lang=en>
- [3] DIN DEUTSCHES INSTITUT FÜR NORMUNG E. V.: ISO/DIS 14880-1:2017:2017-09
- [4] HOU, TINGXIU ; ZHENG, CHONG ; BAI, SHI ; MA, QIAN ; BRIDGES, DENZEL ; HU, ANMING ; DULEY, W. W.: Fabrication, characterization, and applications of microlenses. In: *Applied Optics* Bd. 54 (2015), Nr. 24, S. 7366
- [5] KANG, S. ; SU-DONG MOON: Design and fabrication of micro optical components for optical data storage by micromolding. In: *Technical Digest. CLEO/Pacific Rim 2001. 4th Pacific Rim Conference on Lasers and Electro-Optics (Cat. No.01TH8557)*. Bd. 2. Chiba, Japan : IEEE, 2001 — ISBN 978-0-7803-6738-8, S. II-16-II-17
- [6] JAHNS, J. ; BRENNER, K.-H. (Hrsg.) ; RHODES, W. T. (Hrsg.): *Microoptics: From Technology to Applications, Springer Series in Optical Sciences*. Bd. 97. New York, NY : Springer New York, 2004 — ISBN 978-1-4419-1931-1
- [7] NUSSBAUM, PH ; VÖLKELE, R ; HERZIG, H P ; EISNER, M ; HASELBECK, S: Design, fabrication and testing of microlens arrays for sensors and microsystems. In: *Pure and Applied Optics: Journal of the European Optical Society Part A* Bd. 6 (1997), Nr. 6, S. 617–636
- [8] GUPTA, K. (Hrsg.): *Micro and Precision Manufacturing, Engineering Materials*. Cham : Springer International Publishing, 2018 — ISBN 978-3-319-68800-8
- [9] WU, CHENG-HSIEN ; LIU, CHUN-YU: Closed-die compression molding for optical lenses. In: *2010 International Symposium on Computer, Communication, Control and Automation (3CA)*. Tainan, Taiwan : IEEE, 2010 — ISBN 978-1-4244-5565-2, S. 208–210
- [10] MOON, SU-DONG: Fabrication of polymeric microlens of hemispherical shape using micromolding. In: *Optical Engineering* Bd. 41 (2002), Nr. 9, S. 2267
- [11] HARVEY, JAMES E.: Total integrated scatter from surfaces with arbitrary roughness, correlation widths, and incident angles.  
In: *Optical Engineering* Bd. 51 (2012), Nr. 1, S. 013402



- [12] Optik und Photonik – Erstellung von Zeichnungen für optische Elemente und Systeme – Teil 8: Oberflächengüte; Rauheit und Welligkeit (ISO 10110-8:2010). In: DIN DEUTSCHES INSTITUT FÜR NORMUNG E. V. (Hrsg.) , Beuth Verlag GmbH (2012)
- [13] DIN DEUTSCHES INSTITUT FÜR NORMUNG E.V.: Geometrische Produktspezifikation (GPS) – Oberflächenbeschaffenheit: Flächenhaft – Teil 1: Angabe von Oberflächenbeschaffenheit (ISO 25178-1:2016); Deutsche Fassung EN ISO 25178-1:2016, 2016
- [14] SINZINGER, STEFAN ; JAHNS, JURGEN: *Microoptics*. 2nd rev. and enlarged ed. Weinheim : Wiley-VCH, 2003 — ISBN 978-3-527-40355-4
- [15] OTTEVAERE, H ; COX, R ; HERZIG, H P ; MIYASHITA, T ; NAESSENS, K ; TAGHIZADEH, M ; VÖLKEL, R ; WOO, H J ; U. A.: Comparing glass and plastic refractive microlenses fabricated with different technologies. In: *Journal of Optics A: Pure and Applied Optics* Bd. 8 (2006), Nr. 7, S. S407–S429
- [16] MUKAIDA, MAO ; YAN, JIWANG: Ductile machining of single-crystal silicon for microlens arrays by ultraprecision diamond turning using a slow tool servo. In: *International Journal of Machine Tools and Manufacture* Bd. 115 (2017), 'S. 2–14
- [17] ZHOU, TIAN-FENG ; RUAN, BEN-SHUAI ; ZHOU, JIA ; DONG, XIAO-BIN ; LIANG, ZHI-QIANG ; WANG, XI-BIN: Mechanism of brittle fracture in diamond turning of microlens array on polymethyl methacrylate. In: *Advances in Manufacturing* Bd. 7 (2019), Nr. 2, S. 228–237
- [18] DALY, D ; STEVENS, R F ; HUTLEY, M C ; DAVIES, N: The manufacture of microlenses by melting photoresist. In: *Measurement Science and Technology* Bd. 1 (1990), Nr. 8, S. 759–766
- [19] ZIMMERMANN, ANDRÉ: Vorlesungsmanuskript Aufbau und Verbindungstechnik für Mikrosysteme - Sensor und Systemaufbau - 4 Vielfalt von Mikrosensoren (Vorlesungsmanuskript). Stuttgart, 2017
- [20] KOIKE, YASUHIRO: Optical Functional Materials 2019 - Display Applications (Vorlesungsmanuskript). Yokohama, 2019
- [21] SIELER, MARCEL ; SCHREIBER, PETER ; DANNBERG, PETER ; BRÄUER, ANDREAS ; TÜNNERMANN, ANDREAS: Ultraslim fixed pattern projectors with inherent homogenization of illumination. In: *Applied Optics* Bd. 51 (2012), Nr. 1, S. 64
- [22] FÜCHSEL, KEVIN: Lighting the way to your car. In: *Lighting the way to your car* (2015), Nr. 10/2015, S. 2

- [23] YUAN, WEI ; LI, LI-HUA ; LEE, WING-BUN ; CHAN, CHANG-YUEN: Fabrication of Microlens Array and Its Application: A Review. In: *Chinese Journal of Mechanical Engineering* Bd. 31 (2018), Nr. 1
- [24] SYMMONS, ALAN ; SCHAUB, MICHAEL P.: *Field guide to molded optics, SPIE field guides*. Bellingham, Washington USA : SPIE Press, 2016 — ISBN 978-1-5106-0124-6
- [25] SCHAUB, MICHAEL P.: *The Design of Plastic Optical Systems* : SPIE, 2009— ISBN 978-0-8194-7890-0
- [26] DOUSHKINA, VALENTINA ; FLEMING, ERIK: Optical and mechanical design advantages using polymer optics. In: HATHEWAY, A. E. (Hrsg.): San Diego, CA, 2009, S. 74240Q
- [27] SCHAUB, MICHAEL ; SCHWIEGERLING, JIM ; FEST, ERIC ; SHEPARD, R. HAMILTON ; SYMMONS, ALAN: *Molded Optics: Design and Manufacture*, 2016 — ISBN 978-1-4398-3258-5
- [28] SIMMONS, BLAKE A.: Micromolding (Injection and Compression Molding). In: LI, D. (Hrsg.): *Encyclopedia of Microfluidics and Nanofluidics*. Boston, MA : Springer US, 2014 — ISBN 978-3-642-27758-0, S. 1–10
- [29] HECKELE, M ; SCHOMBURG, W K: Review on micro molding of thermoplastic polymers. In: *Journal of Micromechanics and Microengineering* Bd. 14 (2004), Nr. 3, S. R1–R14
- [30] WEBER, MARVIN J.: *Handbook of optical materials, The CRC Press laser and optical science and technology series*. Boca Raton : CRC Press, 2003 — ISBN 978-0-8493-3512-9
- [31] KOIKE, YASUHIRO: Optical Functional Materials 2019 - Refractive Index (Vorlesungsmanuskript). Yokohama, 2019
- [32] EDMUND OPTICS GMBH: *SPEZIFIKATIONEN FÜR OPTISCHES GLAS*. URL <https://www.edmundoptics.de/resources/application-notes/optics/optical-glass/>
- [33] KOIKE, YASUHIRO: Optical Functional Materials 2019 - Wavelength and Temperature Dependence of Refractive Index. Yokohama, 2019
- [34] YASUHIRO, KOIKE: Optical Functional Materials 2019. Birefringence. Yokohama, 2019
- [35] LI, HUI ; LI, LIKAI ; NAPLES, NEIL J. ; ROBLEE, JEFFREY W. ; YI, ALLEN Y.: Micro-optical fabrication by ultraprecision diamond machining and precision molding. In: *Frontiers of Mechanical Engineering* Bd. 12 (2017), Nr. 2, S. 181–192

- [36] CLAYTOR, NELSON E. ; CLAYTOR, RICHARD N.: Polymer imaging optics for the thermal infrared. In: ANDRESEN, B. F. ; FULOP, G. F. (Hrsg.): Orlando, FL, 2004, S. 107
- [37] ABDUL MANAF, AHMAD ROSLI ; YAN, JIWANG: Press molding of a Si–HDPE hybrid lens substrate and evaluation of its infrared optical properties. In: *Precision Engineering* Bd. 43 (2016), S. 429–438
- [38] HORWITZ, JAMES W.: Infrared refractive index of polyethylene and a polyethylene-based material. In: *Optical Engineering* Bd. 50 (2011), Nr. 9, S. 093603
- [39] EHRENSTEIN, GOTTFRIED W.: *Polymer-Werkstoffe: Struktur - Eigenschaften - Anwendung*. 3. Aufl. München : Hanser, 2011 — ISBN 978-3-446-42967-3
- [40] EGERTON UNIVERSITY, PHYSICS DEPARTMENT, P.O. BOX 536 EGERTON-20115, KENYA ; NDEGWA, NJOROGI G. ; NDIRITU, F. G. ; EGERTON UNIVERSITY, PHYSICS DEPARTMENT, P.O. BOX 536 EGERTON-20115, KENYA ; HUSSEIN, GOLICHA S. A. ; EGERTON UNIVERSITY, PHYSICS DEPARTMENT, P.O. BOX 536 EGERTON-20115, KENYA ; KAMWERU, P. K. ; CHUKA UNIVERSITY, DEPARTMENT OF PHYSICAL SCIENCES, P.O. BOX 107 CHUKA-60400, KENYA ; U. A.: Reflectance, Transmittance and Absorptance of HDPE, LDPE, Glass and Sand Layer Used in a SAH. In: *International Journal of Applied Physics and Mathematics* Bd. 4 (2014), Nr. 6, S. 406–416
- [41] MARSHALL, IAN: Molded plastic lens design. In: BRAAT, J. J. M. (Hrsg.): . Glasgow, United Kingdom, 1996, S. 698–708
- [42] BRYDSON, J. A.: *Plastics materials*. 7th ed. Oxford ; Boston : Butterworth-Heinemann, 1999 — ISBN 978-0-7506-4132-6
- [43] RÖTTING, O. ; RÖPKE, W. ; BECKER, H. ; GÄRTNER, C.: Polymer microfabrication technologies. In: *Microsystem Technologies* Bd. 8 (2002), Nr. 1, S. 32–36
- [44] HUTLEY, M C: Microlens arrays. In: *Physics Education* Bd. 29 (1994), Nr. 3, S. 160–163
- [45] YANG, HSIHARNG ; CHAO, CHING-KONG ; WEI, MAU-KUO ; LIN, CHE-PING: High fill-factor microlens array mold insert fabrication using a thermal reflow process. In: *Journal of Micromechanics and Microengineering* Bd. 14 (2004), Nr. 8, S. 1197–1204

- [46] BECKERT, ERIK ; KEMPER, FALK ; SCHREIBER, PETER ; REIF, MAXIMILIAN ; DANNBERG, PETER: Inkjet printing of microlens arrays on large, lithographic structured substrates. In: VON FREYMAN, G. ; SCHOENFELD, W. V. ; RUMPF, R. C. (Hrsg.): *Advanced Fabrication Technologies for Micro/Nano Optics and Photonics XII*. San Francisco, United States : SPIE, 2019 — ISBN 978-1-5106-2502-0, S. 11
- [47] LUO, YU ; WANG, LI ; DING, YUCHENG ; WEI, HUIFEN ; HAO, XIUQING ; WANG, DONGDONG ; DAI, YANG ; SHI, JINFENG: Direct fabrication of microlens arrays with high numerical aperture by ink-jetting on nanotextured surface. In: *Applied Surface Science* Bd. 279 (2013), S. 36–40
- [48] HAYES, D.J. ; COX, W.R.: Micro-jet printing of polymers for electronics manufacturing. In: *Proceedings of 3rd International Conference on Adhesive Joining and Coating Technology in Electronics Manufacturing 1998 (Cat. No.98EX180)*. Binghamton, NY, USA : IEEE, 1998 — ISBN 978-0-7803-4934-6, S. 168–173
- [49] VILMI, P. ; MYLLYLÄ, R. ; FABRITIUS, T.: Inkjet printed microlens array on patterned substrate. In: VON FREYMAN, G. ; SCHOENFELD, W. V. ; RUMPF, R. C. (Hrsg.): . San Francisco, California, USA, 2013, S. 861317
- [50] GERCHNAN, MARK C.: Specifications And Manufacturing Considerations Of Diamond Machined Optical Components. In: FISCHER, R. E. ; SMITH, W. J. (Hrsg.): . Los Angeles, CA, 1986, S. 36
- [51] DAVIES, MATTHEW A. ; EVANS, CHRISTOPHER J. ; VOHRA, RASHMI R. ; BERGNER, BRENT C. ; PATTERSON, STEVEN R.: Application of precision diamond machining to the manufacture of microphotronics components. In: KLEY, E.-B. ; HERZIG, H. P. (Hrsg.): . San Diego, California, USA, 2003, S. 94
- [52] GLÄBE, RALF ; RIEMER, OLTMANN: Diamond machining of micro-optical components and structures. In: THIENPONT, H. ; VAN DAELE, P. ; MOHR, J. ; ZAPPE, H. (Hrsg.): . Brussels, Belgium, 2010, S. 771602
- [53] CHEN, CHUN-CHIEH ; CHENG, YUAN-CHIEH ; HSU, WEI-YAO ; CHOU, HSIAO-YU ; WANG, PEI-JEN ; TSAI, DIN PING: Slow tool servo diamond turning of optical freeform surface for astigmatic contact lens. In: BURGE, J. H. ; FÄHNLE, O. W. ; WILLIAMSON, R. (Hrsg.): . San Diego, California, USA, 2011, S. 812617
- [54] ROEDER, MARCEL ; GUENTHER, THOMAS ; ZIMMERMANN, ANDRÉ: Review on Fabrication Technologies for Optical Mold Inserts. In: *Micromachines* Bd. 10 (2019), Nr. 4, S. 233
- [55] MANAF, AHMAD ROSLI ABDUL ; SUGIYAMA, TSUNETOSHI ; YAN, JIWANG: Design and fabrication of Si-HDPE hybrid Fresnel lenses for infrared imaging systems. In: *Optics Express* Bd. 25 (2017), Nr. 2, S. 1202

- [56] ZIMMERMANN, ANDRÉ: Vorlesung Grundlagen der Mikrotechnik - 9. Mikrotechnische Bauteile aus Kunststoff (Vorlesungsmanuskript). Stuttgart, 2017
- [57] JACOB, STEFFEN: Temperieren direkt an der Werkzeugwand. In: *Mikroproduktion*. Leipzig (2017)
- [58] CHAKRABARTI, M. ; DAM-HANSEN, C. ; STUBAGER, J. ; PEDERSEN, T. F. ; PEDERSEN, H. C.: Replication of optical microlens array using photoresist coated molds. In: *Optics Express* Bd. 24 (2016), Nr. 9, S. 9528
- [59] WU, CHENG-HSIEN ; LU, CHIEN-HUNG: Fabrication of an LCD light guide plate using closed-die hot embossing. In: *Journal of Micromechanics and Microengineering* Bd. 18 (2008), Nr. 3, S. 035006
- [60] MOON, SU-DONG ; LEE, NAMSUK ; KANG, SHINILL: Fabrication of a microlens array using micro-compression molding with an electroformed mold insert. In: *Journal of Micromechanics and Microengineering* Bd. 13 (2003), Nr. 1, S. 98–103
- [61] YAO, DONGGANG ; KIM, BYUNG ; YI, ALLEN: Embossing-Based Process Variants for Polymer Microfabrication. Atlanta, 2005
- [62] Kunststoffe - Fachwörterverzeichnis (ISO 472:2013); Dreisprachige Fassung EN ISO 472:2013, Beuth Verlag GmbH (2013)
- [63] ONG, N.S ; KOH, Y.H ; FU, Y.Q: Microlens array produced using hot embossing process. In: *Microelectronic Engineering* Bd. 60 (2002), Nr. 3–4, S. 365–379
- [64] LOALDI, DARIO ; QUAGLIOTTI, DANILO ; CALAON, MATTEO ; PARENTI, PAOLO ; ANNONI, MASSIMILIANO ; TOSELLO, GUIDO: Manufacturing Signatures of Injection Molding and Injection Compression Molding for Micro-Structured Polymer Fresnel Lens Production. In: *Micromachines* Bd. 9 (2018), Nr. 12, S. 653
- [65] BU, QIU XIANG ; ZHU, JIAN YI ; YIN, QING ZHEN: Injection Compression Molding Process and Mould Design of Plastic Optical Lens. In: *Key Engineering Materials* Bd. 501 (2012), S. 321–324
- [66] ROEDER, MARCEL ; DREXLER, MARC ; ROTHERMEL, THILO ; MEISSNER, THOMAS ; GUENTHER, THOMAS ; ZIMMERMANN, ANDRÉ: Injection Compression Molded Microlens Arrays for Hyperspectral Imaging. In: *Micromachines* Bd. 9 (2018), Nr. 7, S. 355
- [67] SPECTOR, DAVID P. ; KINGSBURY, JEFFREY M.: Schutzrecht 4,836,960, *Fabrication of thermoplastic components by injection/compression molding*, eingereicht 05.10.1987, und veröffentlicht 06.06.1989.

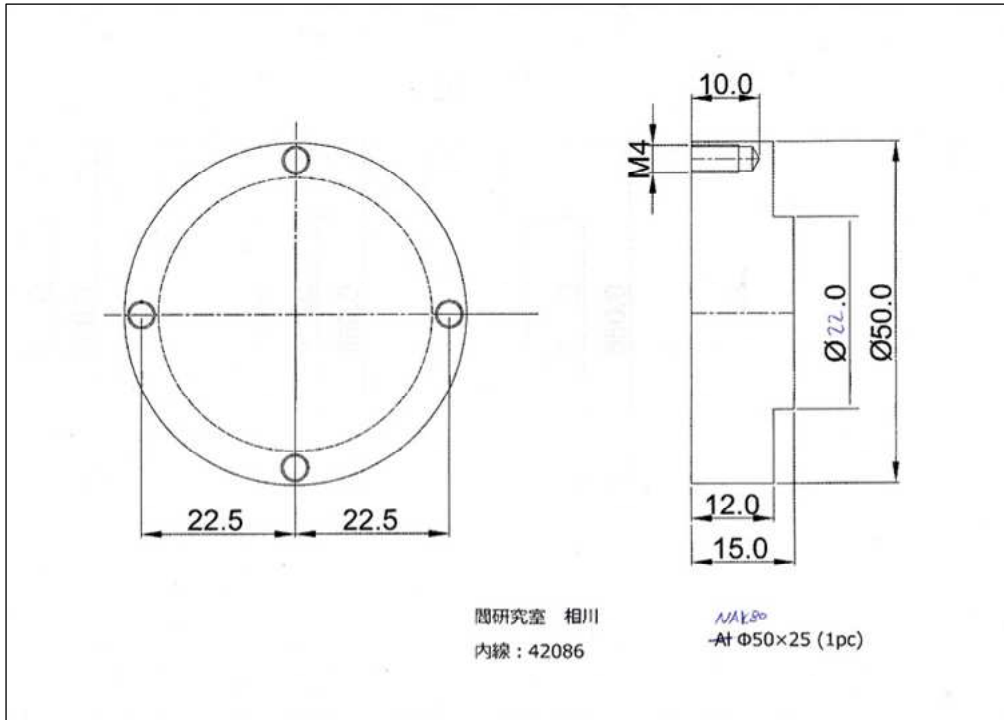
- [68] LI, KANGSEN ; XU, GANG ; HUANG, XINFANG ; XIE, ZHIWEN ; GONG, FENG: Manufacturing of Micro-Lens Array Using Contactless Micro-Embossing with an EDM-Mold. In: *Applied Sciences* Bd. 9 (2018), Nr. 1, S. 85
- [69] ROSATO, DOMINICK V. ; ROSATO, DONALD V. ; ROSATO, MATTHEW V.: *Plastic Product Material and Process Selection Handbook* : Elsevier, 2004 — ISBN 978-1-85617-431-2
- [70] BOURQUE, DAVID: Manufacturing plastic injection optical molds. In: KOSHEL, R. J. ; GREGORY, G. G. ; MOORE, JR., J. D. ; KREVER, D. H. (Hrsg.): San Diego, California, USA, 2008, S. 706117
- [71] SYMMONS, ALAN ; AUZ, BRYAN: Design considerations and manufacturing limitations of Insert Precision Glass Molding (IPGM). In: KREVER, D. H. ; BEICH, W. S. ; SCHAUB, M. P. ; BÄUMER, S. M. (Hrsg.): San Diego, California, USA, 2012, S. 84890H
- [72] LEE, TAE YOON ; HAN, KYUDONG ; PARK, DANIEL S. ; SOPER, STEVEN S. ; BATZER, MARK A. ; NIKITPOULOS, DIMITRIS E. ; MURPHY, MICHAEL C.: A multi-function, microfluidic module for mutation detection. In: *TRANSDUCERS 2009 - 2009 International Solid-State Sensors, Actuators and Microsystems Conference*. Denver, CO, USA : IEEE, 2009 — ISBN 978-1-4244-4190-7, S. 120–123
- [73] BRINKSMEIER, E. ; GLÄBE, R. ; OSMER, J.: Diamond Machining of Nitrocarburized Steel Molds for the Mass Production of Optical Components. In: SCHUH, G. ; NEUGEBAUER, R. ; UHLMANN, E. (Hrsg.): *Future Trends in Production Engineering*. Berlin, Heidelberg : Springer Berlin Heidelberg, 2013 — ISBN 978-3-642-24490-2, S. 191–199
- [74] KIRSCHLING, GÜNTER: *Qualitätssicherung und Toleranzen*. Berlin, Heidelberg : Springer Berlin Heidelberg, 1988 — ISBN 978-3-540-18482-9
- [75] DIN DEUTSCHES INSTITUT FÜR NORMUNG E. V.: DIN ISO 10110-12:2016-04 Optics and photonics - Preparation of drawings for optical elements and systems - Part 12: Aspheric surfaces (ISO 10110-12:2007 + Amd 1:2013), 2016
- [76] Datasheet Takiron Polycarbonate sheet. In: C.I. TAKIRON CORPORATION (Hrsg.) (2018)
- [77] kuraray Datasheet メタクリル樹脂注型板 paraglass メタクリル樹脂押出板 comoglass. In: KURARAY CO. LTD. (Hrsg.) (2018)
- [78] TATSUYA OKADA ; KOUSAI KOUJI: Inquiry „Thermal Properties Comoglas P (transparent)“.

- [79] kuraray Safety data sheet メタクリル樹脂押出板 comoglass.  
In: KURARAY CO. LTD. (Hrsg.) (2019)
- [80] ROEDER, M. ; SCHILLING, P. ; FRITZ, K.-P. ; GUENTHER, T. ; ZIMMERMANN, A.:  
Challenges in the fabrication of microstructured polymer optics. In: *WCMNM 2018 World Congress on Micro and Nano Manufacturing*. Slovenia :Research Publishing Services, 2018 — ISBN 978-981-11-2728-1, S. 33–36
- [81] DIN DEUTSCHES INSTITUT FÜR NORMUNG E. V.: Geometrical Product Specifications (GPS) - Surface texture: Profile method - Rules and procedures for the assessment of surface texture (ISO 4288:1996), 1998
- [82] DIN DEUTSCHES INSTITUT FÜR NORMUNG E. V.: Geometrical product specifications (GPS) - Filtration - Part 21: Linear profile filters: Gaussian filters (ISO 16610-21:2011), 2016
- [83] MITAKA KOHKI CO., LTD.: *Mitaka Kohki Industrial Equipment*. URL <http://www.mitakakohki.co.jp/english/industry/>. - abgerufen am 2019-08-26
- [84] ABDUL MANAF, AHMAD ROSLI ; YAN, JIWANG: Improvement of form accuracy and surface integrity of Si-HDPE hybrid micro-lens arrays in press molding. In: *Precision Engineering* Bd. 47 (2017), S. 469–479
- [85] SPECIALCHEM S.A.: *Shrinkage - Contraction of Plastic Molded PArt*. URL <https://omnexus.specialchem.com/polymer-properties/properties/shrinkage>. - abgerufen am 2019-09-13. — Omnexus - The material selection platform

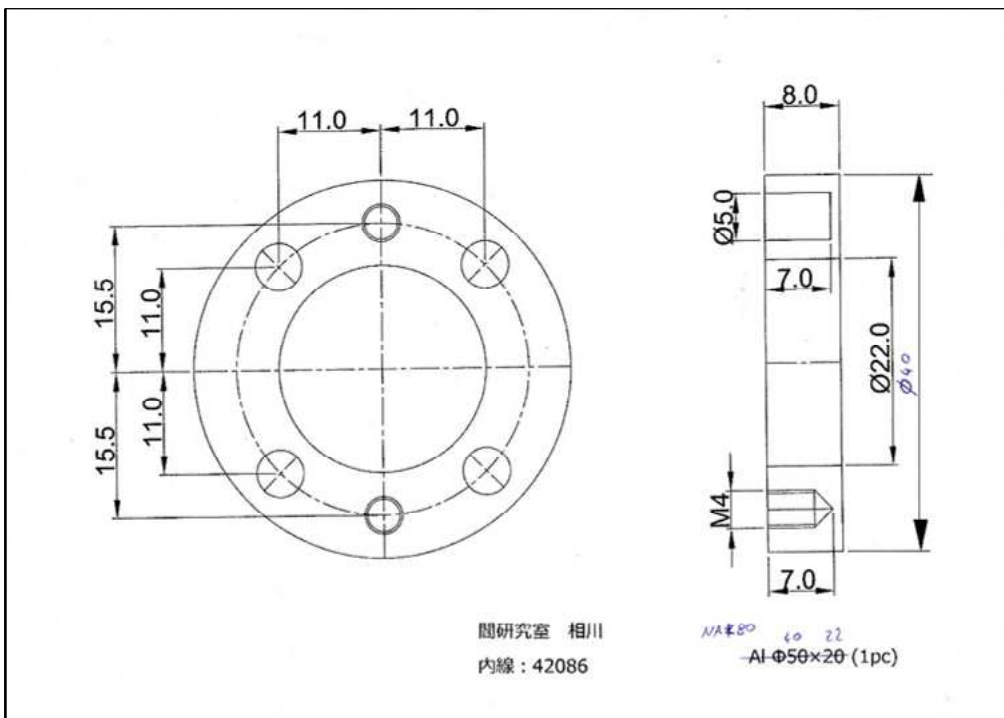
# Appendix

## Mold – Technical Drawings and Datasheets

### (1) TD Upper Mold – Yan Lab Design

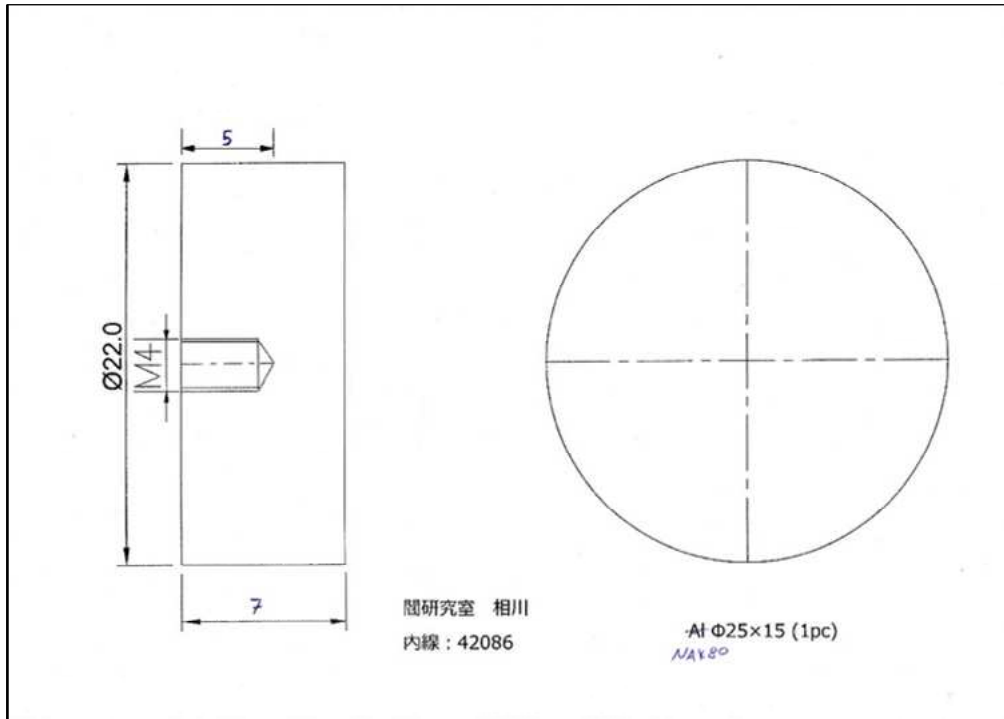


### (2) TD Lower Mold Part 1 – Yan Lab Design

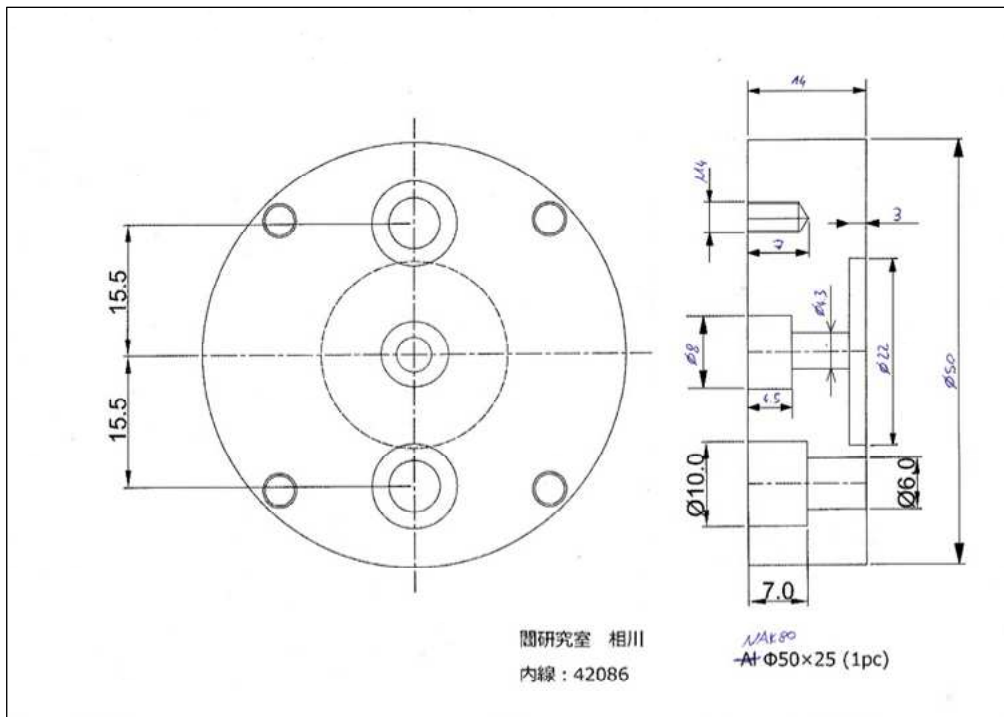




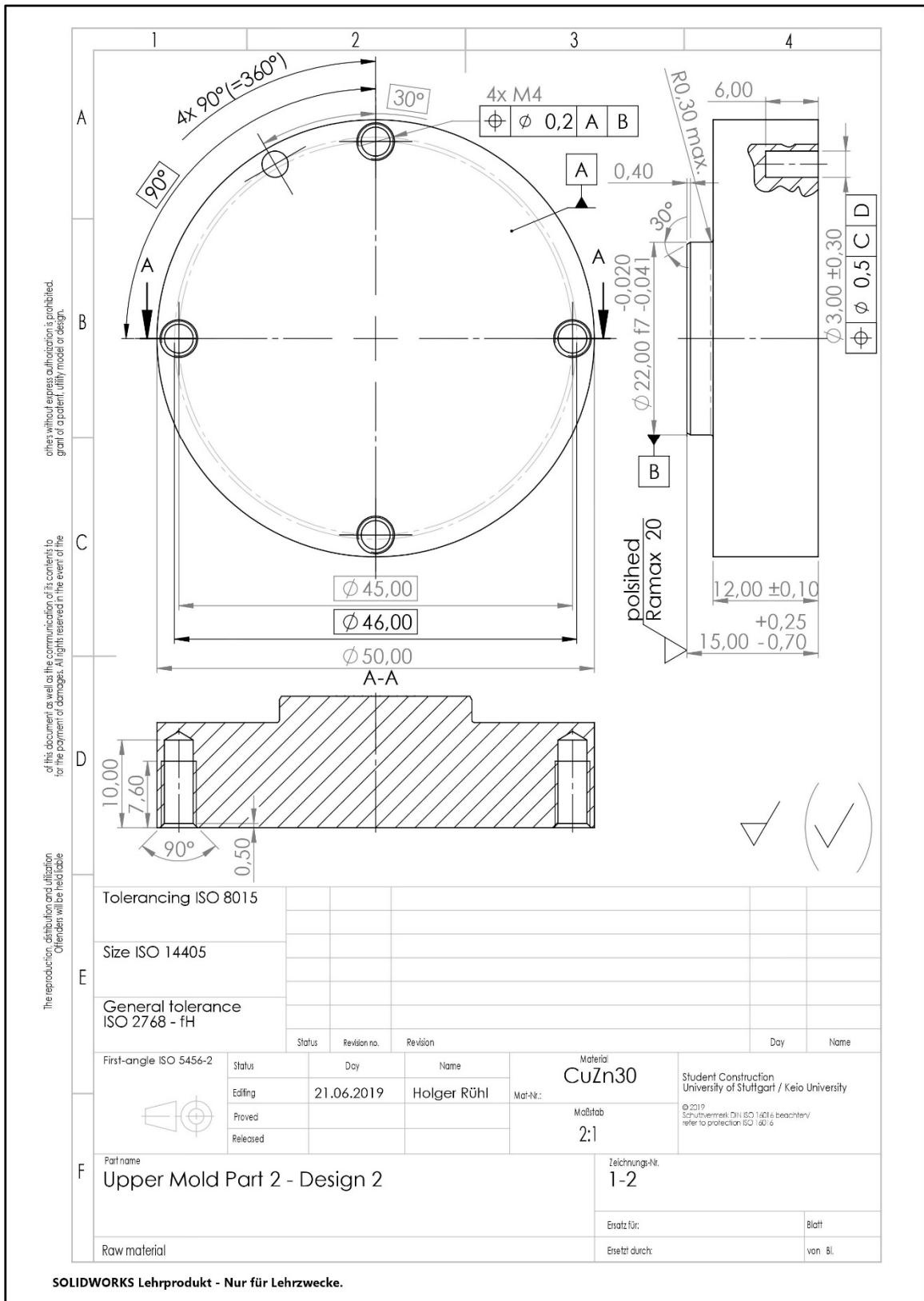
(3) TD Lower Mold Part 2 – Yan Lab Design



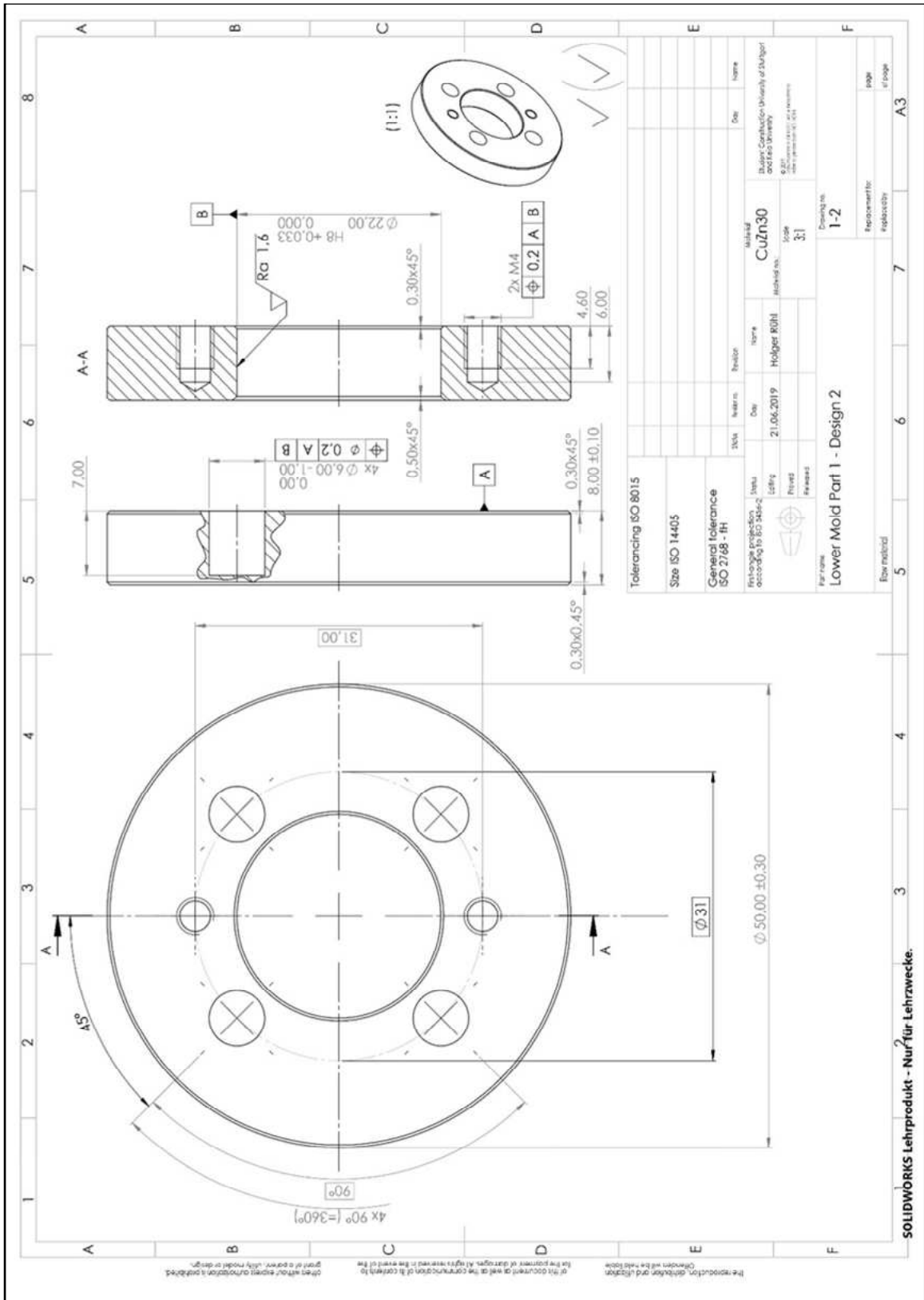
(4) TD Lower Mold Part 3 – Yan Lab Design



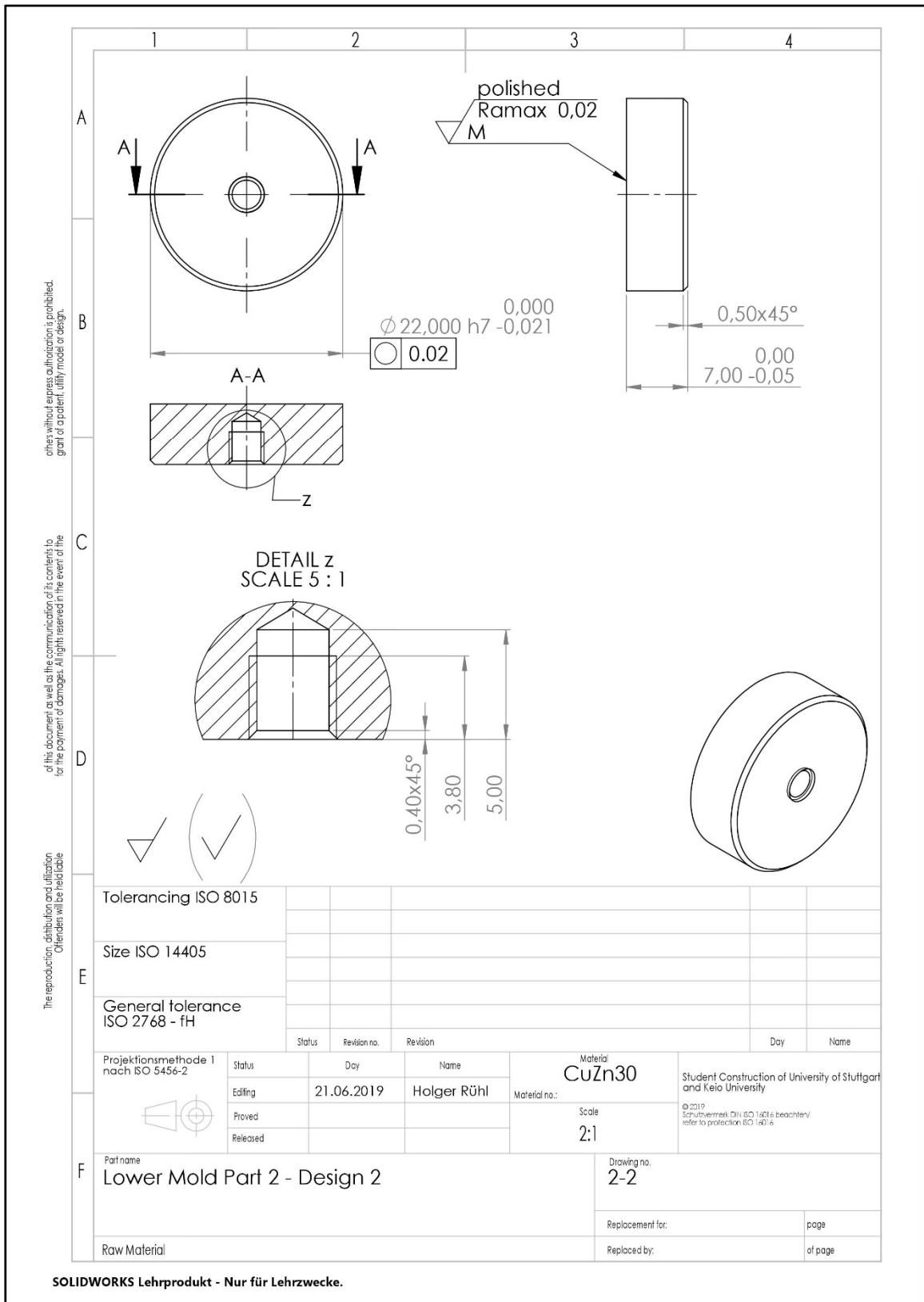
(5) TD Upper Mold



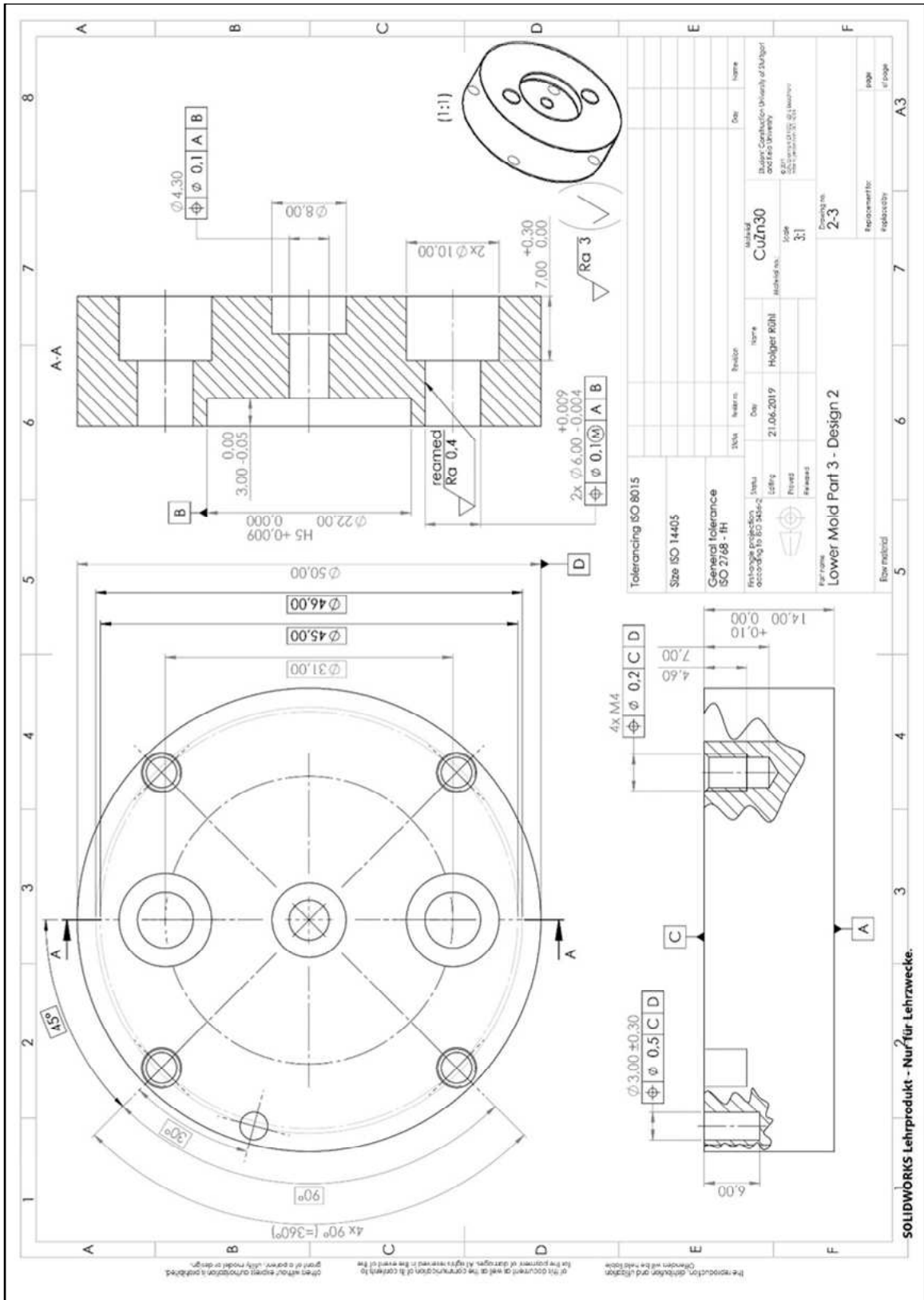
(6) TD Lower Mold Part 1



(7) TD Lower Mold Part 2




(8) TD Lower Mold Part 3



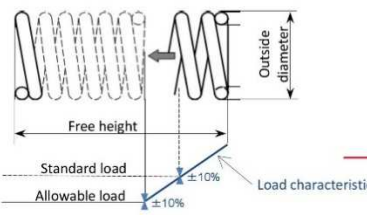
(9) DS compression springs DC519 by Accurate Inc., Japan

page1



## UltraSpring™ Compression Spring

ウルトラスプリング・圧縮コイルばね



<b>C series</b> (230items)	Numbered by the "Standard load" which is originally standardized by Accurate Inc. and regarding the Japanese standardization of springs (JSMA No.7). (社)日本ばね工業会制定の規格を基に、当社独自の管理項目(基準荷重)を追加し配列した規格です。
<b>DC series</b> (525items)	Numbered by the "Standard load" which is originally standardized by Accurate Inc. and regarding the German standardization of springs (DIN2098). 欧州において普及しているドイツの規格(DIN2098)圧縮ばねを参考に、当社独自の管理項目(基準荷重)を追加し、配列した規格です。
<b>P series</b> (212items)	Original Standard series. オリジナルシリーズ

**SPECIFICATIONS** 規格及びばね仕様

Material 材質	Wire diameter 線径	Kinds of steel 鋼種
<b>C series</b>	All	SUS304WPB (18-8 stainless steel wire for springs)
<b>DC series</b>	Less than φ0.5 Greater than φ0.5 through φ5.0 φ5.0 and greater	SUS304WPB (18-8 stainless steel wire for springs) SWP-B (Music wire) SWP-A (Music wire) or SWO-B
<b>P series</b>	Less than φ5.0 φ5.0 and greater	SWP-B (Music wire) SWP-A (Music wire) or SWO-B

**Load characteristic** 荷重特性

Controlled by 2 points of load characteristic.  
次の二点で荷重管理しています。

		Tolerance
Allowable load 許容荷重	Defined by 80% of allowable torsional stress given from JIS B 2704.	許容ねじり応力を、JIS B 2704の約80%と定め、その時の荷重を許容荷重と設定しています。
Standard load 基準荷重	Defined by 60% of allowable load.	許容荷重の約60%を基準荷重と設定しています。

\*Please avoid usage exceeding allowable load.  
許容荷重を超えてのご使用はおやめください。

**Free height** 自由高さ

Generally, free height is a reference value when the load characteristic is specified.  
荷重特長の指定がある場合は一般的に参考値となります。

**Outside coil diameter** コイル外径

Controlled by outside diameter with the tolerance of JIS class 2.  
コイル径は外径基準で管理しています。許容差はJIS 2級に基づいています。

	Class	Tolerance (JIS class 2)
D/d	Greater than 4 up to 8	±1.5% min ±0.20mm
	Greater than 8 up to 15	±2.0% min ±0.30mm
	Greater than 15 up to 22	±3.0% min ±0.50mm

D/d=Spring index, is the ratio of mean coil diameter and wire diameter.  
ばね指数、コイル平均径と線径の比です。

**Number of total coils** 総巻数

Generally, number of total coils is a reference value when the load characteristic is specified.  
荷重条件により、参考値です。


**Direction of wind** 巻方向

Right hand coil  
右巻き


**Ends shape** 端末形状

Ends shape depends on the wire diameter. Please find the below table for grind treatment as well.  
研削処理の有無については、以下の通りです。規格や線径サイズによって異なります。

	Wire diameter	Grind treatment
<b>C series</b>	Less than φ0.8 - Not ground φ0.8 and greater - Ground	Closed クローズドエンド
<b>DC series</b>	Less than φ0.5 - Not ground φ0.5 and greater - Ground	
<b>P series</b>	All - Ground	



Closed, Not ground  
クローズドエンド 研削無し



Closed, Ground  
クローズドエンド 研削有り

\*Colour of appearance or gloss level may be seen differently by production lots though this is caused by low temperature annealing and does not affect spring characteristics.  
製造ロットにより外観色・光沢に若干差が生じることがありますが、これは低温焼鈍(テンパー)によるもので、ばね特性に影響はありません。

\*Specifications are subject to change without notice.  
仕様は予告なく変更する場合があります。

\* C288 is Grounded.(Wire diameter φ0.7mm)  
C288は研削ありです。(線径φ0.7mm)



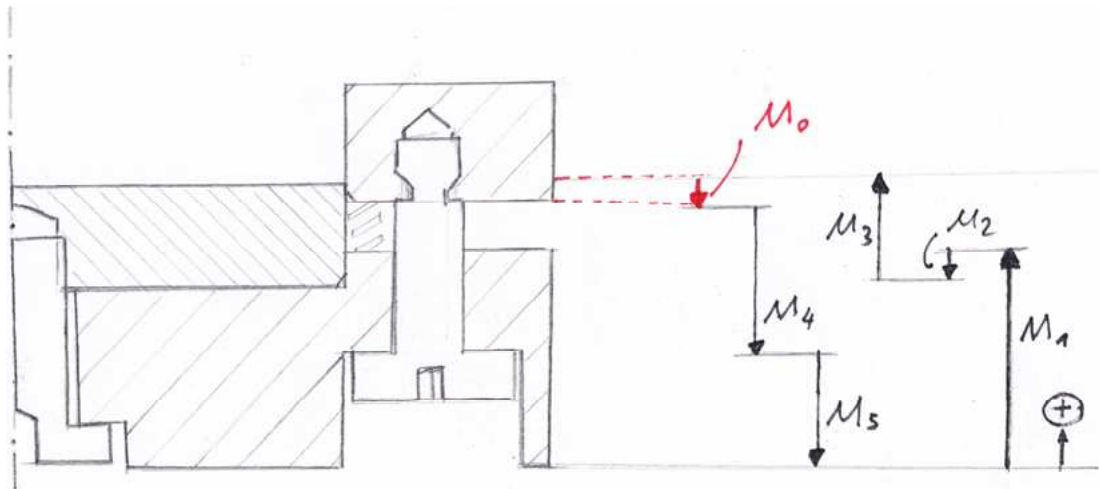
Helical compression spring

圧縮コイルばね

SWP-B

Part No. 製品番号	Standard Load 基準荷重 (P1) N	Standard Height 荷重高さ (H1) mm	Free Height 自由高さ (HF) mm	Wire Diameter 線径 (d) mm	Outer Coil Diameter 外径 (OD) mm	Number of Total Coils 総巻数 (Nt)	Spring Rate ばね定数 (k) N/mm	Allowable Load 許容荷重 (P2) N	Allowable Height 許容荷重時高さ (H2) mm	Solid Height 密着高さ (Hs) mm	Packing Quantity パック内個数
DC500	3.49	12.17	20.0	0.50	6.8	7.50	0.461	5.98	6.69	3.80	20
DC501	3.49	17.89	30.0	0.50	6.8	10.50	0.304	5.98	9.43	5.30	20
DC502	3.49	26.20	44.0	0.50	6.8	14.50	0.206	5.98	13.74	7.30	10
DC503	3.49	38.65	65.0	0.50	6.8	20.50	0.137	5.98	20.22	10.30	10
DC504	3.49	8.52	13.5	0.50	6.8	5.50	0.726	5.98	5.03	2.80	20
DC505	4.39	12.88	20.5	0.50	5.5	10.50	0.608	7.26	7.88	5.30	20
DC506	4.39	18.80	30.0	0.50	5.5	14.50	0.412	7.26	11.44	7.30	20
DC507	4.39	27.92	44.5	0.50	5.5	20.50	0.275	7.26	17.03	10.30	10
DC508	4.39	6.26	9.4	0.50	5.5	5.50	1.461	7.26	4.20	2.80	20
DC509	4.39	9.07	14.0	0.50	5.5	7.50	0.932	7.26	5.83	3.80	20
DC510	5.44	14.58	24.5	0.63	8.6	7.50	0.569	8.92	8.28	4.70	10
DC511	5.44	21.67	37.0	0.63	8.6	10.50	0.373	8.92	11.93	6.60	10
DC512	5.44	32.45	55.0	0.63	8.6	14.50	0.245	8.92	18.13	9.10	10
DC513	5.44	47.13	80.5	0.63	8.6	20.50	0.167	8.92	25.93	12.90	10
DC514	5.44	9.65	16.0	0.63	8.6	5.50	0.892	8.92	5.68	3.50	10
DC515	5.49	10.13	15.0	0.50	4.5	10.50	1.167	8.83	7.15	5.30	20
DC516	5.49	14.33	21.5	0.50	4.5	14.50	0.794	8.83	9.95	7.30	20
DC517	5.49	20.39	31.0	0.50	4.5	20.50	0.539	8.83	13.91	10.30	20
DC518	5.49	4.99	7.0	0.50	4.5	5.50	2.834	8.83	3.77	2.80	20
→ DC519	5.49	6.85	10.0	0.50	4.5	7.50	1.814	8.83	4.92	3.80	20 ←
DC520	6.87	11.41	16.0	0.50	3.7	14.50	1.559	10.59	8.94	7.30	20
DC521	6.87	16.70	23.5	0.50	3.7	20.50	1.049	10.59	13.04	10.30	20
DC522	6.87	4.21	5.5	0.50	3.7	5.50	5.570	10.59	3.52	2.80	20
DC523	6.87	5.88	7.9	0.50	3.7	7.50	3.530	10.59	4.79	3.80	20
DC524	6.87	8.38	11.5	0.50	3.7	10.50	2.285	10.59	6.70	5.30	20
DC525	6.91	10.85	17.0	0.63	6.9	7.50	1.167	11.08	7.11	4.70	20
DC526	6.91	15.99	25.5	0.63	6.9	10.50	0.755	11.08	10.21	6.60	20
DC527	6.91	22.51	36.5	0.63	6.9	14.50	0.510	11.08	14.02	9.10	10
DC528	6.91	33.30	54.0	0.63	6.9	20.50	0.343	11.08	20.73	12.90	10
DC529	6.91	7.58	11.5	0.63	6.9	5.50	1.834	11.08	5.21	3.50	20
DC530	8.71	12.51	18.5	0.63	5.6	10.50	1.520	13.53	9.23	6.60	20
DC531	8.71	17.19	26.0	0.63	5.6	14.50	1.030	13.53	12.36	9.10	10
DC532	8.71	25.46	38.5	0.63	5.6	20.50	0.696	13.53	18.32	12.90	10
DC533	8.71	6.03	8.5	0.63	5.6	5.50	3.687	13.53	4.68	3.50	20
DC534	8.71	8.63	12.5	0.63	5.6	7.50	2.354	13.53	6.50	4.70	20
DC535	8.8	13.35	17.5	0.50	3.0	20.50	2.206	12.75	11.50	10.30	20
DC536	8.8	3.62	4.4	0.50	3.0	5.50	11.572	12.75	3.26	2.80	20
DC537	8.8	4.87	6.1	0.50	3.0	7.50	7.424	12.75	4.32	3.80	20
DC538	8.8	6.79	8.7	0.50	3.0	10.50	4.795	12.75	5.94	5.30	20
DC539	8.8	9.20	12.0	0.50	3.0	14.50	3.266	12.75	7.94	7.30	20

- (10) Tolerance stack analysis – Axial guidance length between Imp 1 and Imp 2  
 Calculation according to [74]:



Scale (2:1)

$i$	$M_i$ [mm]	$N_i$ [mm]	$E_{ci}$ [mm]	$k_i$ [mm]	$T_i$ [mm]
0	$1 \begin{smallmatrix} +0.300 \\ -0.450 \end{smallmatrix}$	1	-0.075	-1	0.750
1	$14 \begin{smallmatrix} +0.100 \\ 0 \end{smallmatrix}$	14	0.050	+1	0.10
2	$3 \begin{smallmatrix} 0 \\ -0.050 \end{smallmatrix}$	3	-0.025	-1	0.050
3	$7 \begin{smallmatrix} +0.050 \\ -0.050 \end{smallmatrix}$	7	0	+1	0.100
4	$10 \begin{smallmatrix} +0.100 \\ -0.100 \end{smallmatrix}$	10	0	-1	0.200
5	$7 \begin{smallmatrix} +0.300 \\ 0 \end{smallmatrix}$	7	0.150	-1	0.300

Nominal dimension: 
$$N_0 = -\frac{1}{k_0} \sum_{i=1}^m k_i N_i \quad (0-1)$$

Center tolerance deviation: 
$$E_{c0} = -\frac{1}{k_0} \sum_{i=1}^m k_i E_{ci} \quad (0-2)$$

Component tolerance: 
$$T_0 = \sum_{i=1}^m T_i \quad (0-3)$$

General dimension: 
$$M_0 = N_0 + E_{c0} \pm \frac{T_0}{2} \quad (0-4)$$



Calculation of  $M_0$ :

$$N_0 = -\frac{1}{-1} (1 * 14 - 1 * 3 + 1 * 7 - 1 * 10 - 1 * 7) = 1 \quad (0-5)$$

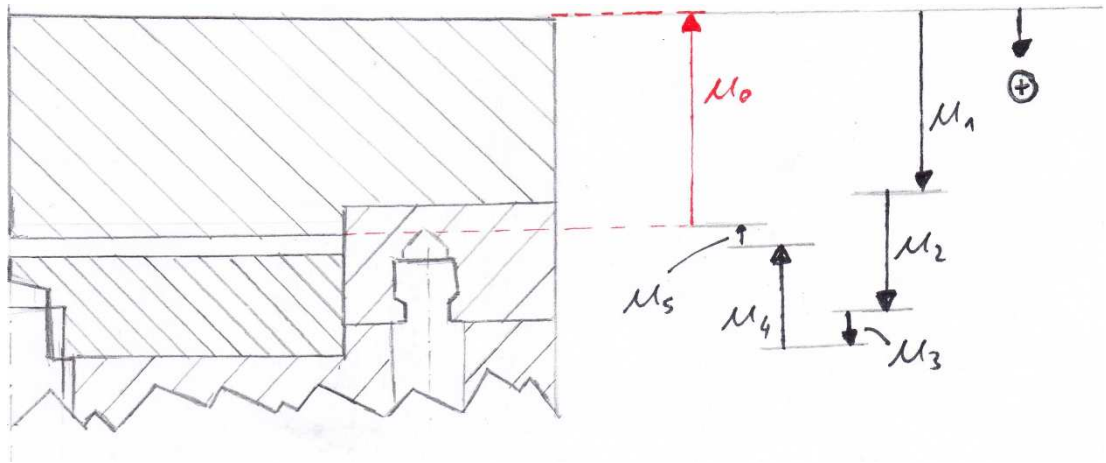
$$E_{c0} = -\frac{1}{-1} (1 * 0.050 - 1 * (-0.025) - 1 * 0.150) = -0.075 \quad (0-6)$$

$$T_0 = 0.100 + 0.050 + 0.100 + 0.200 + 0.300 = 0.750 \quad (0-7)$$

$$M_0 = 1 + (-0.075) \pm \frac{0.750}{2} = 1 \begin{matrix} +0.300 \\ -0.450 \end{matrix} \quad (0-8)$$

(11) Tolerance stack analysis – Plunger length at upper mold part

Calculation according to [74]:



Scale (2:1)

$i$	$M_i$ [mm]	$N_i$ [mm]	$E_{ci}$ [mm]	$k_i$ [mm]	$T_i$ [mm]
0	$15 \begin{smallmatrix} +0.250 \\ -0.700 \end{smallmatrix}$	15	-0.225	-1	0.950
1	$12 \pm 0.100$	12	0	+1	0.200
2	$8 \pm 0.100$	8	0	+1	0.200
3	$3 \begin{smallmatrix} 0 \\ -0.050 \end{smallmatrix}$	3	-0.025	+1	0.050
4	$7 \pm 0.050$	7	0	-1	0.100
5	$1 \begin{smallmatrix} +0.400 \\ 0 \end{smallmatrix}$	1	0.200	-1	0.400

Calculation of  $M_0$ :

$$N_0 = -\frac{1}{-1} (1 * 12 + 1 * 8 + 1 * 3 - 1 * 7 - 1 * 1) = 15 \quad (0-9)$$

$$E_{c0} = -\frac{1}{-1} (1 * (-0.025) - 1 + 0.200) = -0.225 \quad (0-10)$$

$$T_0 = T_0 = \sum_{i=1}^m T_i = 0.950 \quad (0-11)$$

$$M_0 = 15 + (-0.225) \pm \frac{0.950}{2} = 15 \begin{smallmatrix} +0.250 \\ -0.700 \end{smallmatrix} \quad (0-12)$$

## Extracts from Polymer Data Sheets

(12) C.I. Takiron Polycarbonate Material Data Sheet



Polycarbonate Plates

# ポリカーボネートプレート

## — 総合技術資料 —

Comprehensive Technical Data

2018年4月改訂版

Revised April 2018

タキロンシーアイ株式会社

### 3. ポリカーボネートプレートの特性 Polycarbonate Properties

#### (1) 一般物性 General physical properties

	評価項目	試験法	単位	特性値	JIS K 6735 規格値	
機械的性質	Density	比重	JIS K 7112	-	1.2	-
	Tensile yield stress	引張降伏応力	JIS K 7161-2	MPa	63	55以上
	Nominal strain	引張破壊時伸びひずみ	JIS K 7161-2	%	90	60以上
	Elastic modulus	引張弾性率	JIS K 7161-2	MPa	2250	2200以上
	Compressive strength	圧縮降伏応力	ASTM D 695 JIS K 7181	MPa	78	-
	Shear strength	剪断破壊応力	JIS K 7214	MPa	65 (厚さ3mm)	-
	Flexural modulus	曲げ応力	JIS K 7171	MPa	91	-
		曲げ弾性率	JIS K 7171	MPa	2300	-
	Tensile impact strength	引張衝撃強さ	JIS K 7160	kJ/m <sup>2</sup>	220 (厚さ3mm)	150以上 (厚さ<4mm)
	Charpy impact strength	シャルピー衝撃値	JIS K 7111	kJ/m <sup>2</sup>	84 (厚さ3mm) 13 (厚さ5mm)	- 6以上 (厚さ≥4mm)
Hardness	ロックウェル硬度	JIS K 7202	-	M-67 R-125	-	
熱的性質	Deflection temperature	荷重たわみ温度	JIS K 7191-2A	℃	139	130以上
	Softening temperature	ピカット軟化温度	JIS K 7206	℃	150	145以上
	Embrittlement temperature	脆化温度	ASTM D 764	℃	-100以下	-
	Thermal conductivity	熱伝導率	ASTM D 177	W/m・K	0.19	-
	Thermal expansion coefficient	線膨張係数	JIS K 7140-1	℃ <sup>-1</sup>	6.5×10 <sup>-5</sup>	-
電気的性質		比誘電率 (60 Hz)	ASTM D 150	-	2.95	-
		比誘電率 (1 MHz)	ASTM D 150	-	2.90	-
		アーク抵抗	ASTM D 495	sec	110	-
Refractive index	屈折率	ASTM D 542	-	1.587	-	
Transmission	全光線透過率	JIS K 7361-1	%	90 (厚さ3mm)	85以上 (厚さ3mm)	

※試験片の厚さが記載されていない場合の記載数値は、試験片厚さ 5 mm の実測値であって保証値ではありません。

### (2)－7 耐擦傷性

ポリカーボネートプレートの耐擦傷性について試験を行ない、その結果を他の材料と比較して下記表に示します。

試験項目	試験方法	単位	ポリカーボネート PC1600	ポリカーボネート PCMR56620	ポリカーボネート PCMRMS61600	ガラス	アクリル
テーパー 摩耗試験	JISK6735 CS-10F・ 500g 100回転 TYPE4	△H	36.6	4.7	5.8	0.2	23.2
鉛筆硬度	JISK600-5-4	-	4B	HB~F	HB~F	8H	2H

### (3) 熱的性質 Thermal Properties

#### (3)－1 耐熱性

ポリカーボネートは合成樹脂中、熱変形温度が最も高い部類に属しており、しかも荷重の大小によって大幅に変化しないのが大きな特長です。

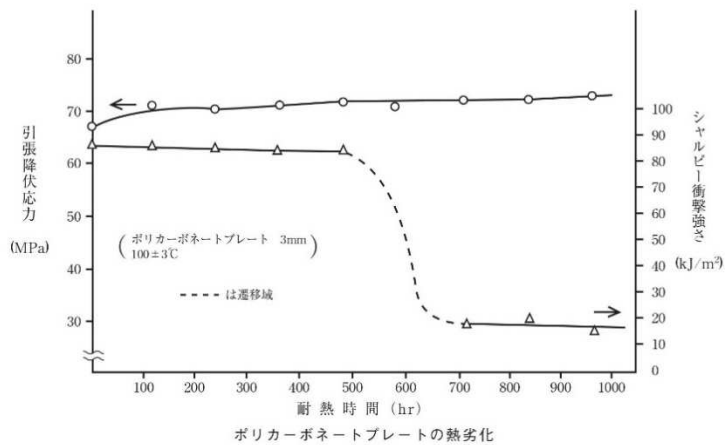
実用使用最高温度（連続） **Maximum temperature of use = 120 °C**

使用条件、材料の種類などによって異なりますが、一般に空气中で使用の場合は熱変形温度から約 15 ~ 20°C 差し引いた温度が実用最高温度（連続）となります。

このことからポリカーボネートの乾燥空气中での実用最高温度（連続）は約 120°C となります。

#### 熱劣化試験

ポリカーボネートプレート（厚さ 3mm）を 100°C ± 3°C の恒温乾燥機中に放置し、各時間ごとに取り出して試験片作成後試験を行ないました。

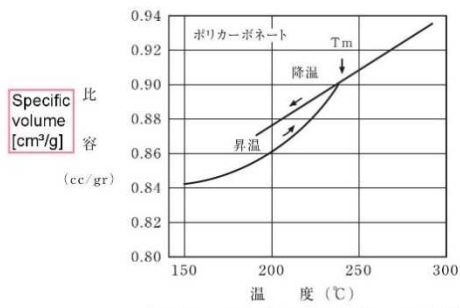
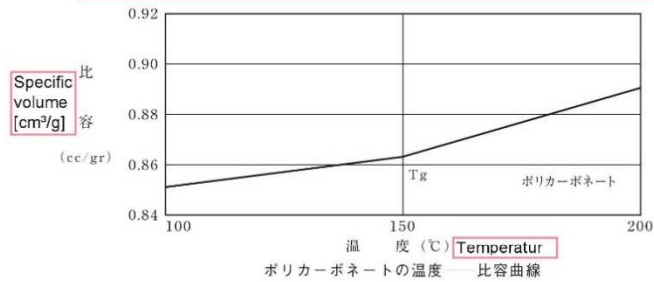


Class transition point (secondary transition point) and melting temperature (first order transition point)

(3) - 2 ガラス転移点 (二次転移点) および熔融温度 (一次転移点)

熱膨張法 (Dilatometry) によるポリカーボネートのガラス転移点  $T_g$  は約  $150^\circ\text{C}$  であり、熔融温度  $T_m$  は約  $240^\circ\text{C}$  です。

The glass transition temperature  $T_g$  of the polycarbonate is about  $150^\circ\text{C}$ , the decomposition temperature  $T_m$  is about  $240^\circ\text{C}$ .



結晶性ポリカーボネートの温度—比容曲線  
Temperature curve of crystalline polycarbonate

ガラス転移点は一般に分子運動が凍結される温度とされており、これを越えると分子運動が始まって容積、誘電率、屈折率、圧縮率、熱伝導率などの物理特性が急激に変化します。また、熔融温度は分子量、結晶化度などによって異なり、また高分子物質では明瞭に認められ難く、普通ある範囲をもちます。

プラスチックのガラス転移点および熔融温度

種類	ガラス転移点 (°C)	熔融温度 (°C)
Polycarbonate ポリカーボネート	150	240
Nylon 66 ナイロン 66	47	250~265
Polyacetal ポリアセタール	-	264
PVC 硬質塩化ビニル	70~77	-
アクリル (MMA)	60~105	-
高密度ポリエチレン	-21~-24	105~115
ポリプロピレン	-35	160~170
ポリスチレン	80~105	230

Polycarbonate:  
Glass transition temperature  
 $T_g = 150^\circ\text{C}$   
Decomposition temperature =  
 $240^\circ\text{C}$

## 基本物性

## 新JIS規格による物性値

COMOGLAS

項目	試験方法	単位	パラガラス。	コモグラス。	コモグラス。	コモグラス。	
			一般グレード	一般グレード	KHC2	HI70	
一般物性	Density 比重	JIS K7112	—	1.19	1.19	1.19	1.17
	吸水率	JIS K7209	%	0.3	0.3	0.3	0.3
	燃焼性	JIS K6911 (A法)	—	可燃性	可燃性	可燃性	可燃性
UL94		—	HB	HB	HB	HB	
All light transmission	全光線透過率	JIS K7361-1	%	93	93	93	91
Visible light transmission	可視光線透過率	JIS R3106	%	92	92	92	90
光学的性質	ヘイズ	JIS K7136	%	0.2	0.2	0.2	0.7
	屈折率	JIS K7142	—	1.49	1.49	1.49	1.49
Refractive Index	日射透過率	JIS R3106	%	88	88	88	87
Tensile yield strength	引張強さ	JIS K7162	MPa	76	73	73	49
Tensile breaking strength	引張破断ひずみ	JIS K7162	%	6	5	5	20
Bending strength	曲げ強さ	JIS K7171	MPa	120	113	113	74
Flexural modulus	曲げ弾性率	JIS K7171	MPa	3200	3200	3200	2200
Hardness	ロックウェル硬度	JIS K7202-2	Mスケール	100	97	97	61
	アイゾット衝撃強さ	JIS K7110	KJ/m <sup>2</sup>	2.1	1.8	1.8	5.3
Charpy impact strength	シャルピー衝撃強さ	JIS K7111	KJ/m <sup>2</sup>	18	17	17	80
Spec. heat capacity	比熱容量	JIS K7123	J/g・°C	1.5	1.5	1.5	1.5
熱的性質	荷重たわみ温度	JIS K7191-2 (A法)	°C	105	92	92	84
	線膨張係数	JIS K7197	°C <sup>-1</sup>	7×10 <sup>-5</sup>	7×10 <sup>-5</sup>	7×10 <sup>-5</sup>	8×10 <sup>-5</sup>
電氣的性質	表面抵抗率	JIS K6911	Ω	>10 <sup>16</sup>	>10 <sup>16</sup>	>10 <sup>16</sup>	>10 <sup>16</sup>
	電荷半減時間	JIS L1094	sec	∞	∞	∞	∞
耐久性	テーパ-摩耗 <sup>*1</sup>	JIS K7204	ヘイズ (%)	18	20	5	—
	落砂摩耗	ASTM D673	ヘイズ (%)	50	52	3	—

☆上記の数値は、代表値であり保証値ではありません。

1MPa=10.2kgf/cm<sup>2</sup>

\*1…500gの荷重で円筒形砥石(CS-10F)を100回転させた後のヘイズ(曇り)を測定

## 耐候性

促進暴露試験を行い材料劣化の初期段階に現れる変色をハンター(Hunter)の色差ΔEで表しますと

下表のように「パラガラス」、「コモグラス」の変色が少ないことが分かります。

材料	促進暴露期間			
	200hr	400hr	1000hr	2000hr
パラガラス。(透明)	0.05	0.27	0.45	1.50
コモグラス。(透明)	0.05	0.21	0.40	1.42
硬質ポリ塩化ビニール(透明)	0.91	1.74	2.30	—
硬質ポリ塩化ビニール(乳半)	1.84	2.00	2.22	—
ポリスチレン	1.40	1.65	1.76	—
ポリカーボネート	1.77	3.16	4.89	—
ポリエステル	1.30	1.65	1.75	—

# (14) Kuraray Co. Ltd. PMMA Safety Data Sheet

製品名 : コモグラス、CG P (透明系)、管理番号 : R12-010 P.1/8

作成日 2019年02月01日 Year/Month/Day

## 安全データシート Safety Data Sheet

### 1. 製品及び会社情報 Product and Company Information

製品名 : **コモグラス** Comoglas transparent  
製品コード : CG P (透明系)  
\* 共通品番 [HPM, UV40, KD1, DK3, E30] [430L, 431L, 432L, 452L]  
[120K, 130K, 144K, 150K, 148K, 125K, 135K, 145K, 155K, 530K, 550K]  
[9041K, 9053K] [DFA2 P, DFA2 148K, DFA2 446L] [DSF2 0157L]  
[KHC1, KHC2] [TH1] \*特注色[6170K, 7054K]  
Company 会社名 : **株式会社クラレ** Kuraray Co., Ltd.  
住 所 : 〒100-8115 東京都千代田区大手町 1-1-3 大手センタービル  
担当部門 : 機能材料カンパニー メタアクリル事業部 シート販売部  
電話番号 : 03-6701-1526 FAX 番号 : 03-6701-1577  
緊急連絡先 : 株式会社クラレ新潟事業所 代表電話  
緊急電話番号 : 0254-43-2521  
推奨用途及び : 表面保護シート、電飾看板、照明カバー、パーティション、  
ディスプレイ等  
使用上の制限 R12-010

### 2. 危険有害性の要約

GHS 分類 :

物理化学的危険性 :	火薬類	分類対象外
	可燃性・引火性ガス	分類対象外
	可燃性・引火性エアゾール	分類対象外
	支燃性・酸化性ガス	分類対象外
	高压ガス	分類対象外
	引火性液体	分類対象外
	可燃性固体	分類できない
	自己反応性化学品	分類できない
	自然発火性液体	分類対象外
	自然発火性固体	区分外
	自己発熱性化学品	分類できない
	水反応可燃性化学品	区分外
	酸化性液体	分類対象外
	酸化性固体	分類対象外
	有機過氧化物	分類対象外
	金属腐食性物質	分類できない
人健康有害性 :	急性毒性 (経口、経皮、吸入)	分類できない
	皮膚腐食性・刺激性	分類できない
	眼に対する重篤な損傷・眼刺激性	分類できない
	呼吸器感受性	分類できない
	皮膚感受性	分類できない
	生殖細胞変異原性	分類できない
	発がん性	分類できない



## 9. 物理的及び化学的性質 Physical and Chemical Properties

物理的状態、形状：	固体（シート塊状）
色：	無色
臭い：	無臭
pH：	該当しない
融点・凝固点	データなし
沸点、初留点及び沸騰範囲：	データなし
引火点：	280～300℃ <sup>1)</sup>
爆発範囲：	データなし
蒸気圧：	データなし
蒸気密度：	データなし
<span style="border: 1px solid black; padding: 2px;">Density</span> 比重（相対密度）：	1.17～1.20 g/cm <sup>3</sup> <sup>2)</sup>
溶解度：	
溶媒に対する溶解性	水に対する溶解性 不溶 <sup>4)</sup>
溶媒の溶解性	アセトン、酢酸エチルに可溶 <sup>3)</sup>
n-オクタノール/水分配係数：	データなし
自然発火温度：	450～462℃ <sup>1)</sup>
<span style="border: 1px solid black; padding: 2px;">Decomposition temperature</span> 分解温度：	約 220℃ <sup>5)</sup>
燃焼性：	可燃性 (UL94 HB) <sup>3)</sup>
その他のデータ：	比熱容量 1.5 J/g℃ <sup>3)</sup>
<span style="border: 1px solid black; padding: 2px;">Refractive Index</span> 屈折率	1.49 <sup>3)</sup>

## 10. 安定性及び反応性

安定性：	一般的な貯蔵、取扱いにおいては安定である。
危険有害反応可能性：	特になし
避けるべき条件：	特になし
混触危険物質：	特になし
危険有害な分解生成物：	データなし

## 11. 有害性情報

急性毒性：	データなし
皮膚腐食性・刺激性：	データなし
眼に対する重篤な損傷・刺激性：	データなし
呼吸器感受性又は皮膚感受性：	データなし
生殖細胞変異原性：	データなし
発がん性：	データなし
生殖毒性：	データなし
特定標的臓器・全身毒性－単回曝露：	データなし
特定標的臓器・全身毒性－反復曝露：	データなし
吸引力呼吸器有害性：	データなし

## Press-Molding Parameters to be set at the Toshiba GMP211

- (15) Explanation of the compression molding parameters with reference to Figure 6-8:  
Toshiba GMP211 compression molding process, page 41

Position Parameters Z [mm]	
Z1	Position of the lower mold during heating
Z2	Position of the lower mold when compression is started
Cylinder Motion Speed V [mm/min]	
V1	Speed to position Z1
V2	Speed to position Z2
V3	Motion speed after temperature T4 is reached
Pressing Parameters P [kN]	
P1	Compression force
P2	Compression force 1 applied during cooling
P3	Compression force 2 applied during cooling
Temperature Parameters T [°C]	
T1	Material preheating temperature
T2	Temperature before mold closing
T3	Cooling temperature 1
T4	Cooling temperature 2 / Demolding temperature
Time Parameters t [s]	
Pt1	Compression time during P1
St1	T1-holding time
St2	T2-holding time
St3	T2-holding time during compression

# Experiment Documentation

(16) TS3no1xx

Date / time	30.07.2019 / 13:40	Machine operator:	Holger RÜHL
Test series	3	Sample no.	1
Machine:	Toshiba GMP211		
Mold material (ISO/JIS)	CuZn30 / C2600		
Press material	HDPE		
Raw material form	Granules		
Press material weight [g]	0.448	Balance:	Shimadzu TW3323N

Parameter value [unit]	Parameter definition
<b>Position Parameters Z [mm]</b>	
Z1	48.00
Z2	48.00
<b>Cylinder motion speed V [mm/min]</b>	
V1	500.00 *
V2	20.00 *
V3	500.00 *
<b>Pressure P [kN]</b>	
P1	1
P2	1
P3	1
<b>Temperature T [°C]</b>	
T1	125
T2	125
T3	125
T4	60
<b>Time Parameters t [s]</b>	
Pt1	410
St1	60
St2	60
St3	20

\* Pre-set parameters adopted

**Observations**  
 Press-Molding time [s]: 815  
 Others:

(17) TS3no2xx

Date / time	30.07.2019 / 14:52	Machine operator:	Holger RÜHL
Test series	3	Sample no.	2
Machine:	Toshiba GMP211		
Mold material (ISO/JIS)	CuZn30 / C2600		
Press material	HDPE		
Raw material form	Granules		
Press material weight [g]	0.447	Balance:	Shimadzu TW3323N
Parameter value [unit]		Parameter definition	
Position Parameters Z [mm]			
Z1	48.00	Position lower mold during heating	
Z2	48.00	Position lower mold during compression	
Cylinder motion speed V [mm/min]			
V1	500.00*	Speed to Z1	
V2	20.00*	Speed to Z2	
V3	500.00*	Motion speed after T4	
Pressure P [kN]			
P1	1	Compression pressure	
P2	1	Compression pressure 1 while cooling	
P3	1	Compression pressure 2 while cooling	
Temperature T [°C]			
T1	128	Material Preheating Temperature	
T2	128	Temperature for mold closing	
T3	128	Cooling Temperature 1	
T4	60	Demolding Temperature	
Time Parameters t [s]			
Pt1	410	Compression time during P1	
St1	60	T1-Temperature holding time	
St2	60	Holding time until T2	
St3	20	T2-Temperature holding time while compression	
* Pre-set parameters adopted			
<b>Observations</b>			
Press-Molding time [s]:	820		
Others:			

(18) TS3no3xx

Date / time	30.07.2019 / 15:30	Machine operator:	Holger RÜHL
Test series	3	Sample no.	3
Machine:	Toshiba GMP211		
Mold material (ISO/JIS)	CuZn30 / C2600		
Press material	HDPE		
Raw material form	Granules		
Press material weight [g]	0.448	Balance:	Shimadzu TW3323N
Parameter value [unit]		Parameter definition	
Position Parameters Z [mm]			
Z1	48.00	Position lower mold during heating	
Z2	48.00	Position lower mold during compression	
Cylinder motion speed V [mm/min]			
V1	500.00*	Speed to Z1	
V2	20.00*	Speed to Z2	
V3	500.00*	Motion speed after T4	
Pressure P [kN]			
P1	1	Compression pressure	
P2	1	Compression pressure 1 while cooling	
P3	1	Compression pressure 2 while cooling	
Temperature T [°C]			
T1	131	Material Preheating Temperature	
T2	131	Temperature for mold closing	
T3	131	Cooling Temperature 1	
T4	80	Demolding Temperature	
Time Parameters t [s]			
Pt1	410	Compression time during P1	
St1	60	T1-Temperature holding time	
St2	60	Holding time until T2	
St3	20	T2-Temperature holding time while compression	
* Pre-set parameters adopted			
<b>Observations</b>			
Press-Molding time [s]:	827		
Others:			

(19) TS3no4xx

Date / time	30.07.2019 / 16:30	Machine operator:	Holger RÜHL
Test series	3	Sample no.	4
Machine:	Toshiba GMP211		
Mold material (ISO/JIS)	CuZn30 / C2600		
Press material	HDPE		
Raw material form	Granules		
Press material weight [g]	0.446	Balance:	Shimadzu TW3323N
Parameter value [unit]		Parameter definition	
Position Parameters Z [mm]			
Z1	48.00	Position lower mold during heating	
Z2	48.00	Position lower mold during compression	
Cylinder motion speed V [mm/min]			
V1	500.00*	Speed to Z1	
V2	20.00*	Speed to Z2	
V3	500.00*	Motion speed after T4	
Pressure P [kN]			
P1	1.2	Compression pressure	
P2	1.2	Compression pressure 1 while cooling	
P3	1.2	Compression pressure 2 while cooling	
Temperature T [°C]			
T1	131	Material Preheating Temperature	
T2	131	Temperature for mold closing	
T3	131	Cooling Temperature 1	
T4	8	Demolding Temperature	
Time Parameters t [s]			
Pt1	410	Compression time during P1	
St1	60	T1-Temperature holding time	
St2	60	Holding time until T2	
St3	20	T2-Temperature holding time while compression	
* Pre-set parameters adopted			
<b>Observations</b>			
Press-Molding time [s]:	686		
Others:			

(20) TS3no5xx

Date / time	30.07.2019 / 17:25	Machine operator:	Holger RÜHL
Test series	3	Sample no.	5
Machine:	Toshiba GMP211		
Mold material (ISO/JIS)	CuZn30 / C2600		
Press material	HDPE		
Raw material form	Granules		
Press material weight [g]	0.445	Balance:	Shimadzu TW3323N
Parameter value [unit]		Parameter definition	
Position Parameters Z [mm]			
Z1	48.00	Position lower mold during heating	
Z2	48.00	Position lower mold during compression	
Cylinder motion speed V [mm/min]			
V1	500.00*	Speed to Z1	
V2	20.00*	Speed to Z2	
V3	500.00*	Motion speed after T4	
Pressure P [kN]			
P1	1.2	Compression pressure	
P2	1.2	Compression pressure 1 while cooling	
P3	1.2	Compression pressure 2 while cooling	
Temperature T [°C]			
T1	131	Material Preheating Temperature	
T2	131	Temperature for mold closing	
T3	131	Cooling Temperature 1	
T4	80	Demolding Temperature	
Time Parameters t [s]			
Pt1	410	Compression time during P1	
St1	60	T1-Temperature holding time	
St2	60	Holding time until T2	
St3	20	T2-Temperature holding time while compression	
* Pre-set parameters adopted			
<b>Observations</b>			
Press-Molding time [s]:	683		
Others:			

(21) TS3no6xx

Date / time	30.07.2019 / 18:20	Machine operator:	Holger RÜHL
Test series	3	Sample no.	6
Machine:	Toshiba GMP211		
Mold material (ISO/JIS)	CuZn30 / C2600		
Press material	HDPE		
Raw material form	Granules		
Press material weight [g]	0.446	Balance:	Shimadzu TW3323N
Parameter value [unit]		Parameter definition	
Position Parameters Z [mm]			
Z1	48.00	Position lower mold during heating	
Z2	48.00	Position lower mold during compression	
Cylinder motion speed V [mm/min]			
V1	500.00*	Speed to Z1	
V2	20.00*	Speed to Z2	
V3	500.00*	Motion speed after T4	
Pressure P [kN]			
P1	1.4	Compression pressure	
P2	1.4	Compression pressure 1 while cooling	
P3	1.4	Compression pressure 2 while cooling	
Temperature T [°C]			
T1	131	Material Preheating Temperature	
T2	131	Temperature for mold closing	
T3	131	Cooling Temperature 1	
T4	80	Demolding Temperature	
Time Parameters t [s]			
Pt1	410	Compression time during P1	
St1	60	T1-Temperature holding time	
St2	60	Holding time until T2	
St3	60	T2-Temperature holding time while compression	
* Pre-set parameters adopted			
<b>Observations</b>			
Press-Molding time [s]:	690		
Others:			



(22) TS2no1xx

Date / time	22.08.2019 / 17:15	Machine operator:	Holger RÜHL
Test series	2	Sample no.	1
Machine:	Toshiba GMP211		
Mold material (ISO/JIS)	CuZn30 / C2600		
Press material	Polycarbonate		
Raw material form	Sheet		
Press material weight [g]	0.447	Balance:	Shimadzu TW3323N

Parameter value [unit]		Parameter definition
Position Parameters Z [mm]		
Z1	48.00	Position lower mold during heating
Z2	48.00	Position lower mold during compression
Cylinder motion speed V [mm/min]		
V1	500.00 *	Speed to Z1
V2	20.00	Speed to Z2
V3	500.00 *	Motion speed after T4
Pressure P [kN]		
P1	1.0	Compression pressure
P2	1.0	Compression pressure 1 while cooling
P3	1.0	Compression pressure 2 while cooling
Temperature T [°C]		
T1	175	Material Preheating Temperature
T2	175	Temperature for mold closing
T3	175	Cooling Temperature 1
T4	80	Demolding Temperature
Time Parameters t [s]		
Pt1	410	Compression time during P1
St1	60	T1-Temperature holding time
St2	60	Holding time until T2
St3	20	T2-Temperature holding time while compression

\* Pre-set parameters adopted

**Observations**  
Press-Molding time [s]: 799  
Others: Part sticking to the mold

## (23) TS2no2xx

Date / time	21.08.2019	Machine operator:	Holger RÜHL
Test series	2	Sample no.	2
Machine:	Toshiba GMP211	826 sek	
Mold material (ISO/JIS)	CuZn30 / C2600	Sticks to the upper mold	
Press material	Polycarbonate		
Raw material form	Sheet		
Press material weight [g]	0.549	Balance:	Shimadzu TW3323N

Parameter value [unit]	Parameter definition
<b>Position Parameters Z [mm]</b>	
Z1	48.00
Z2	48.00
<b>Cylinder motion speed V [mm/min]</b>	
V1	500.00 *
V2	20.00 *
V3	500.00 *
<b>Pressure P [kN]</b>	
P1	1.0
P2	1.0
P3	1.0
<b>Temperature T [°C]</b>	
T1	182
T2	182
T3	182
T4	80
<b>Time Parameters t [s]</b>	
Pt1	410
St1	60
St2	60
St3	20

\* Pre-set parameters adopted

**Observations**  
 Press-Molding time [s]: 826  
 Others: Part sticking to the mold

(24) TS2no3xx

Date / time	21.08.2019	Machine operator:	Holger RÜHL
Test series	2	Sample no.	3
Machine:	Toshiba GMP211		
Mold material (ISO/JIS)	CuZn30 / C2600		
Press material	Polycarbonate		
Raw material form	Sheet		
Press material weight [g]	0.55	Balance:	Shimadzu TW3323N

Parameter value [unit]	Parameter definition
<b>Position Parameters Z [mm]</b>	
Z1	48.00
Z2	48.00
<b>Cylinder motion speed V [mm/min]</b>	
V1	500.00*
V2	20.00*
V3	500.00*
<b>Pressure P [kN]</b>	
P1	1.0
P2	1.0
P3	1.0
<b>Temperature T [°C]</b>	
T1	189
T2	189
T3	189
T4	80
<b>Time Parameters t [s]</b>	
Pt1	410
St1	60
St2	60
St3	20

\* Pre-set parameters adopted

**Observations**  
 Press-Molding time [s]: 840  
 Others:

(25) TS2no4xx

Date / time	21.08.2019	Machine operator:	Holger RÜHL
Test series	2	Sample no.	4
Machine:	Toshiba GMP211		
Mold material (ISO/JIS)	CuZn30 / C2600		
Press material	Polycarbonate		
Raw material form	Sheet		
Press material weight [g]	0.553	Balance:	Shimadzu TW3323N

Parameter value [unit]	Parameter definition
<b>Position Parameters Z [mm]</b>	
Z1	48.00
Z2	48.00
<b>Cylinder motion speed V [mm/min]</b>	
V1	500.00*
V2	20.00*
V3	500.00*
<b>Pressure P [kN]</b>	
P1	0.8
P2	0.8
P3	0.8
<b>Temperature T [°C]</b>	
T1	182
T2	182
T3	182
T4	80
<b>Time Parameters t [s]</b>	
Pt1	410
St1	60
St2	60
St3	20

\* Pre-set parameters adopted

**Observations**  
Press-Molding time [s]: 794  
Others:

(26) TS2no5xx

Date / time	21.08.2019	Machine operator:	Holger RÜHL
Test series	2	Sample no.	4
Machine:	Toshiba GMP211		
Mold material (ISO/JIS)	CuZn30 / C2600		
Press material	Polycarbonate		
Raw material form	Sheet		
Press material weight [g]	0.55	Balance:	Shimadzu TW3323N
Parameter value [unit]		Parameter definition	
Position Parameters Z [mm]			
Z1	48.00	Position lower mold during heating	
Z2	48.00	Position lower mold during compression	
Cylinder motion speed V [mm/min]			
V1	500.00*	Speed to Z1	
V2	20.00*	Speed to Z2	
V3	500.00*	Motion speed after T4	
Pressure P [kN]			
P1	0.8	Compression pressure	
P2	0.8	Compression pressure 1 while cooling	
P3	0.8	Compression pressure 2 while cooling	
Temperature T [°C]			
T1	182	Material Preheating Temperature	
T2	182	Temperature for mold closing	
T3	182	Cooling Temperature 1	
T4	80	Demolding Temperature	
Time Parameters t [s]			
Pt1	410	Compression time during P1	
St1	60	T1-Temperature holding time	
St2	60	Holding time until T2	
St3	20	T2-Temperature holding time while compression	
* Pre-set parameters adopted			
<b>Observations</b>			
Press-Molding time [s]:	815		
Others:	Part sticking to the mold		

(27) TS2no6xx

Date / time	21.08.2019	Machine operator:	Holger RÜHL
Test series	2	Sample no.	6
Machine:	Toshiba GMP211		
Mold material (ISO/JIS)	CuZn30 / C2600		
Press material	Polycarbonate		
Raw material form	Sheet		
Press material weight [g]	Balance:	Shimadzu TW3323N	
Parameter value [unit]		Parameter definition	
Position Parameters Z [mm]			
Z1	48.00	Position lower mold during heating	
Z2	48.00	Position lower mold during compression	
Cylinder motion speed V [mm/min]			
V1	500.00 *	Speed to Z1	
V2	20.00 *	Speed to Z2	
V3	500.00 *	Motion speed after T4	
Pressure P [kN]			
P1	1.4	Compression pressure	
P2	1.4	Compression pressure 1 while cooling	
P3	1.4	Compression pressure 2 while cooling	
Temperature T [°C]			
T1	182	Material Preheating Temperature	
T2	182	Temperature for mold closing	
T3	182	Cooling Temperature 1	
T4	80	Demolding Temperature	
Time Parameters t [s]			
Pt1		Compression time during P1	
St1		T1-Temperature holding time	
St2		Holding time until T2	
St3		T2-Temperature holding time while compression	
* Pre-set parameters adopted			
<b>Observations</b>			
Press-Molding time [s]: 783			
Others:			

(28) TS4no1xx

Date / time	05.09.2019 / 14:20	Machine operator:	Holger RÜHL
Test series	4	Sample no.	1
Machine:	Toshiba GMP211		
Mold material (ISO/JIS)	CuZn30 / C2600		
Press material	PMMA		
Raw material form	Sheet		
Press material weight [g]		Balance:	Shimadzu TW3323N
Parameter value [unit]		Parameter definition	
Position Parameters Z [mm]			
Z1	48.00	Position lower mold during heating	
Z2	48.00	Position lower mold during compression	
Cylinder motion speed V [mm/min]			
V1	500.00 *	Speed to Z1	
V2	20.00	Speed to Z2	
V3	500.00 *	Motion speed after T4	
Pressure P [kN]			
P1	1.0	Compression pressure	
P2	1.0	Compression pressure 1 while cooling	
P3	1.0	Compression pressure 2 while cooling	
Temperature T [°C]			
T1	175	Material Preheating Temperature	
T2	175	Temperature for mold closing	
T3	175	Cooling Temperature 1	
T4	80	Demolding Temperature	
Time Parameters t [s]			
Pt1	410	Compression time during P1	
St1	60	T1-Temperature holding time	
St2	60	Holding time until T2	
St3	20	T2-Temperature holding time while compression	
* Pre-set parameters adopted			
<b>Observations</b>			
Press-Molding time [s]:	672		
Others:			

(29) TS4no2xx

Date / time	05.09.2019 / 18:13	Machine operator:	Holger RÜHL
Test series	2	Sample no.	2
Machine:	Toshiba GMP211		
Mold material (ISO/JIS)	CuZn30 / C2600		
Press material	PMMA		
Raw material form	Sheet		
Press material weight [g]	0.56	Balance:	Shimadzu TW3323N
Parameter value [unit]		Parameter definition	
Position Parameters Z [mm]			
Z1	48.00	Position lower mold during heating	
Z2	48.00	Position lower mold during compression	
Cylinder motion speed V [mm/min]			
V1	500.00*	Speed to Z1	
V2	20.00*	Speed to Z2	
V3	500.00*	Motion speed after T4	
Pressure P [kN]			
P1	1.0	Compression pressure	
P2	1.0	Compression pressure 1 while cooling	
P3	1.0	Compression pressure 2 while cooling	
Temperature T [°C]			
T1	182	Material Preheating Temperature	
T2	182	Temperature for mold closing	
T3	182	Cooling Temperature 1	
T4	80	Demolding Temperature	
Time Parameters t [s]			
Pt1	410	Compression time during P1	
St1	60	T1-Temperature holding time	
St2	60	Holding time until T2	
St3	20	T2-Temperature holding time while compression	
* Pre-set parameters adopted			
<b>Observations</b>			
Press-Molding time [s]: 682 sek			
Others: Part sticking to the mold			



## (30) TS4no3xx

Date / time	05.09.2019 / 15:30	Machine operator:	Holger RÜHL
Test series	2	Sample no.	3
Machine:	Toshiba GMP211		
Mold material (ISO/JIS)	CuZn30 / C2600		
Press material	PMMA		
Raw material form	Sheet		
Press material weight [g]	0.55	Balance:	Shimadzu TW3323N

Parameter value [unit]		Parameter definition
Position Parameters Z [mm]		
Z1	48.00	Position lower mold during heating
Z2	48.00	Position lower mold during compression
Cylinder motion speed V [mm/min]		
V1	500.00*	Speed to Z1
V2	20.00*	Speed to Z2
V3	500.00*	Motion speed after T4
Pressure P [kN]		
P1	1.0	Compression pressure
P2	1.0	Compression pressure 1 while cooling
P3	1.0	Compression pressure 2 while cooling
Temperature T [°C]		
T1	189	Material Preheating Temperature
T2	189	Temperature for mold closing
T3	189	Cooling Temperature 1
T4	80	Demolding Temperature
Time Parameters t [s]		
Pt1	410	Compression time during P1
St1	60	T1-Temperature holding time
St2	60	Holding time until T2
St3	20	T2-Temperature holding time while compression

\* Pre-set parameters adopted

**Observations**  
Press-Molding time [s]: 650  
Others:

## (31) TS4no4xx

Date / time	05.09.2019 / 16:10	Machine operator:	Holger RÜHL
Test series	2	Sample no.	4
Machine:	Toshiba GMP211		
Mold material (ISO/JIS)	CuZn30 / C2600		
Press material	PMMA		
Raw material form	Sheet		
Press material weight [g]	0.564	Balance:	Shimadzu TW3323N

Parameter value [unit]	Parameter definition
<b>Position Parameters Z [mm]</b>	
Z1	Position lower mold during heating
Z2	Position lower mold during compression
<b>Cylinder motion speed V [mm/min]</b>	
V1	Speed to Z1
V2	Speed to Z2
V3	Motion speed after T4
<b>Pressure P [kN]</b>	
P1	Compression pressure
P2	Compression pressure 1 while cooling
P3	Compression pressure 2 while cooling
<b>Temperature T [°C]</b>	
T1	Material Preheating Temperature
T2	Temperature for mold closing
T3	Cooling Temperature 1
T4	Demolding Temperature
<b>Time Parameters t [s]</b>	
Pt1	Compression time during P1
St1	T1-Temperature holding time
St2	Holding time until T2
St3	T2-Temperature holding time while compression

\* Pre-set parameters adopted

**Observations**  
Press-Molding time [s]: 714 sek  
Others: Sticking to the mold

## (32) TS4no5xx

Date / time	05.09.2019 / 17:00		Machine operator:	Holger RÜHL
Test series	4	Sample no.	5	
Machine:	Toshiba GMP211			
Mold material (ISO/JIS)	CuZn30 / C2600			
Press material	PMMA			
Raw material form	Sheet			
Press material weight [g]	0.565	Balance:	Shimadzu TW3323N	

Parameter value [unit]		Parameter definition
Position Parameters Z [mm]		
Z1	48.00	Position lower mold during heating
Z2	48.00	Position lower mold during compression
Cylinder motion speed V [mm/min]		
V1	500.00*	Speed to Z1
V2	20.00*	Speed to Z2
V3	500.00*	Motion speed after T4
Pressure P [kN]		
P1	1.2	Compression pressure
P2	1.2	Compression pressure 1 while cooling
P3	1.2	Compression pressure 2 while cooling
Temperature T [°C]		
T1	140	Material Preheating Temperature
T2	140	Temperature for mold closing
T3	140	Cooling Temperature 1
T4	80	Demolding Temperature
Time Parameters t [s]		
Pt1	410	Compression time during P1
St1	60	T1-Temperature holding time
St2	60	Holding time until T2
St3	20	T2-Temperature holding time while compression

\* Pre-set parameters adopted

**Observations**  
Press-Molding time [s]: 746 sek  
Others: Part sticking to the mold

(33) TS4no6xx

Date / time	05.09.2019 / 17:33	Machine operator:	Holger RÜHL
Test series	4	Sample no.	6
Machine:	Toshiba GMP211		
Mold material (ISO/JIS)	CuZn30 / C2600		
Press material	PMMA		
Raw material form	Sheet		
Press material weight [g]	0.561	Balance:	Shimadzu TW3323N
<b>Parameter value [unit]</b>			
<b>Position Parameters Z [mm]</b>			
Z1	48.00	Position lower mold during heating Position lower mold during compression	
Z2	48.00		
<b>Cylinder motion speed V [mm/min]</b>			
V1	500.00*	Speed to Z1	
V2	20.00*	Speed to Z2	
V3	500.00*	Motion speed after T4	
<b>Pressure P [kN]</b>			
P1	1.4	Compression pressure	
P2	1.4	Compression pressure 1 while cooling	
P3	1.4	Compression pressure 2 while cooling	
<b>Temperature T [°C]</b>			
T1	140	Material Preheating Temperature	
T2	140	Temperature for mold closing	
T3	140	Cooling Temperature 1	
T4	80	Demolding Temperature	
<b>Time Parameters t [s]</b>			
Pt1	410	Compression time during P1	
St1	60	T1-Temperature holding time	
St2	60	Holding time until T2	
St3	20	T2-Temperature holding time while compression	
* Pre-set parameters adopted			
<b>Observations</b>			
Press-Molding time [s]:	700 sek		
Others:	Part sticking to the mold		